DISPERSED GAS PROJECT

GRI CONTRACT NO. 5080-321-0398

QUARTERLY REPORT

(AUGUST, SEPTEMBER, OCTOBER, 1982)

Prepared by

Bureau of Economic Geology
The University of Texas at Austin
W. L. Fisher, Director

TABLE OF CONTENTS

PART 1

ASSESSMENT OF UNCONVENTIONAL GAS RESOURCE IN TEXAS

by

A. R. Gregory, Z. S. Lin

and R. S. Reed

Dispersed Gas Project

GRI Contract No. 5080-321-0398

Bureau of Economic Geology

The University of Texas at Austin

University Station, Box X

Austin, Texas 78712

September 1982

September 9, 1982

ASSESSMENT OF UNCONVENTIONAL GAS RESOURCE IN TEXAS

Methods, procedures, and source
material used in assessment

by

Bureau of Economic Geology
The University of Texas at Austin

Geopressured Sandstones

Solution gas only — Data for this assessment were taken from the BEG report to DOE (Gregory and others, 1980). This assessment was for onshore Texas only, below 8,000 ft. The in-place solution gas is 690 Tcf and recoverable gas (28 Tcf) is 4% of the in-place solution gas (table 1). Distribution of this resource is tabulated by formation and by subdivision (table 2); the location of subdivisions number 1-24 are given in figure 1. Distribution of the resource is also tabulated by major fault zones (table 3). Locations of the fault zones are shown in figure 2.

Co-production, gas and water — This assessment is for non-associated natural gas in onshore and offshore Texas. Data were taken from a publication by the API, AGA, and CPA (1980). In this assessment the recoverable unconventional free gas resource R is defined by equation (1) below.

$$R = [\,OGIP - (GR + CGP)\,] \times F \qquad (1)$$

where OGIP = original gas-in-place = (GR + CGP)/f
GR = proven gas reserves
CGP = cumulative primary gas production
F = recovery factor, percentage of gas remaining in reservoir after primary production
f = recovery factor for primary production (% of OGIP)

Tabulated data include gas in geopressured and hydropressured reservoirs (table 1). Calculations are shown in table 4. The value of 33 percent used for the recovery factor F (table 4) is a conservative estimate based on the calculated recoveries of 50% and 51% of remaining gas from field data (table 5) and is equivalent to a value of 10 percent of the OGIP.

Hydropressured Sandstones (or aquifers)

Solution gas only — In-place data for this assessment (table 6) were obtained from five different areas in Texas designated as Gulf Coast, Central Texas, Panhandle, East Texas, and West Texas (fig. 3). References are listed separately for each area. A 3 percent recovery factor is assumed for the tabulation (table 1).

Undiscovered Gas

Data for the assessment (table 1) were obtained from Dolton and others (1981), Fisher (1978), and Miller and others (1975). Recovery is assumed to be 10 percent of the OGIP. Detailed computations are shown in table 7.

Wet Gas-Bearing Shale

Data for this assessment are not given in table 1 but a summary of the methodology is outlined in table 8. The recoverable gas in onshore and offshore Texas is estimated to be 2.7 Tcf (or about 10 percent of the recoverable solution gas estimated for geopressured sandstones in table 1). Pertinent references are Wallace and others (1979) and Garg (1980).

Probability Factors

The probability factors used in this assessment refer to the reliability and accuracy of the listed data (in the opinion of the persons who were responsible for the assessment).

References for the Assessment in Geopressured Sandstones, Gulf Coast of Texas (solution gas only)

Gregory, A. R., Dodge, M. M., Posey, J. S., and Morton, R. A., 1980, Volume and accessibility of entrained (solution) methane in deep geopressured reservoirs—Tertiary formations of the Texas Gulf Coast: The University of Texas at Austin, Bureau of Economic Geology, Report to the U.S. Department of Energy, Division of Geothermal Energy, Contract No. DE-AC08-78ET01580, 390 p.

References for the Assessment of Co-Production of Gas and Water

Reserves of crude oil, natural gas liquids, and natural gas in the United States and Canada as of December 31, 1979: Volume 34, June 1980, published by API, AGA, and CPA, 253 p.

Brinkman, F. P., Increased gas recovery from a moderate water drive reservoir; Journal of Petroleum Technology, December 1981, p. 2475-2480.

Lutes, J. L., Chiang, C. P., Brady, M. M., and Rossen, R. H., Accelerated blowdown of a strong water drive gas reservoir; Journal of Petroleum Technology, December 1977, p. 1533-1538.

Chesney, T. P., Lewis, R. C., and Trice, M. L., Enhanced gas recovery from a moderately strong water drive reservoir; paper SPE 10117 presented at SPE 56th Annual Fall Meeting, San Antonio, Texas, October 5-7, 1981.

References for Assessment in Central Texas (hydropressured aquifers, solution gas only)

A survey of the subsurface saline water of Texas, 1972: Texas Water Development Board Report 157, v. I, p. 3, 6, 43-60.

A survey of the subsurface saline water of Texas, chemical analyses of saline water, 1972: Texas Water Development Board Report 157, v. II, p. 9, 11, 18, 34, 39, 54, 61, 68, 86, 94, 104, 113, 135, 153, 177, 190, 202, 230, 237, 258, 278, 296, 306, 316, 322, 350, 353, 371.

A survey of the subsurface saline water of Texas, aquifer rock properties, 1972: Texas Water Development Board Report 157, v. III, p. 14-17, 24, 25, 38, 42-44, 54-56, 61, 62, 64-69, 87, 95, 96, 104, 105, 110, 133-135, 142, 143, 152-154, 174-176, 188-190, 204, 205, 228, 235-238, 254, 270, 271, 282-285, 293, 294, 301-303, 307-309, 335-343, 360-362.

A survey of the subsurface saline water of Texas, geologic well data Central Texas, 1972: Texas Water Development Board Report 157, v. IV, p. 1-9, 13-24, 36-42, 45-62, 72-101, 116-153, 161-175, 180-196, 202-210, 217-223, 227-234, 259-269, 276-279, 284-297, 303-311, 319-329, 343-361, 385-399, 407-428.

References for Assessment in Texas Panhandle (hydropressured aquifers, solution gas only)

Handford, C. R., 1980, Lower Permian facies of the Palo Duro Basin, Texas: depositional systems, shelf margin evolution, paleogeography, and petroleum potential: The University of Texas at Austin, Bureau of Economic Geology Report of Investigations No. 102, p. 15-25.

Handford, C. R., and Fredericks, P. E., 1980, Facies patterns and depositional history of a Permian Sabkha complex: Red Cave Formation, Texas Panhandle: The University of Texas at Austin, Bureau of Economic Geology Geological Circular 80-9, 10 p.

Handford, C. R., Dutton, S. P., and Fredericks, P. E., 1981, Regional cross sections of the Texas Panhandle: Precambrian to mid-Permian: The University of Texas at Austin, Bureau of Economic Geology.

Oil and gas fields of the Texas and Oklahoma Panhandles, 1961: Panhandle Geological Society.

Selected gas fields of the Texas Panhandle, 1977: Panhandle Geological Society.

References for Assessment in East Texas: (hydropressured aquifers, solution gas only)

Eaton, R. W., and Nichols, P. H., 1964, Occurrence of oil and gas in northeast Texas: East Texas Geological Society Publication No. 5, v. I.

Herald, F. A., 1951, Occurrence of oil and gas in northeast Texas: The University of Texas at Austin, Bureau of Economic Geology Publication No. 5116.

Wood, D. H., and Guevara, E. H., 1981, Regional structural cross sections and general stratigraphy, East Texas Basin: The University of Texas at Austin, Bureau of Economic Geology.

A survey of the subsurface saline water of Texas, 1972: Texas Water Development Board Report 157, v. I, p. 3, 6, 79-83, 87-98.

A survey of the subsurface saline water of Texas, chemical analyses of saline water, 1972: Texas Water Development Board Report 157, v. II, p. 1. 46, 51, 115, 116, 136, 150, 157, 164, 166, 193, 209, 212, 223, 245, 246, 259, 282, 299, 302, 324, 336, 365.

A survey of the subsurface saline water of Texas, aquifer rock properties, 1972: Texas Water Development Board Report 157, v. III, p. 1-3, 47, 48, 52, 106, 113-115, 136, 148-150, 156, 158, 162, 163, 193, 194, 209, 212, 222, 223, 241-243, 255, 269, 272, 273, 286, 287, 310, 319, 355, 356.

A survey of the subsurface saline water of Texas, geologic well data East Texas, 1972: Texas Water Development Board Report 157, v. VII, p. 1-5, 32-40, 68-71, 75-115, 127-131, 145-150, 166-173, 181-196, 206-212, 214-219, 221-233, 240-246, 256-262.

<u>References for assessment in West Texas (hydropressured aquifers, solution gas only)</u>

Oil and gas fields in West Texas symposium, 1966: West Texas Geological Society, Publication No. 66-52.

Oil and gas fields in West Texas symposium volume II, 1969: West Texas Geological Society, Publication No. 69-57.

Gas fields in West Texas symposium volume III, 1977: West Texas Geological Society, Publication No. 1977-67.

Herald, Frank A., 1957, Occurrence of oil and gas in West Texas: The University of Texas at Austin, Bureau of Economic Geology Publication No. 5716.

<u>References for the Assessment of Undiscovered Gas</u>

Dolton, G. L., and others, 1981, Estimates of undiscovered recoverable conventional resources of oil and gas in the United States: Geological Survey Circular 860, p. 24, table 6.

Fisher, W. L., 1978, Texas energy reserves and resources: The University of Texas at Austin, Bureau of Economic Geology Geological Circular 78-5, 30 p.

Miller, B. M., and others, 1975, Geological estimates of undiscovered recoverable oil and gas resources in the United States: U.S. Geological Survey, Circular 725.

References for assessment of wet gas-bearing shale

Garg, S. K., 1980, Shale recharge and production behavior of geopressured reservoirs: Geothermal Resources Council, Transactions v. 4, p. 325-328.

Wallace, R. H., Jr., Kraemer, T. F., Taylor, R. E., and Wesselman, J. B., Assessment of geopressured-geothermal resources in the Northern Gulf of of Mexico basin: in Assessment of Geothermal Resources of the United States-1978, L. J. P. Muffler, Editor, Circular 790, United States Geological Survey, 1979, pp. 132-155.

Table 1. Summary—Assessment of Unconventional Gas Resources in Texas

	Geopressured Sandstones		Hydropressured Sandstones		Undiscov. Gas	TOTAL	Total x Prob. Factors
	Solution Gas Only	Co-Prod. Gas + H_2O	Solution Gas Only	Co-Prod. Gas + H_2O			
OGIP, Tcf	690	285	3,511	—	154	4,640	2,675
(Prob. Factor)	(0.85)	(0.90)	(0.50)		(0.50)		
In Place, Tcf	690	86	3,511	—	46	4,333	2,442
(Prob. Factor)	(0.85)	(0.90)	(0.50)		(0.50)		
Recoverable, Tcf	28	29	105	—	15	177	89
(Prob. Factor)	(0.85)	(0.90)	(0.30)		(0.50)		
Reference	1	2	3	4	5		

1. Gregory and others (1980), DOE report by BEG, 4% recovery assumed.
2. API, AGA & CPS (1980) vol. 34; includes geopressured, and hydropressured, ~~and water-drive reservoirs.~~ Recovery = 10% of OGIP (See text and references)
3. See text and references, 3% recovery assumed.
4. Included under 2.
5. Dolton and others (1981), Geological Survey Circular 860. Recovery assumed to be 10% of OGIP.

Table 2. Geopressured sandstones, in-place dissolved methane, totals for Tertiary net sandstones below 8,000 ft, onshore Texas Gulf Coast (Tcf) (after Gregory and others, 1980)

Subdivision	upper Oligocene-Pleistocene	upper Frio	lower Frio	Vicksburg-Jackson	upper Claiborne (Yegua)	lower Claiborne	upper Wilcox	middle Wilcox	lower Wilcox	Total by subdivision
1	4.71	33.07	25.37	35.37	—	—	—	—	—	98.52
2	0.06	47.60	63.18	25.65	—	—	—	—	—	136.49
3	—	8.80	6.72	3.88	—	—	—	—	—	19.40
4	—	2.90	19.62	5.35	—	—	—	—	—	27.87
5	4.01	6.19	25.73	1.88	—	—	—	—	—	37.81
6	1.79	3.00	21.81	0.56	—	—	—	—	—	27.16
7	—	—	—	1.17	—	—	0.69	—	—	1.86
8	—	—	—	1.24	—	—	1.64	0.02	—	2.90
9	—	—	—	—	—	—	1.79	0.31	—	2.10
10	—	—	—	—	—	—	2.14	1.19	0.70	4.03
11	—	—	—	—	1.97	—	0.35	0.78	0.40	3.50
12	—	—	0.36	—	7.78	0.25	6.22	5.48	—	20.09
13	—	—	—	—	—	—	6.50	0.25	—	6.75
14	—	—	—	—	—	—	9.91	1.63	—	11.54
15	—	—	—	—	—	—	3.01	3.49	10.40	16.90
16	—	—	—	—	—	—	4.61	3.82	28.69	37.12
17	—	—	—	—	0.13	0.01	11.53	8.79	59.07	79.53
18	—	—	—	—	0.14	—	11.36	8.25	11.47	31.22
19	—	—	—	—	—	—	—	—	0.28	0.28
20	—	—	—	—	—	—	—	0.05	0.31	0.36
21	—	—	—	—	—	—	—	0.09	6.83	6.92
22	—	—	—	—	—	—	—	0.22	13.88	14.10
23	—	—	—	—	—	—	0.78	3.62	49.05	53.45
24	—	—	—	—	—	—	3.23	6.25	39.53	49.01
Total by formation	10.57	101.56	162.79	75.59	10.02	0.26	63.76	44.24	220.83	688.91

Total methane (net sandstones) = 690×10^{12} SCF

Table 3. Geopressured sandstones, distribution of in-place methane dissolved in formation waters, Tertiary sandstones below 8,000 ft, onshore Texas Gulf Coast.

	Methane (Tcf)	% Total Methane
Vicksburg-Frio fault zone (Subdivisions 1-6)	348	50.4
Updip of Vicksburg-Frio fault zone (Subdivisions 7-12)	33	4.8
Wilcox fault zone (Subdivisions 13-16)	183	26.5
Updip of Wilcox fault zone (Subdivisions 19-24)	126	18.3
Total	690	

Table 4. Calculation of Recoverable Non-Associated Gas in Texas by Co-Production of Gas and Water

Using equation (1) in the text:

(1) GR = 39.454 Tcf (API, AGA, AND CPA, 1980, p. 110 and 115)

(2) Ultimate Recovery = 199.773 Tcf (API, AGA, and CPA, 1980, p. 200)

(3) $CGP = 199.773 - GR$
$= 199.773 - 39.45 = 160.319$ Tcf

(4) $OGIP = (GR + CGP)/f$
$= 199.773/0.7 = 285.4$ Tcf

(5) $R = [OGIP - (GR + CGP)] \times F$
$= [285.4 - 199.773] \times 33\%$
$= 29$ Tcf

Table 5. Summary of Recovery Factors of Published Field Data

	Lovells Lake Field (Brinkman, 1981)	Katy Field (Lutes and others, 1977)	North Alazan Field (Chesney and others, 1981)
Original gas in place (OGIP), Bcf	175	330	121
Cumulative primary gas production, Bcf	101	151	77
Remaining gas after primary Production, Bcf	74	179	44
Calculated additional recovery, Bcf	37.6	91	> 7.7
Recovery factor F, % of remaining gas	50%*	51%*	>18%
Calculated recovery factor, % OGIP	21%**	28%**	> 6%

$$* \text{ Recovery factor F} = \frac{\text{additional recovery}}{\text{remaining gas after primary production}} \times 100\%$$

$$** \text{ Recovery factor} = \frac{\text{additional gas recovery}}{\text{OGIP}} \times 100\%$$

Table 6. Assessment of in-Place Solution Gas in Hydropressured Sandstones (aquifers) in Texas

	Tcf
Gulf Coast	1,050
Central Texas	144
Panhandle	158
East Texas	188
West Texas	1,971
Total	3,511

Table 7. Undiscovered Recoverable Natural Gas Resources in Texas

(1) Undiscovered recoverable gas in Region 5—West Texas and Eastern New Mexico (Dolton and others, 19~~75~~81, p. 24).
= 32.8 Tcf (mean)

(2) Undiscovered recoverable gas in Region 6—Western Gulf Basin (Dolton and others, 19~~75~~81, p. 24).
= 112.6 Tcf (mean)

(3) Fraction of Texas in Region 5 = 0.8609
Fraction of Texas in Region 6 = 0.7043
(from Fisher, 1978; and Miller and others, 1975).

(4) Undiscovered recoverable gas in Texas
=(32.8 x 0.8609) + (112.6 x 0.7043)
= 107.54 Tcf

(5) Original undiscovered gas in-place in Texas
= 107.54/0.7 = 153.6 Tcf

(6) Undiscovered gas in-place in Texas for unconventional resources
= 153.6 x 0.3 = 46 Tcf

(7) Recoverable undiscovered gas for unconventional resources by EGR
= 153.6 x 0.1 = 15.3 Tcf

Table 8

Part A. Calculation of Recoverable Gas From Wet Gas-Bearing Shale

(1) Gas in wet gas-bearing shale = 26,557 Tcf (Wallace and others, 1978)

(2) Recovery factor = 0.01% (see case 2 in part B)

(3) Recoverable gas from wet gas-bearing shale = 26,557 x 0.01% = 2.7 Tcf

Part B. Summary of Calculated Recovery Factors for Wet Gas-Bearing Shale, Based on Reservoir Simulation Study by Garg (1980)

	Vertical Shale Permeability, μd	Uniaxial Shale Compressiblity, psi^{-1}	Cumulative Gas Production, Scf	Recovery * Factor (percent)
Case 1 (Base case)	0	10^{-5}	1.49×10^8	—
Case 2	0.001	10^{-5}	1.51×10^8	0.01
Case 3	0.01	10^{-5}	1.78×10^8	0.15
Case 4	0.1	10^{-5}	3.55×10^8	1.06
Case 5	0.01	10^{-4}	1.79×10^8	0.15
Case 6	0.1	10^{-4}	3.71×10^8	1.15

* Recovery factor (% of gas recovery from shale water)

$$= \frac{\text{cum. gas production} - 1.49 \times 10^8}{\text{amount of gas in shale water initially}} = \frac{\text{cum. gas production} - 1.49 \times 10^8}{1.9384 \times 10^{10}}$$

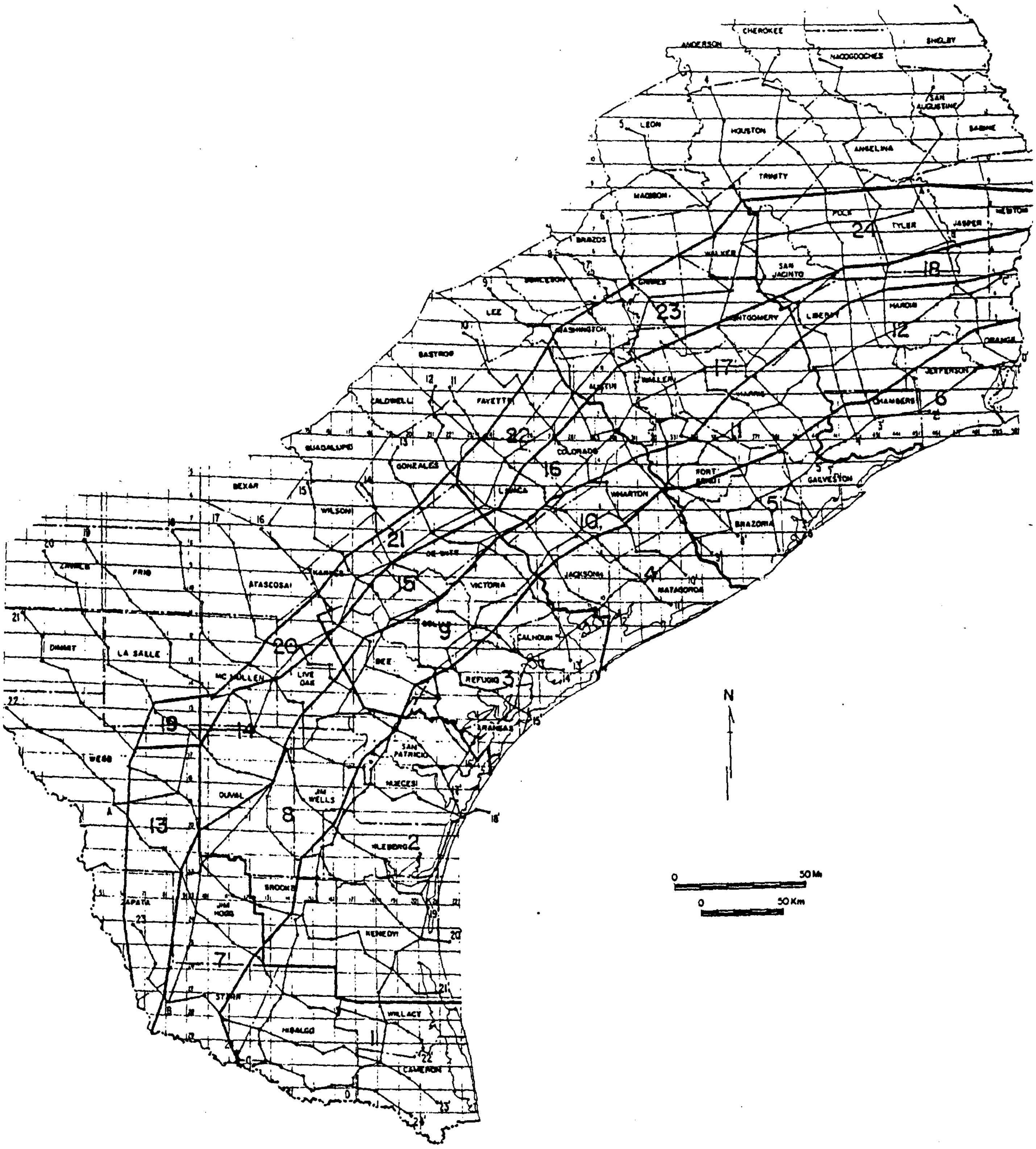

Figure 1. Subdivisions delineated for detailed mapping and calculation of in-place methane resource (geopressured sandstones) after Gregory and others, 1980.

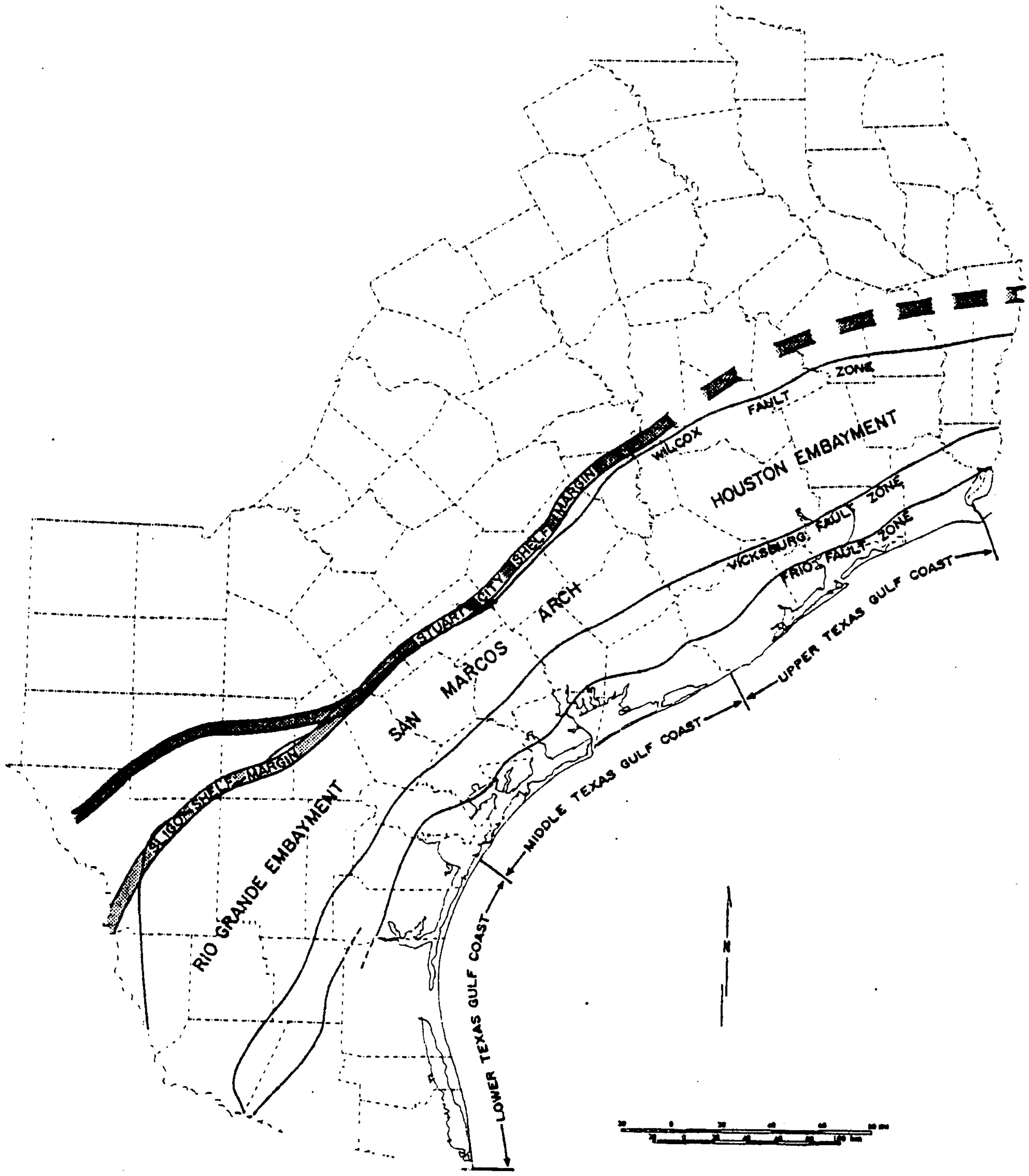

Figure 2. Major structural features of the Texas Gulf Coast (after Gregory and others, 1980).

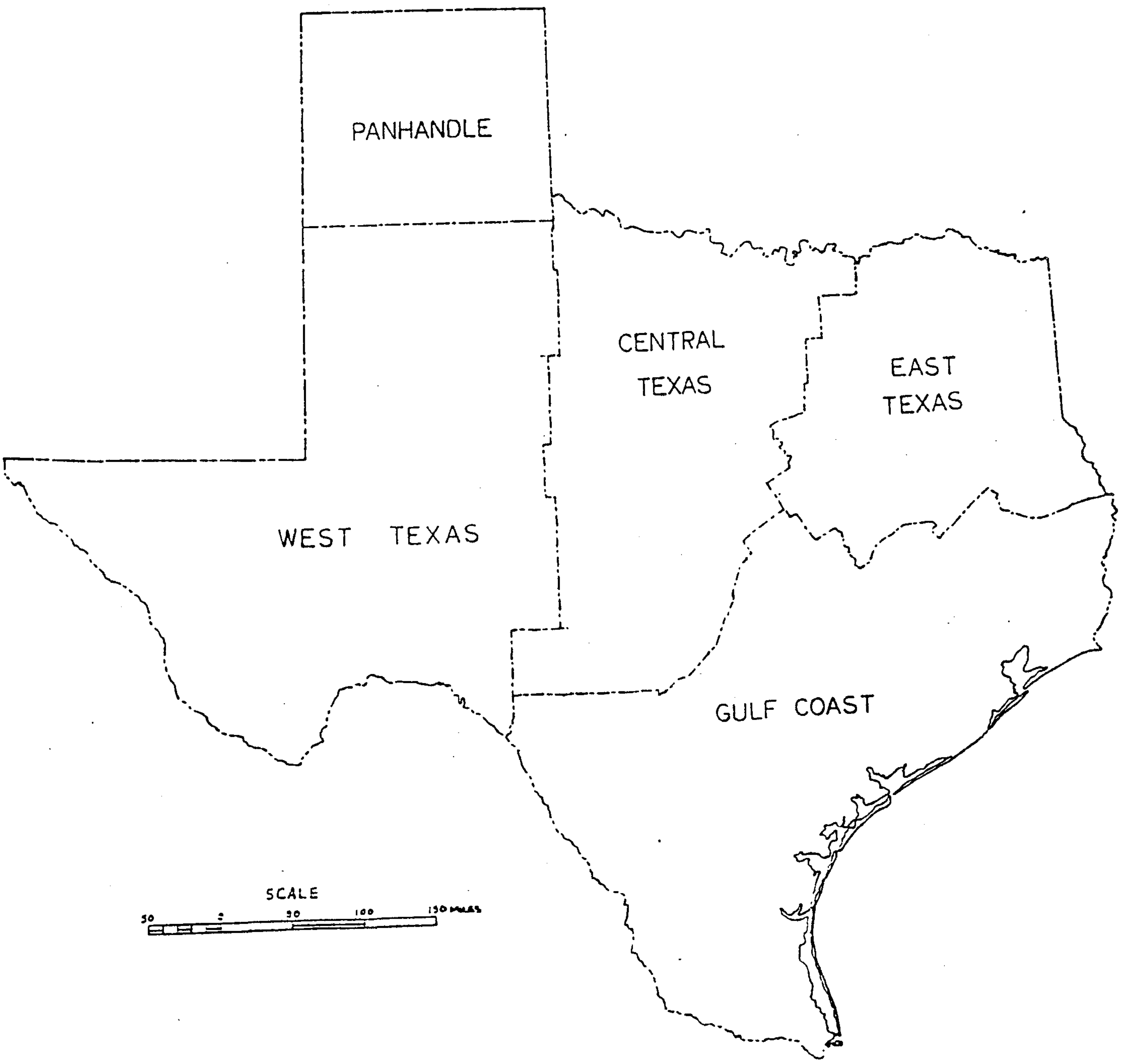

Figure 3. Texas divided into five areas for assessment of solution gas in hydropressured aquifers.

PART 2

SEISMIC PROCESSING AND MODELING

PORT ARTHUR FIELD

JEFFERSON COUNTY, TEXAS

TABLE OF CONTENTS

NOTE: Appendix D and exhibits 1, 2, and 3 (which are mentioned in the text) are not included in this report.

*Trademark of GeoQuest International, Inc.
®Trademark of GeoQuest International, Inc.

INTRODUCTION

At the request of the Bureau of Economic Geology (BEG) and the Gas Research Institute (GRI), GeoQuest International, Inc. (GQI) has processed six seismic lines in the Port Arthur area, Jefferson County, Texas and has performed seismic modeling of the Port Arthur Field.

The object of the processing was to enhance vertical and horizontal resolution to aid the interpretation of the seismic data. The orientation of the seismic lines relative to the Port Arthur Field is shown in Figure 1.

The object of the seismic modeling was to determine if the presence of gas in the Lower Hackberry Sands could be seen on the seismic data and if the extent of gas reservoirs could be delineated with seismic data. An underlying question which the modeling might hope to address concerned detectability of dispersed gas reservoirs versus normally saturated reservoirs.

CONCLUSIONS

Reprocessing of the six seismic lines in the Port Arthur Area has resulted in a modest improvement in the interpretability of the seismic data. The most important contribution of GeoQuest's processing was the shaping of the basic seismic wavelet to a narrow symmetrical wavelet. This made the seismic response to a bed the same on all lines. It also allowed one to associate bed boundaries (for resolved beds) with peaks and troughs in the seismic data.

The objective of enhancing resolution by broadening the spectral band-width and by migration was severely limited by the very poor signal-to-noise ratio in this data. We feel the noise level is such that the data is only suitable for structural interpretation of the seismic data. It is not of sufficient quality for detailed reservoir delineation. Structural interpretation of the seismic data was to be performed by BEG staff.

Recommendations for a seismic data acquisition program to improve one's ability to see reservoir detail with sufficient accuracy are presented in this report. The main conclusions are that 1) a signal-to-noise level four times that seen so far must be achieved; 2) a bandwidth of 10 to 85 hertz would be satisfactory but may be beyond reach; 3) dynamite would be the best source both for signal strength and static corrections but may not be practical in a cultured environment; and 4) recording of the shot signature with a special uphole geophone would improve the wavelet processing.

Seismic modeling along Mobil Line 3 contributed to the above conclusions. It also showed the nature of the seismic response to the thin gas beds of the Port Arthur Field. The model of Figure 10 shows the geologic cross section from which the synthetic seismic sections were derived. Figure 17 is a typical synthetic seismic section; sixteen such sections were generated. Variation of bed velocities produced models that showed the sensitivity of the seismic response to those variations. It also showed that uncertainty in bed acoustic impedances could severely limit one's ability to unravel the details of reservoirs like these which have thin, rapidly changing beds. It is clear that good resolution and exceptional synthetic-seismic ties would be necessary to delineate this type of reservoir using seismic data. The data quality here was inadequate for this.

The question of whether dispersed gas in a depleted reservoir can be seen in the seismic data remains unanswered. There were no measurements of the velocity in dispersed gas reservoirs. In light of that velocity uncertainty, several assumptions were made for the dispersed gas velocity, and models were built for each assumption; however, the seismic data quality was too poor to observe the differences seen in the models. Thus, no comment could be made as to which was the most appropriate velocity.

SEISMIC DATA PROCESSING AND ACQUISITION

Data Acquisition

The data utilized in this project were obtained by purchase of existing seismic data available for sale through oil companies and/or data brokers. This method of obtaining data is relatively inexpensive and quick but has the problem that the line locations may be less than optimum and that there is no control over acquisition parameters or quality. The data selected were the best available for purchase. A base map showing the location of the lines is presented in Exhibit 1. Figure 1 summarizes that map.

Several types of data were obtained:

1. Line K-1 was recorded in 1980 by GeoSource using a thumper as a source. The data were recorded with a 220 foot group interval and a 24 fold stack from a 48 trace cable.

2. Lines 1, 2, and 3 were recorded in 1973 by Western Geophysical using Vibroseis as a source (Sweep 48-12 Hz). A 330 foot group interval, 24 trace cable developed a 12 fold stack.

3. Line MS-7 was recorded in 1979 by Mineral Search using dynamite as a source (10 pounds at 77 feet). A 330 foot group interval 48 trace cable and 12 fold stack were recorded.

4. Line 10 was recorded in 1969 by Teledyne using dynamite as a source (15 pounds at 73 feet). A 300 foot group interval, 24 trace cable and 6 fold stack were used.

This wide variation in source, geometry and stack fold results in appreciable differences in data quality particularly when a broad band spectral content is needed for detailed stratigraphic interpretation. Wavelet processing has compensated for source differences and the resulting character differences.

Seismic Processing by GeoQuest

The object of GeoQuest's processing was to enhance the interpretability of the seismic section. This is done first by shaping the wavelet to a narrow symmetric form (using the SWE* process) and second by migrating the data to enhance lateral resolution. Conversion of wiggly trace seismic data to an acoustic log form of display (SYN-LOG®) can often aid the interpretation by enhancing the acoustic bed boundaries and their continuity. The following discussion elaborates on the processing procedure. Appendix A treats one aspect, wavelet processing, in more detail. A subset of that, SWE*, is treated mathematically in Appendix B. The SYN-LOG** procedure is explained in Appendix C.

The processing sequence included the following:

1. Demultiplexing
2. Correlating if needed
3. Applying a gain leveling function
4. Trace to trace normalization
5. Field statics and geometry corrections
6. Sorting to CDP gathers
7. Velocity determination (one per Km)
8. Residual static corrections
9. Stacking
10. Deconvolution (predictive)
11. Time Variant SWE* (statistical wavelet enhancement)
12. Migration and
13. Conversion to relative acoustic impedance sections (SYNLOG**)

Films were made of true amplitude SWE* section, true amplitude migration section, true amplitude SYN-LOG** section and time variant bandpass filter and AGC of the migrated section. Copies of these sections are included in a supplement to this report. The films have been sent under separate cover.

The processing sequence described above was intended to produce seismic sections with a near zero phase wavelet with the broadest spectral content that can be supported with the signal-to-noise ratio of the data. The SWE* process, described more completely in an appendix, is a

*Trademark of GeoQuest International, Inc.
©Trademark of GeoQuest International, Inc.
**Trademark of GeoQuest International, Inc.

statistical wavelet processing procedure which uses the spectral measurements of auto correlation ($|W|^2 + |N|^2$) and cross correlation ($|W|^2$) sums to develop an operator. These spectral measurements, when combined with a phase assumption (Φ) and a band limiting function (D) yield an operator of the form:

$$F = \frac{|W| \cdot e^{-j\Phi} \cdot D}{|W|^2 + |N|^2}$$

This filter has high output when the noise content is low and a low output when noise content is strong.

Recommendations For Future Seismic Gathering And Processing

The objectives of an investigative survey of this nature dictate that data quality be the best possible. Determination of the thickness, extent and fluid content of sands at these target depths requires seismic data of maximum quality and signal-to-noise ratio. Should another such project be planned, it is recommended that new data be recorded with all parameters designed to produce maximum resolution at the zone of interest.

Among the considerations in planning such a survey is the source to be used. Dynamite has been proven to be a reliable and versatile seismic source with a great deal of penetration and available bandwidth. Static delays due to the near surface low velocity layer can often be effectively corrected from shot hole information. Special uphole geophones, designed to handle strong signals, can provide direct measurements of the propagating wavelet when burried shots are used. Despite the advantages of dynamite shooting, cultural considerations often severely limit the use of dynamite. In the presence of severe cultural limitations Vibroseis may be preferable. Modern vibroseis equipment allows the introduction of a lot of power for penetration, and a broad sweep spectrum can be provided. We recommend that choice of sources be limited to these two and that dynamite be used if possible.

After the choice of sources has been made, selection of parameters and geometries must be based upon the particular objectives of the project. We refer the reader to an excellent article out of the Journal of the Canadian Geophysical Society: "Extending The Resolution Of Seismic Reflection Exploration" by L.R. Denham (Vol. 17, No.1, December 1981). This article details the many different parameters which must be considered in planning a new seismic survey. Some of the parameters discussed there are:

1. Far-trace offset
2. Near-trace offset
3. Geophone-group interval
4. Charge size
5. Charge depth
6. Sample rate
7. Low-cut filter
8. Geophone frequency
9. Geophone array geometry
10. Line length.

We recommend that the principles outlined be used in planning any future data acquisition.

In summary we recommend that future project planning consider the following:

1. Gathering of new seismic data using a source and field parameters designed to provide maximum data quality and resolution in the zone of interest.

2. Processing of these data should include wavelet shaping to zero phase and spectral shaping to the widest possible bandwidth for maximum resolution.

SEISMIC MODELING

Overview

Seismic modeling was undertaken to show the seismic response to presumed subsurface geology. Had good seismic data been available, one could use the synthetic seismic section derived from such a model as a test of the correctness of the model (within the resolution limits of the seismic data). The noise level of the data did not allow this. Furthermore only limited well data was available for predicting acoustic properties. Thus, the focus of the modeling was to test the detectability of the reservoir details in synthetic seismic data and to relate this experience to the real seismic data where possible. The modeling was done for varying conditions of bandwidth, noise and rock velocities.

That portion of Line 3 which corresponds to the modeled synthetic sections is shown in Figure 9. One may wish to compare the synthetic sections with that section. Note that the C-Sand top is 50 ms shallower in the synthetic sections. Note also that there are 9 more traces on the left side of the synthetic sections than on the real data. Observe that the shot point numbers are one half the value of the CDP numbers. Only CDP values are posted on the synthetic seismic sections. To aid the comparison between synthetic and real data, the interpreted C-Sand top has been marked on the real seismic section in Figure 12.

The following sections address the steps in the modeling: 1) Synthetic seismogram generation and tie to the seismic section, 2) Model generation, 3) Bandwidth studies, 4) Noise studies, 5) Alternate rock velocities, and 6) Summary.

Synthetic Seismogram Generation And Tie

A synthetic seismogram display was generated for the Kilroy Booz #1 well. This was tied to the seismic sections for identificaiton of the lower Hackberry Sands in the seismic data.

Only the Booz #1 well had a sonic log; thus a synthetic seismogram could be made for that well alone. This is well number 37 on the BEG maps. In Figure 5 it is seen to be a directional well. In that figure the lines near the Port Arthur Field are shown along with the structure map of the C-Sand (supplied by BEG). At the depth of the C-Sand, the vertical projection of the well bore is very close to Line MS-7 (shotpoint 111).

The synthetic seismogram plot generated for the Booz #1 well is shown in pieces in Figures 6A through 6C. It is also presented at 10 inches per second in Exhibit 2. Figure 6A shows one synthetic seismogram derived from the sonic log. The sonic log is the left-most curve. The SP and resistivity curves are included there only for convenience. Density is needed for the calculation of acoustic impedance ($Z= \rho v$) which in turn is used to compute reflection coefficients ($RC = (Z2 - Z1)/(Z2 + Z1)$). Since the density log was not available, density was estimated through the Gardner Relationship ($\rho = .23 * v ** .25$).

Figure 6B shows several versions of the synthetic seismogram traces for various wavelet assumptions. The wavelets are Butterworth Bandpass (BWBP) Wavelets. They are parameterized by numbers like "13-4/30-3". The numbers 13 and 30 designate the low and high cut frequencies at the half amplitude points. The numbers 4 and 3 indicate the rates of cut off or "filter slopes". They are multiples of 12 db/octave. This range of wavelet bandwidths is useful when the wavelet is not known precisely or when the bandwidth changes with depth.

Figure 6C shows the same traces displayed in Figure 6B but presented in the SYN-LOG** format. These are useful for making ties to SYN-LOG** formated seismic sections. SYN-LOG** sections are discussed in Appendix C. They were not used in our analysis because the data were too poor.

In Figure 7 key parts of the synthetic seismogram display are enlarged in the zone of interest--the vicinity of the Hackberry Sands. The synthetic seismic traces were generated using a 30-4/45-4 BWBP wavelet. This appears to match the data best and is consistent with the spectrum predicted by the SWE* processing (see Figure 4).

The synthetic tie with the seismic data is shown in Figure 8. The correlation is poor but is reinforced by time-depth curves from nearby wells. (A check shot survey from the No. 2 W.H. Gilbert well -- well 40 -- predicts a time of 2.82 seconds for the top of the C-Sand). This poor tie can be due to several causes, the most important being the poor signal-to-noise in the seismic data. The second most important cause for the mistie is that the seismic method samples a large circular area (the Fresnel Zone) of a subsurface bed while the well log sees only inches into the formation. The Fresnel Zone radius is a function of the average velocity and the time to a bed and of the peak frequency in the data. For the C-Sand the Fresnel Zone radius is 2000 feet; therefore, the diameter of one Fresnel Zone is nearly as wide as the reservoir. Migration tends to collaps the Fresnel Zone to a point, but does so in two dimensions only; thus, out of plane variations within 2000 feet of the line are averaged with data in the plane of the section. Thus, rapid changes in lithology and poor signal-to-noise have degraded the tie.

The time-depth relationship and the synthetic seismogram were sufficient to pick the top of the C-Sand to within a cycle. This horizon top was correlated from line to line for the three lines that cross the reservior. The line ties and horizon C correlations are shown in Figure 8. Note that line 3 had to be shifted down 30 ms with respect to line K-1 and line MS-7 had to be shifted down 15m. This kind of shift is not unusual for lines shot with different sources and recorded with different instruments.

**Trademark of GeoQuest International, Inc.

Model Generation

The geologic model was designed in cooperation with BEG geologists. The synthetic seismic sections were produced by GeoQuest using the AIMS® computer programs.

On GeoQuest's request, BEG geologists developed the geologic model shown in Figure 10. This model was derived from well data. Blocked spontaneous potential curves were used to identify beds of sufficient thickness and acoustic impedance contrast to yield an observable seismic response. These beds were at least 20 feet thick. The beds were correlated from well to well and projected onto the line of section that coincides with seismic line 3. The projection was guided by structure maps on the sand tops. Those wells closest to the seismic line 3 are shown on the model in Figure 10.

The velocities assigned to the beds were derived in part from the sonic log of the Booz #1 (well number 37). The velocities used in five different models are shown in Figure 10. The gas sand velocity was the most important velocity to know, but there was no measurement of it. Experience tells us that it may be anywhere between 90% to 70% of the water sand velocity. The 70% values are common in Plio-Pleistocene sands, particularly in unconsolidated sands. Miocene sands tend to have the larger percentages.

In the case of dispersed gas or free gas in pockets, such as is found in a depleted gas reservoir, we have no experience with velocities. Some would argue that velocity effects of gas and oil in consolidated sands are historical influences -- that is hydrocarbons preserve porosity by altering the diagenesis. If this is the case, then the reduction of gas saturation would not affect the velocity. Because of this uncertainty, several gas sand velocities were tried. Reduction of gas saturation will affect density. Density was derived from the Gardner relationship here. Gas sand densities could be 15% less than water sand densities. While this density difference could have a significant effect on acoustic impedance, the uncertainty in density was included in the velocity uncertainty.

The AIMS** modeling program was employed to generate the synthetic seismic sections from the geologic model. The digitized structure model was plotted by AIMS** as shown in Exhibit 3. Velocities were added to this, and synthetic sections with different wavelets and noise levels were produced by AIMS**. The computer listing of Model 3 is given in Appendix ~~I~~ D along with the AIMS** execution cards used to generate one of the synthetic sections.

® Trademark of GeoQuest International, Inc.
** Trademark of GeoQuest International, Inc.

Bandwidth Studies

The effects of bandwidth are explored in the synthetic seismic sections of Figures 11 through 16. Figure 11A reveals the ultimate resolution for the given time sample interval (1 ms for the models). Each bed boundary is represented by a spike two samples wide. These spikes are very broad band (0-500 Hz). The amplitudes and polarities of the reflection coefficients at each bed boundary are portrayed by the size and sign of the spikes. The location of the gas sands is indicated on the spike section by the shaded zones in Figure 11B. The wavelets used in each section are shown on the sections at CDP 205 near time 2.97 seconds. In Figures 13 through 16 four BWBP wavelets are employed: 15-35, 15-45, 15-65 and 16-85. In all cases the filter slopes are 48 db/octave on the low end and 72 db/octave on the high end.

In all four sections two features characterize the presence of gas. One is the dimming of the reflector at the top of the C-Sand over the gas cap. This is due to the reduction of velocity contrast with respect to the overlying shales. This in turn is due to the fact that the sands here have velocities greater than the shales and that the gas sand velocity is assumed to be intermediate between the sand and shale velocities. (These velocities correspond to model 1 where the gas sand velocity is 9500 f/s, which is 86% of the water sand velocity). This is an important clue for identifying gas in the C-Sand. The clue works in the model data because there are no conflicting variations in the overlying bed. This clue or "seismic signature" does not work for the other sands because they are all overlain by beds which are themselves changing laterally. If one looks for an amplitude variation along the C-Sand in the real seismic data of Figure 12, he sees no clear indication of dimming -- only noise fluctuations.

The second common feature indicating gas is the general loss of amplitude in the central portion of the reservoir complex. This dim zone is centered at the structural crest and at a time of 2.82 seconds. The observation is of limited practical use for establishing the details of the reservoir geometry. It simply says that the acoustic contrasts approach zero here. The fact that we know a priori that it represents stacked, closely spaced gas pays does little to help us determine the lateral extent of the pay zones.

It is clear that the broader bandwidth data (Figure 16) brings out details essential to reservoir delineation. This is a necessary but not sufficient condition to map the reservoir: we need well data. Even in this case the only classic hydrocarbon indicator that shows up here, but not in the narrow band sections is the flat spot at 2.83 seconds. It is the base of the E sand. An equally nice flat spot which lies below it; however, is not due to a fluid contact but rather a shale stringer that was nearly flat and limited to a crestal position. Thus, it is apparent that, without good clues, one would not be able to work out the reservoir shapes. The needed clues come from the clear identification of the seismic responses to the sands, which in turn is derived from a good well tie and an accurate measurement of the bed acoustic impedances. The seismic data might then suggest models to try. These models could be verified with comparisons between synthetic sections and the real seismic data.

Interpretation of high acoustic impedance zones has much more ambiguity than interpretation of low acoustic impedance zones. This fact further complicates the story at Port Arthur. The problem with high impedance reservoir rock (high relative to nearby low impedance, non-reservoir rock) is that increased porosity or hydrocarbon content means a reduction of amplitude. A reduction of amplitude can result from other causes, notably thinning of the reservoir bed or contamination by non reservoir rock. This is the cause of the ambiguity. It further complicates the interpretation.

One useful structural clue comes from the synthetic tie and from the modeling. In Figure 12 we see that the interpreted C-Sand top does not roll over into the major fault nearly as much as the model would have it. There is little well control there so this is possible. This shows one benefit of coordinated well and seismic interpretations.

Noise Studies

The influence of noise on detectability of the reservoir elements is studied in Figures 17 and 22. Noise is measured here as the ratio of the largest signal amplitude to the root-mean-squared (RMS) value of the noise. The largest signal amplitude in the sections is the isolated, one trace reflection in the lower left of the figure: the so-called "wavelet". Two suites of noise models are shown in Figures 17 through 19 and 20 through 22 respectively. In each suite there are three signal-to-noise rations, 25.1, 12.6 and 6.3 (in db: 28, 22 and 16). The two suites differ in the wavelets used. The first suite has a wavelet whose bandwidth is 15 to 45 Hz. The second suite has a wavelet whose bandwidth is 15 to 85 Hz.

In the first suite of noise sections (Figures 17, 18 and 19), the detectability of reservoir elements gets progressively worse as the signal-to-noise ratio declines. In Figure 17, the essential elements of the reservoir, as seen in the noise free section of Figure 14, are still discernable in Figure 17. One could still do serious modeling with this level of noise. In Figure 18, only the grossest features of the reservoir are detectable. Figure 19 looks hopeless from a modeling point of view: only structure is detectable. This figure begins to look like the real section of Figure 12. It suggests that the noise level in the real data is four times the maximum tolerable level for modeling.

In the next suite of noise sections (Figures 20 through 22), the higher resolution due to a broader bandwidth seems to have increased the detectability of the reservoir elements. This is due in part to the higher amplitudes resulting from the decline of destructive interference from adjacent beds. The noise and signal amplitude spectrums are identical within each section. In nature, they tend to differ. The noise spectrum is broader and often peaks at low frequencies. If the noise of Figure 19 could be superimposed on the broad band signal of Figure 22, then the two figures may have looked very similar and had a comparable loss of detectability.

Alternate Rock Velocities

Different assumptions about rock velocities are made and the effect on the synthetic sections are observed here. This is useful for understanding how sensitive one's ability to detect reservoir elements is to the knowledge of the bed acoustic impedances.

The first variation to Model 1 is Model 2 (see Figure 10) where the channel sands and others sands are given velocities that differ by 1000 feet per second. The argument for this is that the coarser sands should have higher velocity. Figure 23 shows the result. In comparing it to Figure 14 one sees very little difference.

Changing the gas sand velocity has much more profound effects. Consider Figure 25 which shows the synthetic section from model 4. Here the gas sand velocity has been increased from 9500 feet/second to 10250 feet/second (or 93% of the water sand velocity). The distinction between water sand (at 11000 feet/second) and gas sand decreases while the difference between gas sand and shale (9000 feet/second) increases. When compared to Figure 15, Figure 25 reveals several subtle but important changes. The top of the C-Sand has much less loss of amplitude due to the presence of the gas. Likewise, the top of the D-Sand, which is the second black cycle, shows up more strongly. The fluid contact in Figure 15 is the flat portion of the third black cycle. The gas-water contact in the E channel sand is partially responsible for this reflection but the sidelobe of the shale lense between the E and F sands also contributes. As expected, this flat spot loses amplitude when the gas sand velocity in the model is changed from 9500 feet/second to 10250 feet/second. However, because the sidelobes from other reflectors contribute to the reflection, the effect is small.

It is interesting to observe the seismic response when no gas is present in the reservoir as is the case in Model 5. Figure 26 shows the resultant synthetic seismic section. Notice how more continuous the reflectors look. The amplitude changes are easily related to the coming and going of shale stringers. When this section is compared to Figure 15 (with gas at 9500 feet per second), the clues to the presence of hydrocarbons become dramatically more evident -- the dimming of the top cycle, the central dim spot and the fluid contact. This illustrates nicely the value of alternate models.

One last model jumps to the other extreme. In Model 3 the gas sand velocity is made much lower -- 8000 feet/second. The picture changes drastically. Figure 24 shows the result. Compare this to the no-gas case of Figure 26. The C-Sand reservoir is lost completely because it has no contrast in acoustic impedance with the upper shale. The D and E sands become more visible because the largest amplitudes are those associated with the gas. Here the fluid contacts are reinforced. This is useful, provided one knows what to look for.

<u>Summary</u>

In summary, this modeling effort has shown that the present seismic data is suitable only for structural interpretation. The signal to noise level is too low for any useful modeling or "direct hydrocarbon detection". Nor could the detectability of dispersed gas sands (versus highly saturated gas sands) be determined from this data: no measurements of the dispersed gas sand velocity have been made, and the seismic data was to poor to suggest what velocity best models the seismic response. The models have suggested that a close coupling of well data and good seismic data can help define a reservoir better than either alone. The models also show that the small bed spacing and rapid lateral variation are pushing the limit of seismic definition of this kind of reservoir. Any time the target zone has a seismic signature of dimming as opposed to brightening the problem gets more difficult. This is so because there is an ambiguity between the loss of amplitude due to increased porosity (or gas content) versus the loss of amplitude due to bed thinning. This was evident in the models. The models have been very instructive in showing the possibilities of greater reservoir detection with increased bandwidth and signal to noise. They also showed the utility of varying rock parameters to test their impact on the seismic image and thus the detectability of such changes.

Prepared By:

Edward S Meanley

Dr. Edward S. Meanley

Reviewed By:

D. L. Kelm

J. R. Patch

ESM/lh

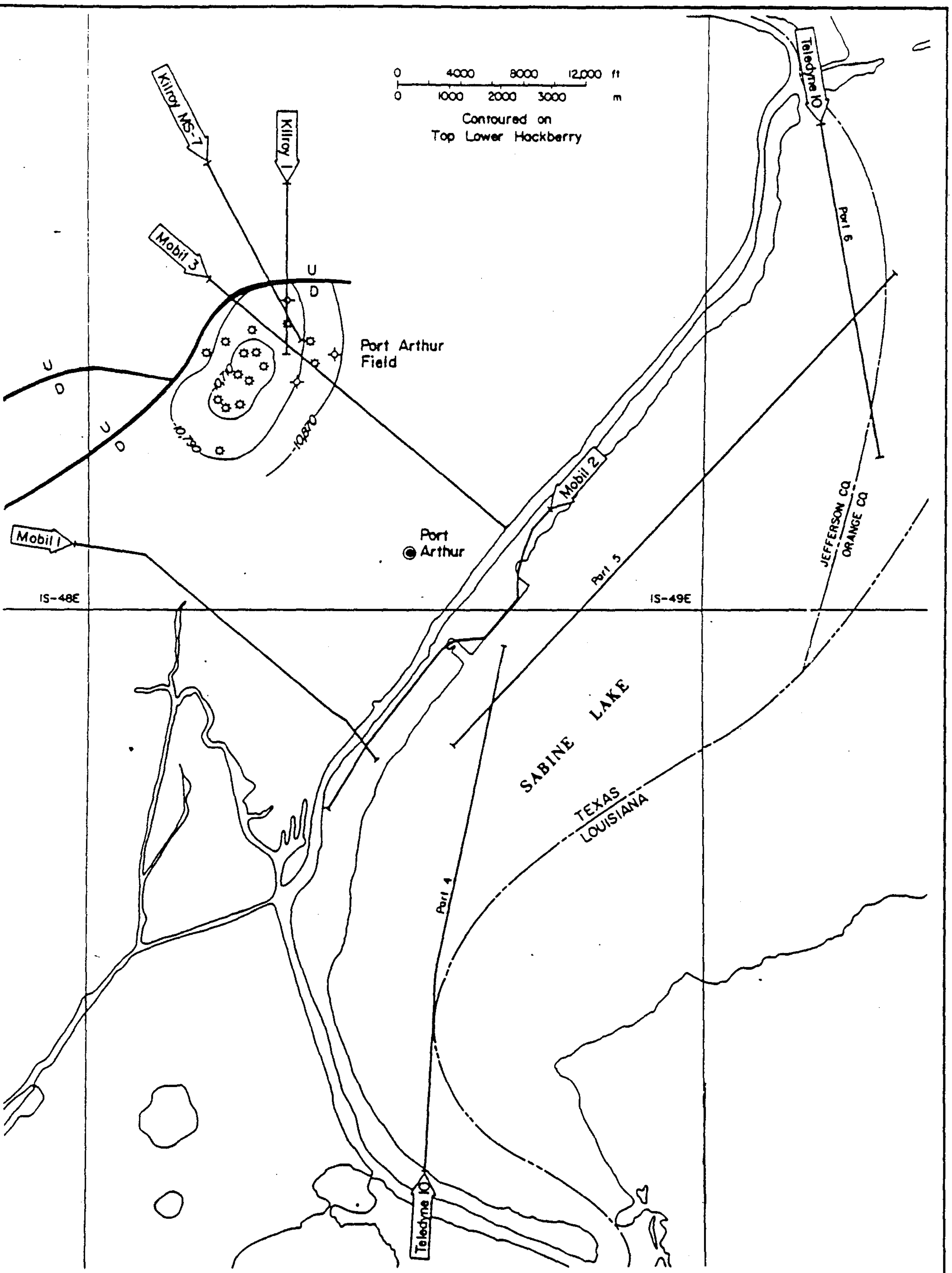

...gure 1. Location of seismic lines in the Port Arthur area, reprocessed by GeoQuest.

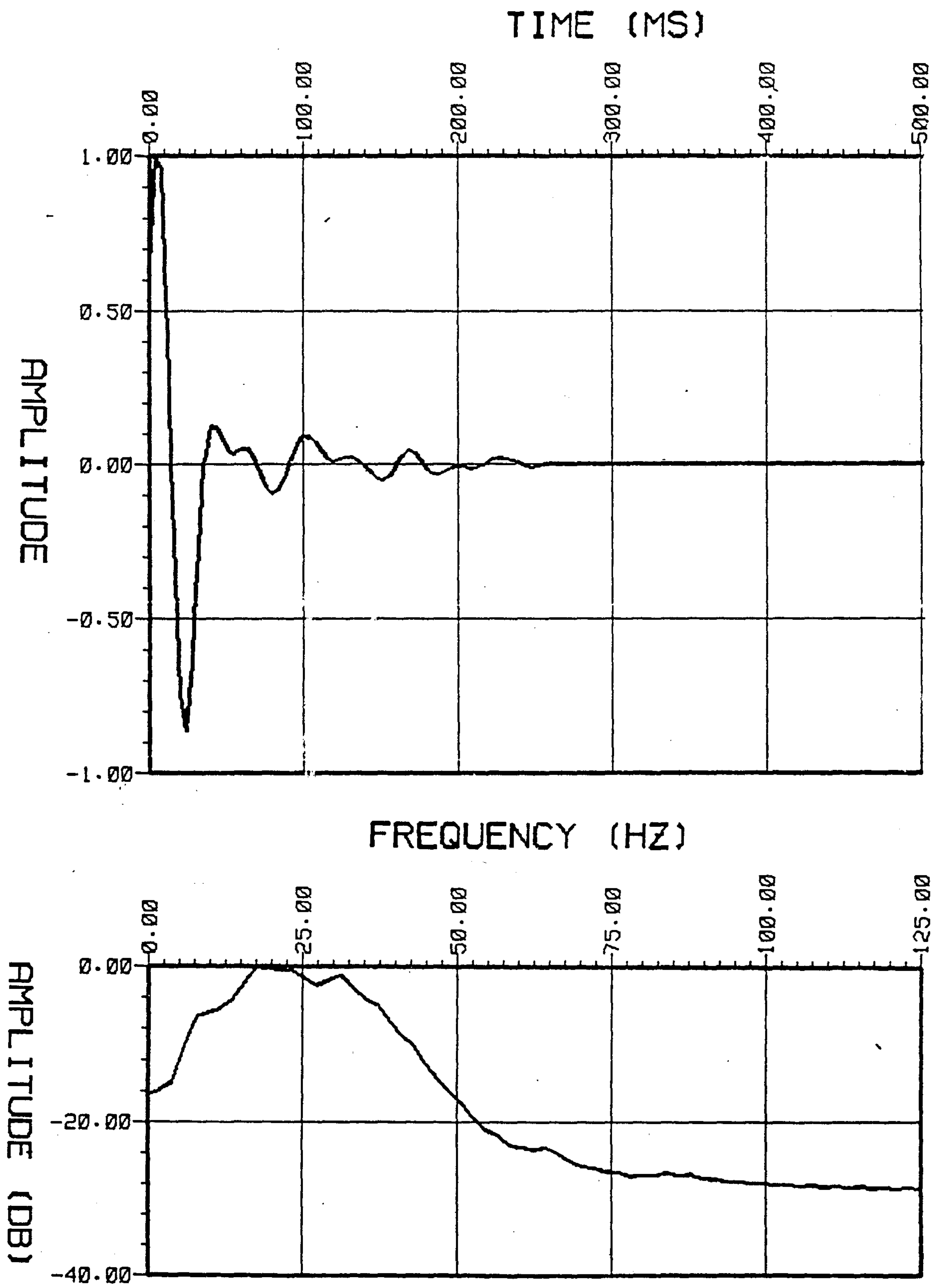

Figure 2. Extracted wavelet and it's spectrum for Kilroy 1 line, prior to SWE.

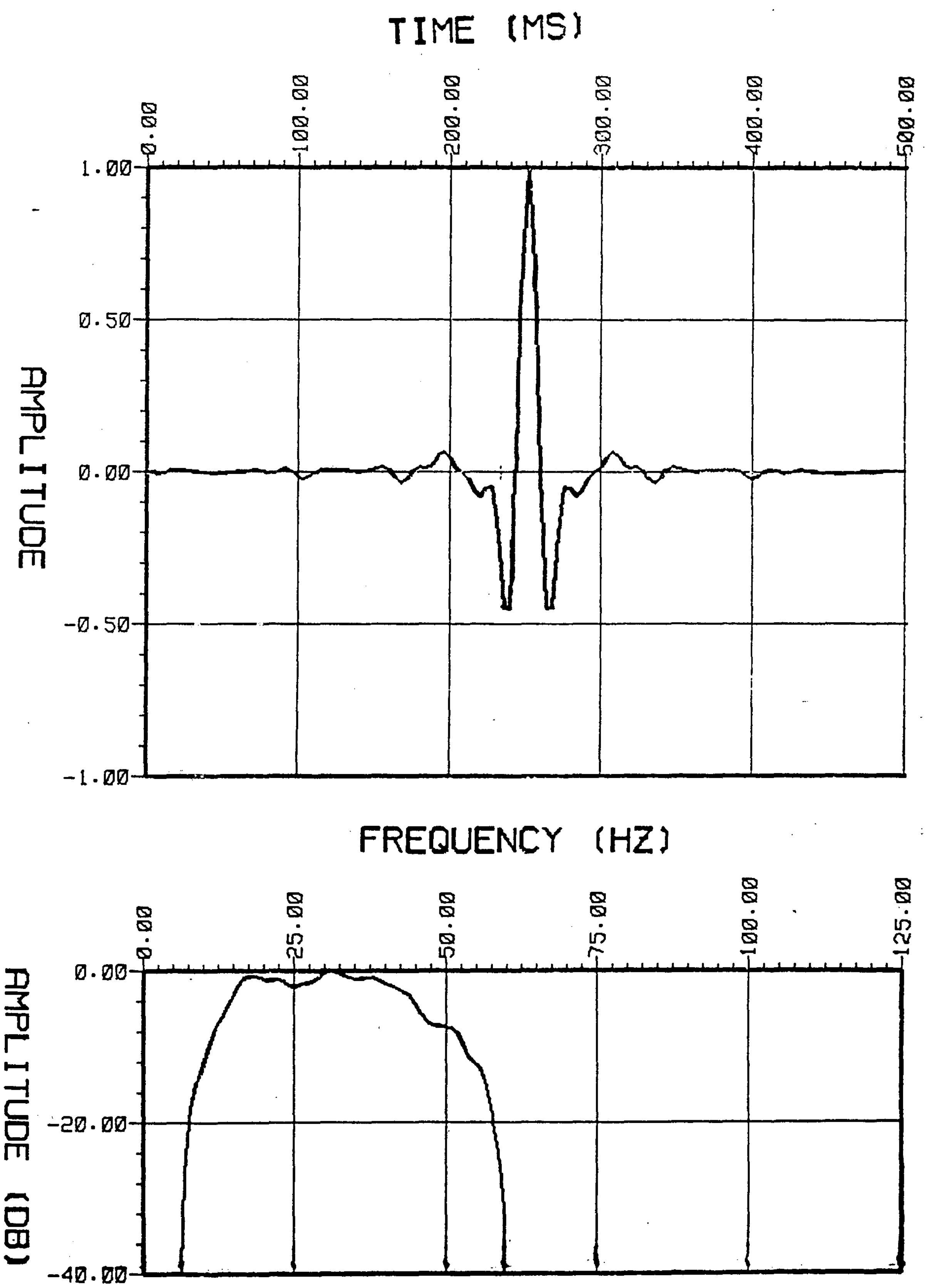

ure 3. Resultant Theoretical wavelet for Kilroy 1 line, after SWE.

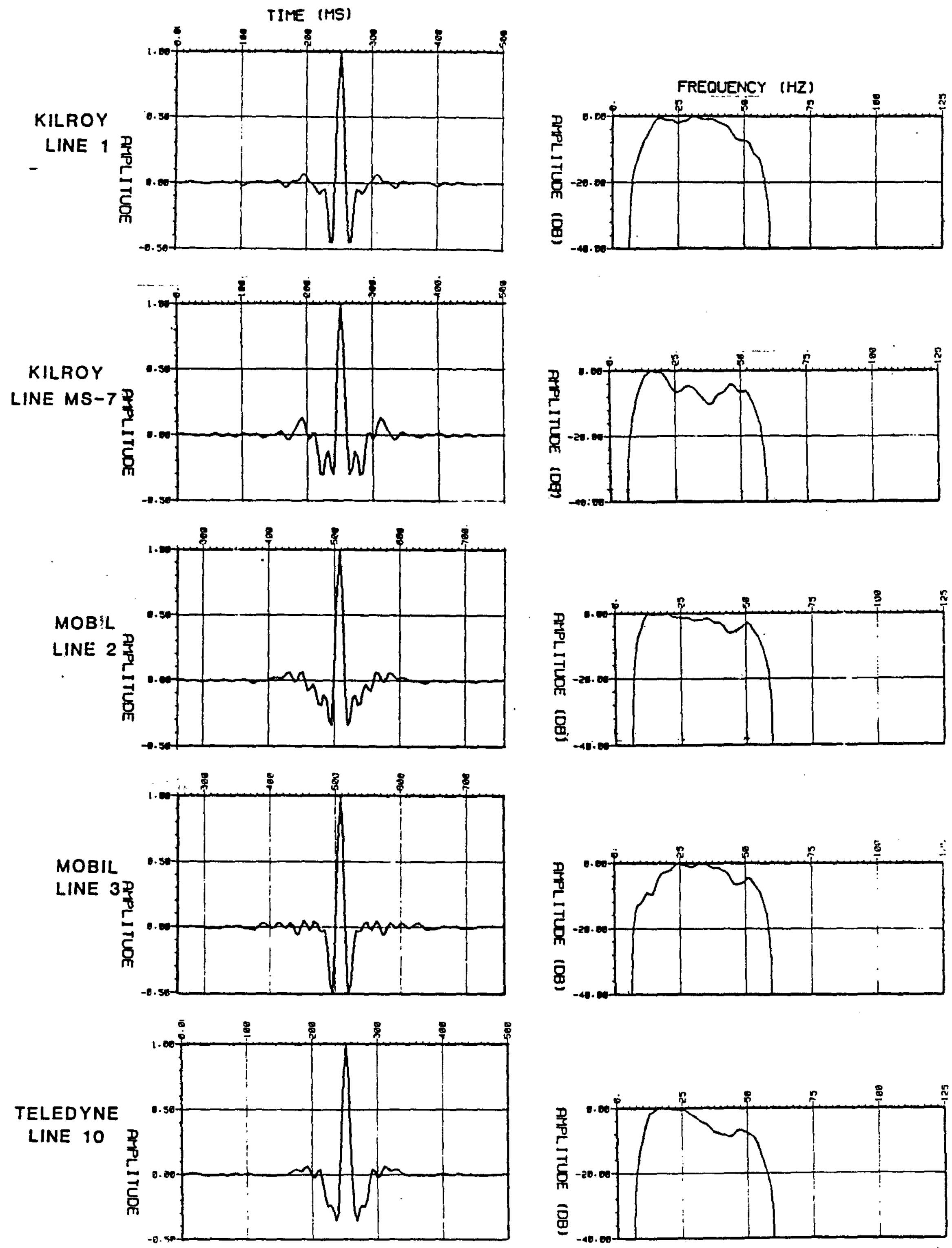

Figure 4. Results of SWE processing for each seismic line. These are the Theoretical zero phase wavelets (and spectrums) in the SWE seismic lines (2.3-3.4 seconds).

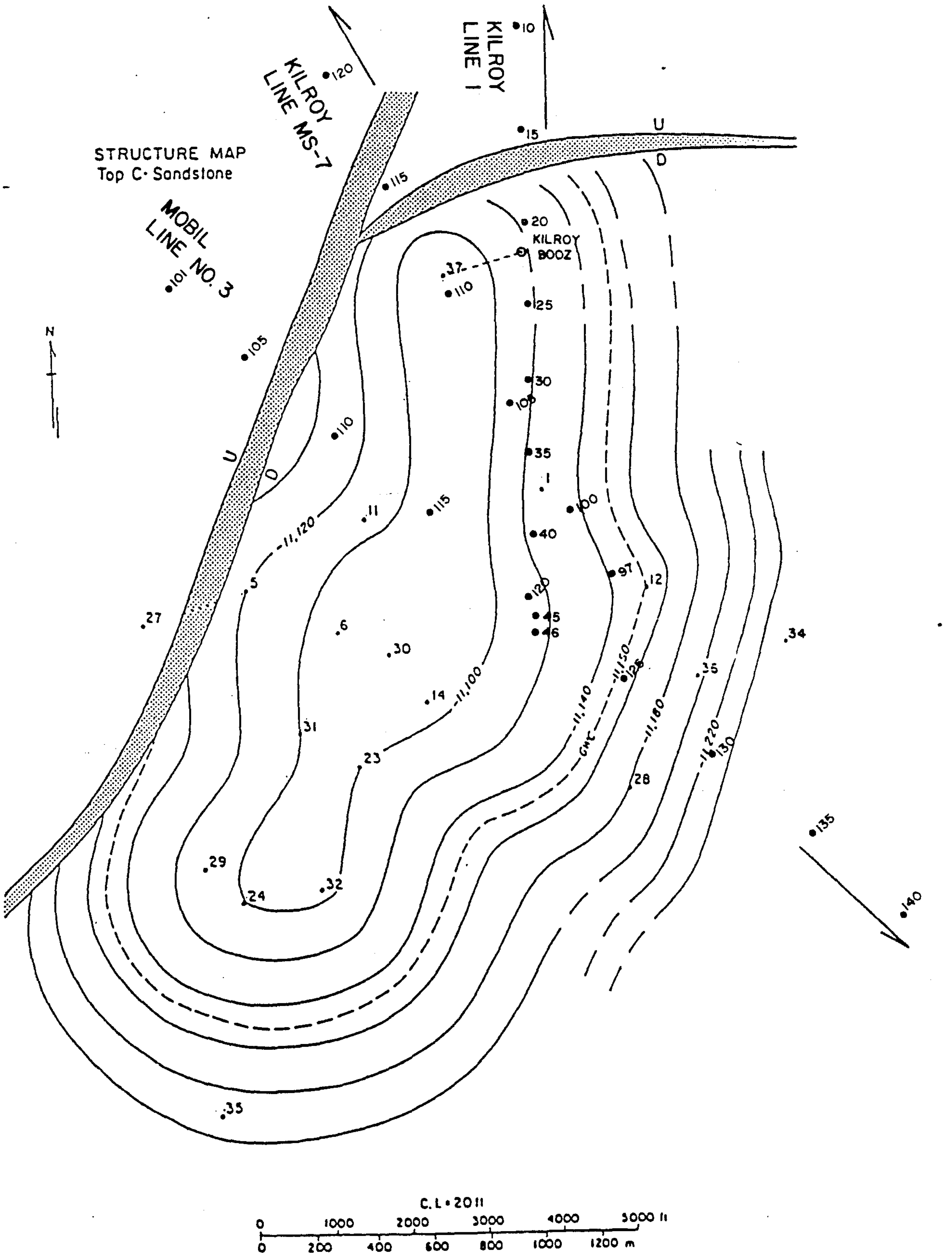

Figure 5. Orientation of seismic lines with respect to the C Sand reservior. (structure map from B.E.G.)

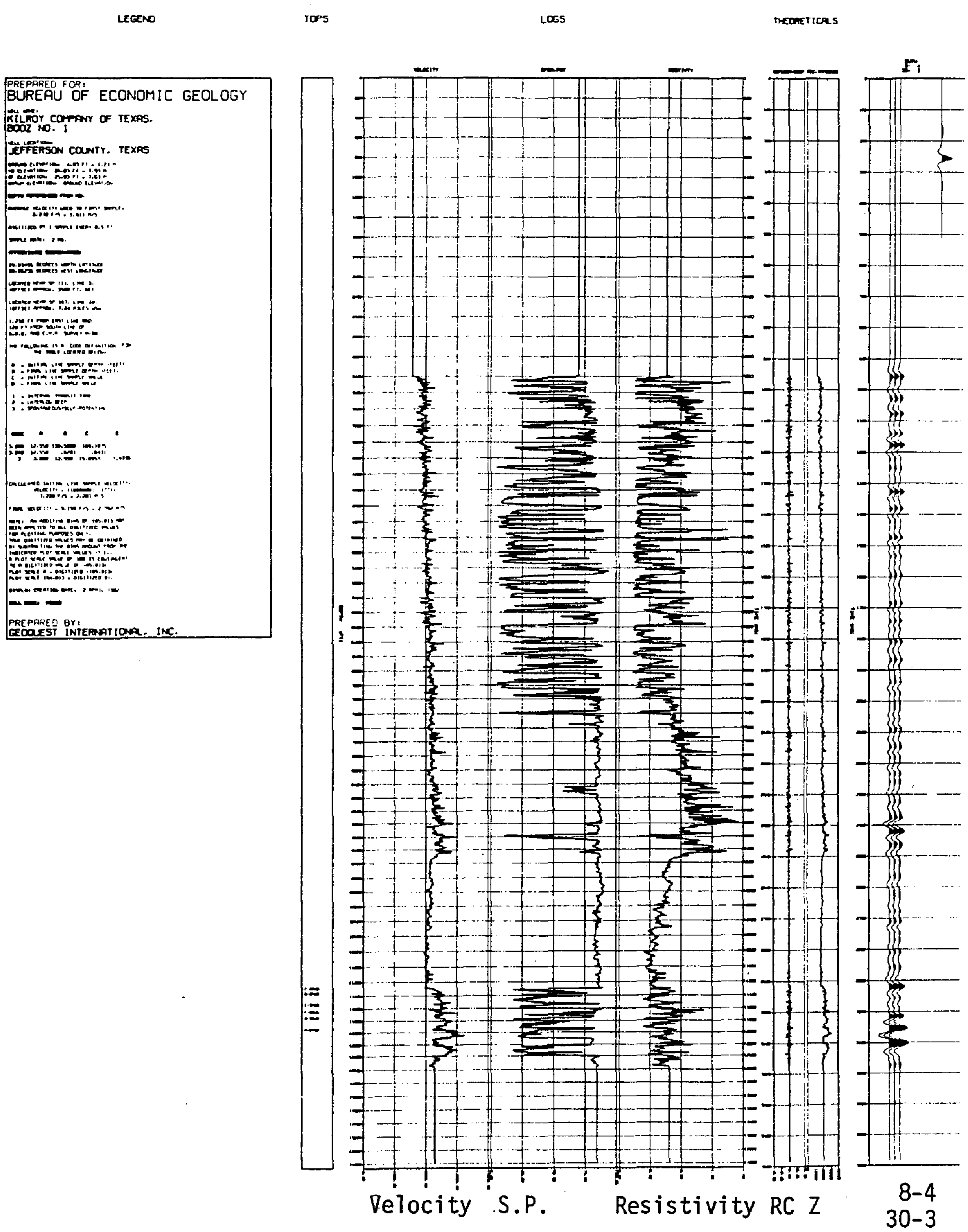

Figure 6A. Synthetic seismogram at the BOOZ #1 well.

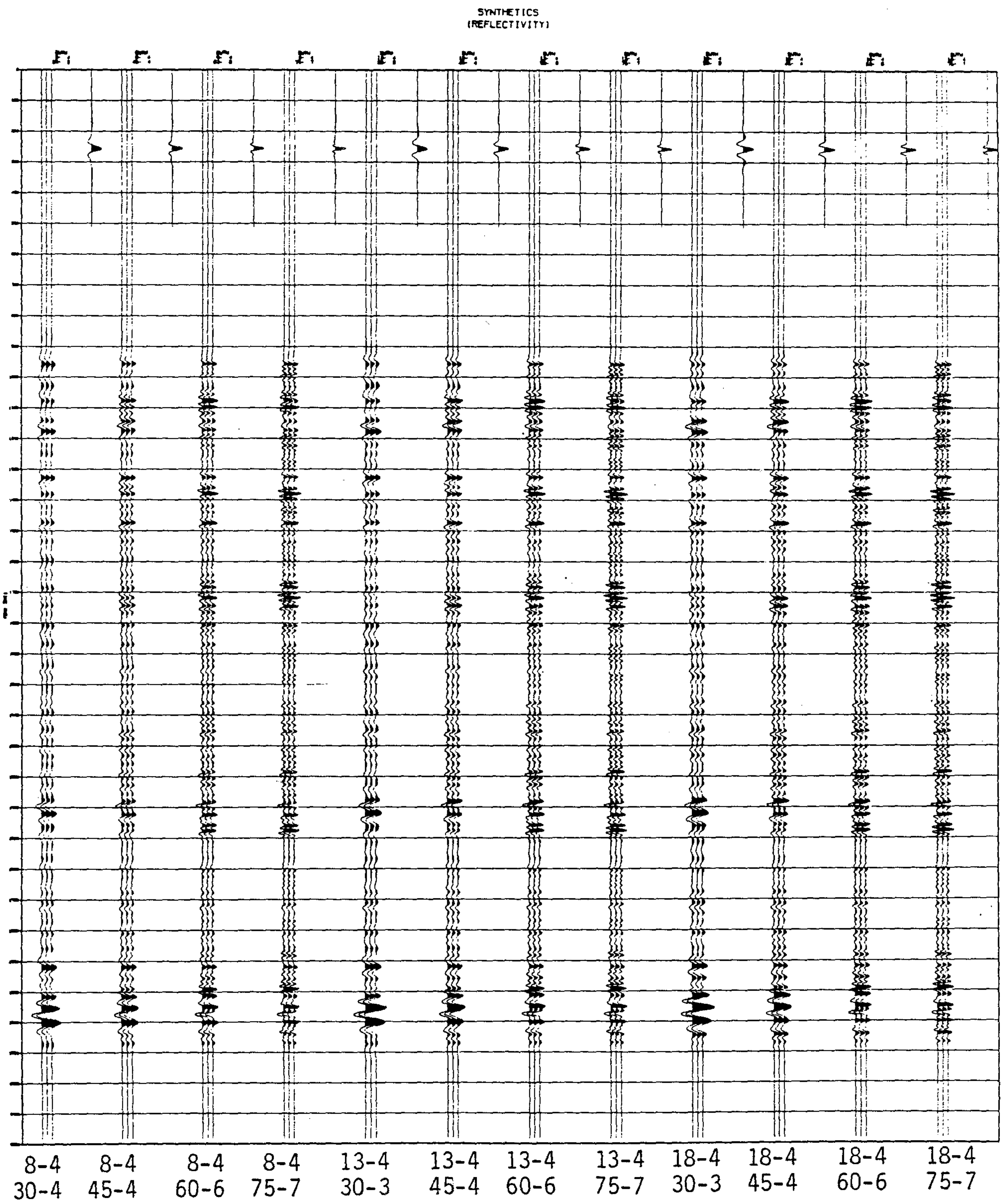

Figure 6B. Synthetic seismogram traces for several bandpass wavelets. This is a continuation of Figure 6A.

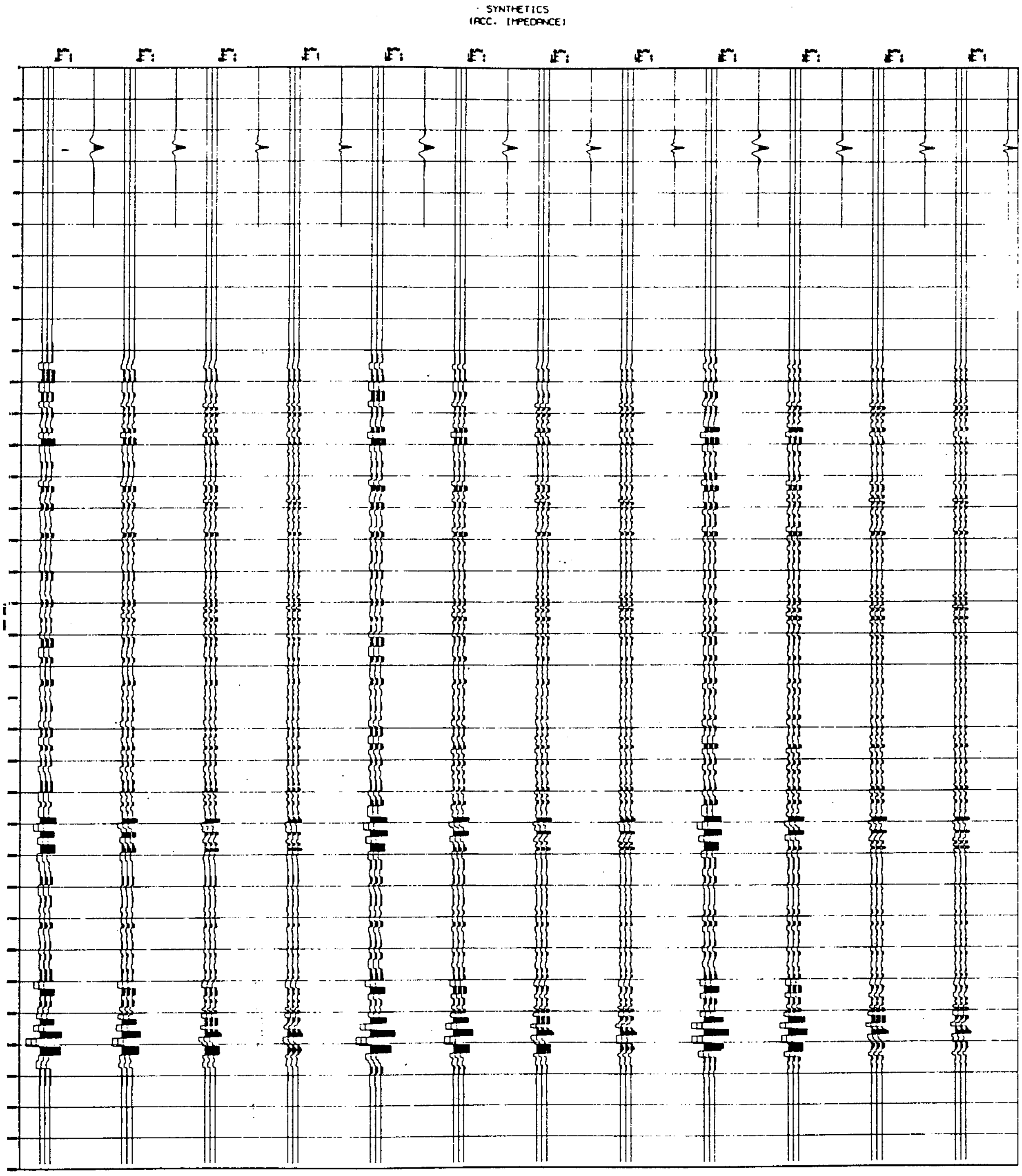

Figure 6C. SYN-LOG representation of the synthetic seismogram traces of Figure 6B.

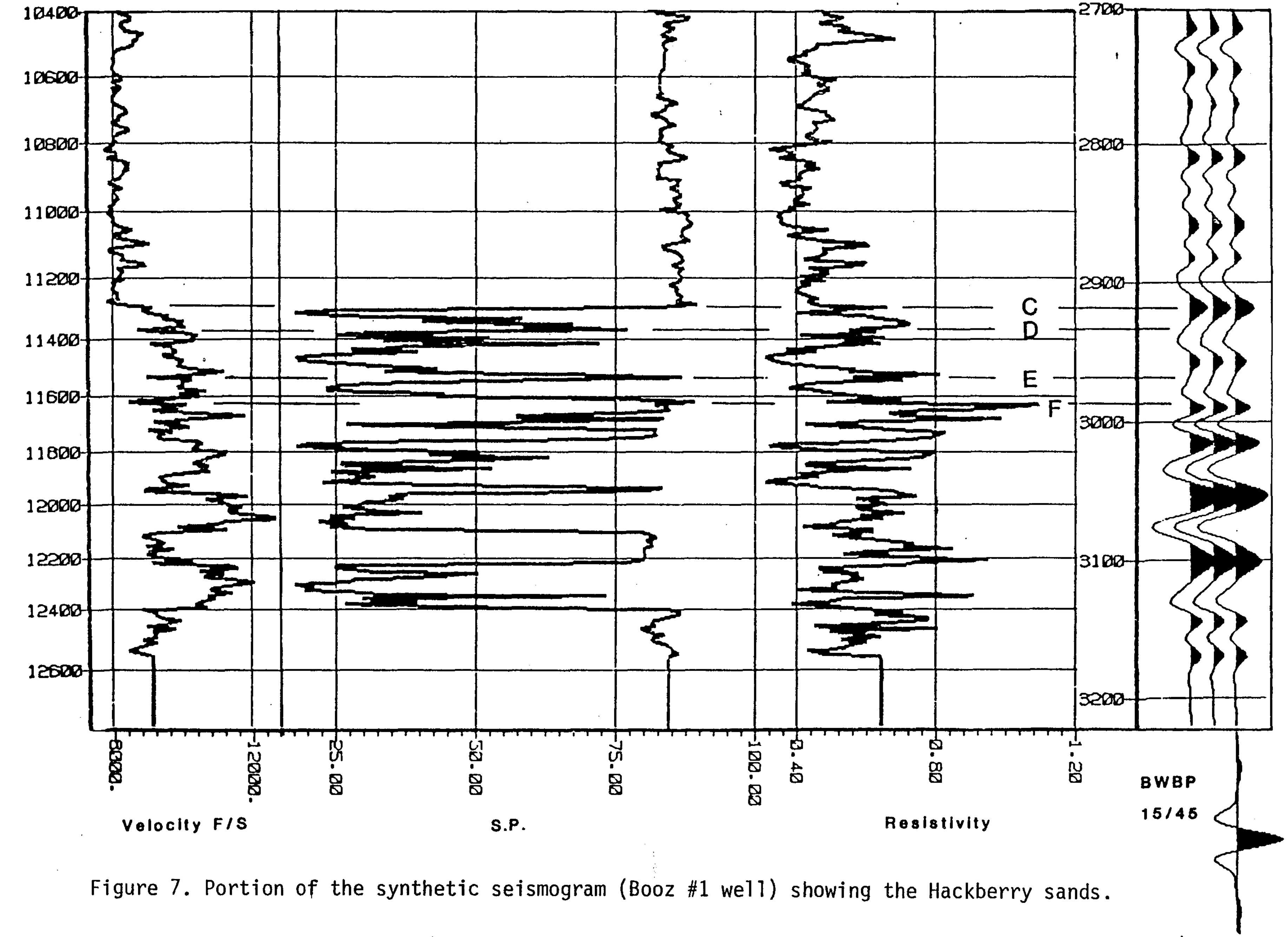

Figure 7. Portion of the synthetic seismogram (Booz #1 well) showing the Hackberry sands.

GeoQuest International, Inc.

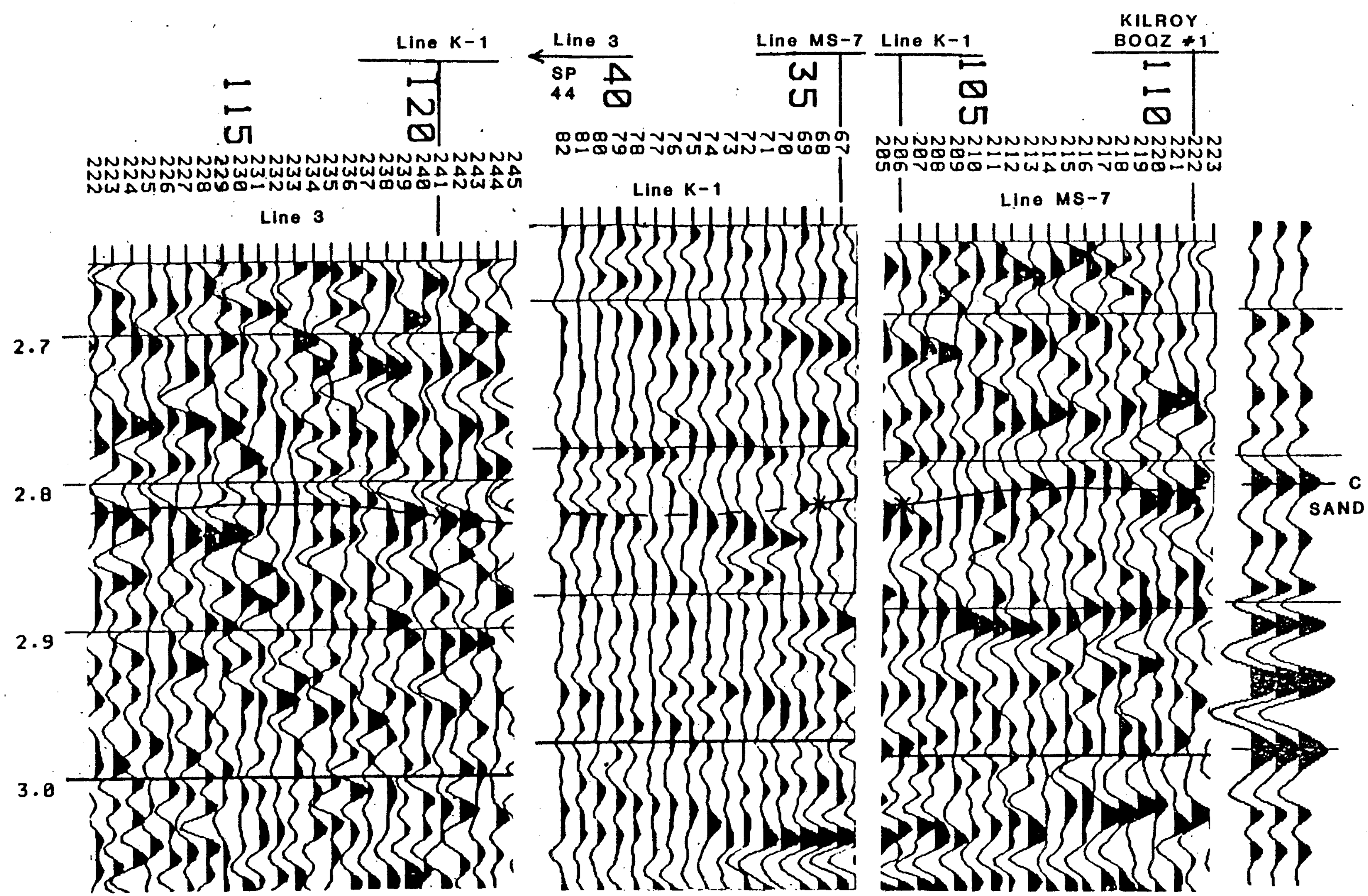

Figure 8. Synthetic-to-section tie and correlation of the C-Sand top along three seismic lines.

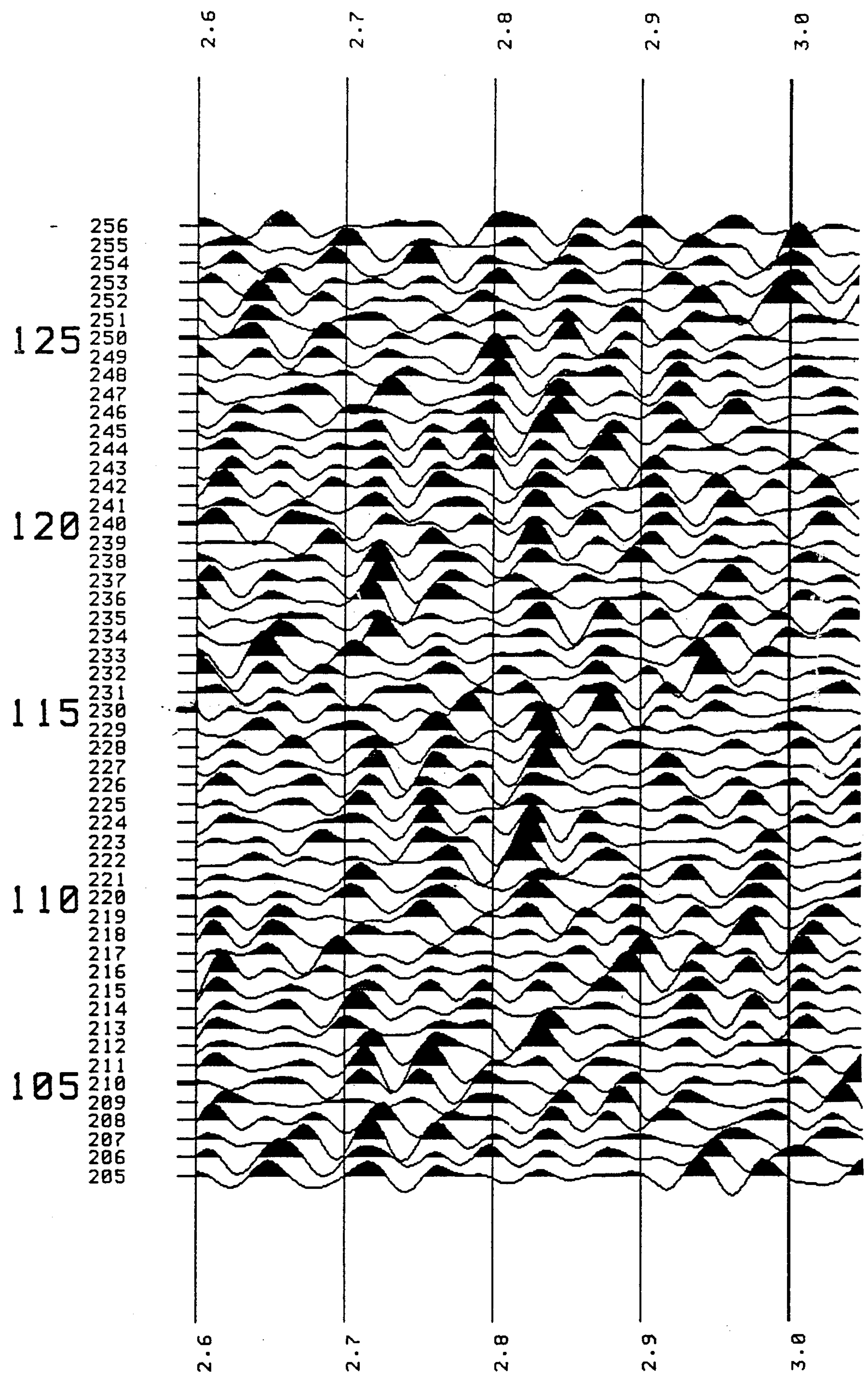

Figure 9. Portion of Mobile Line 3 seismic section which is modeled.

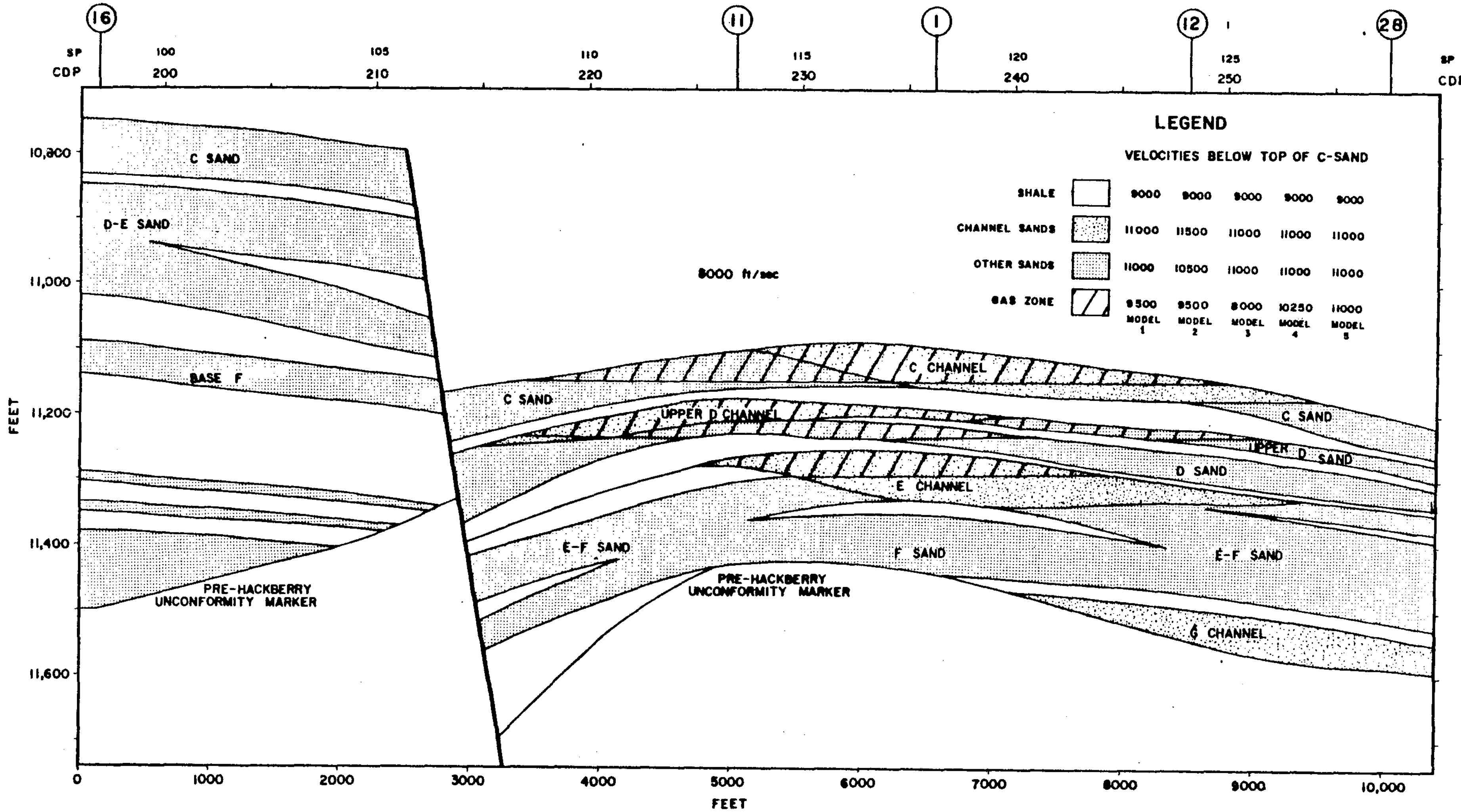

Figure 10. Model of the Hackberry Sands along a cross section following Seismic Line 3.

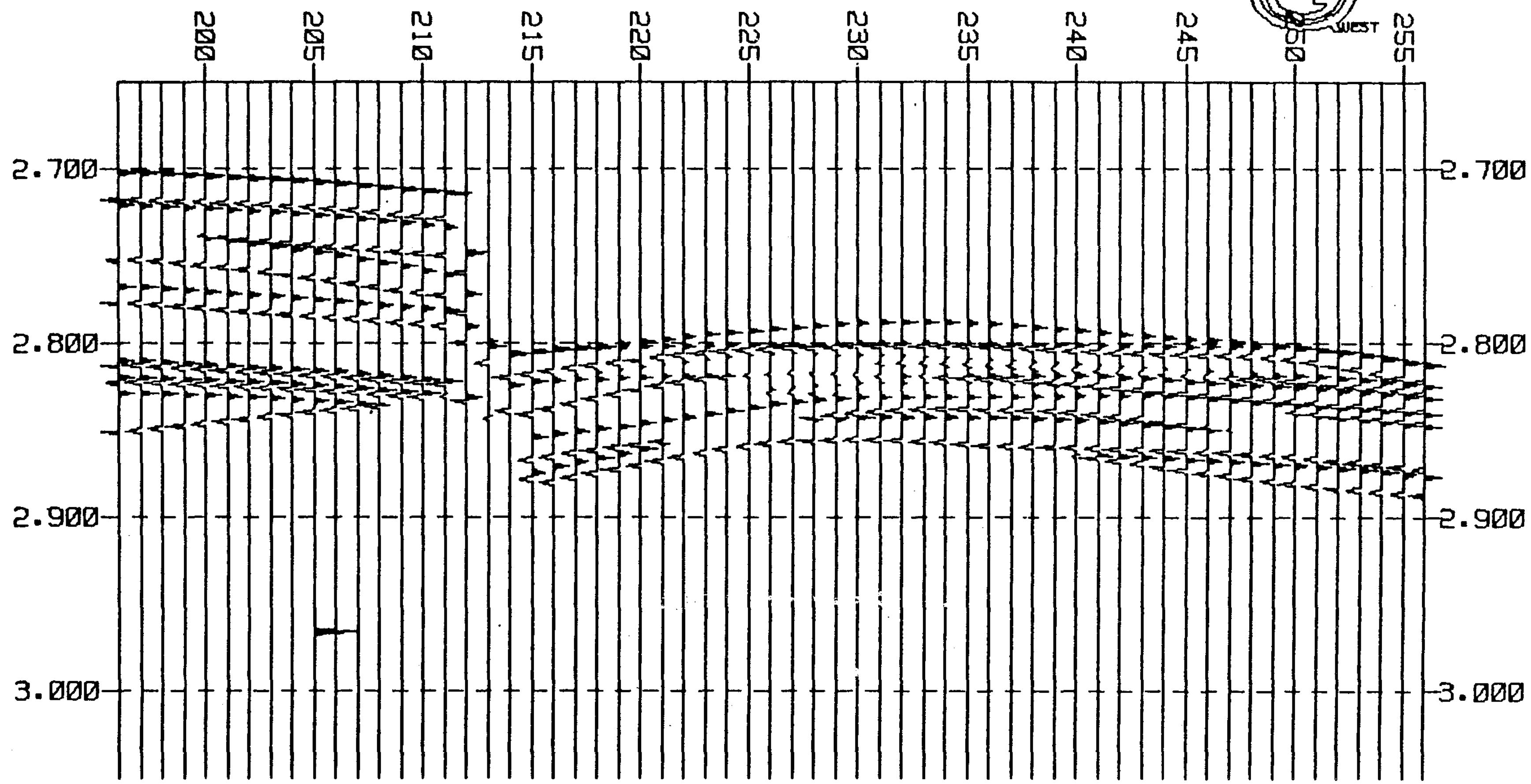

Figure 11a. Spike synthetic seismic section derived from Figure 10.(Model 1)

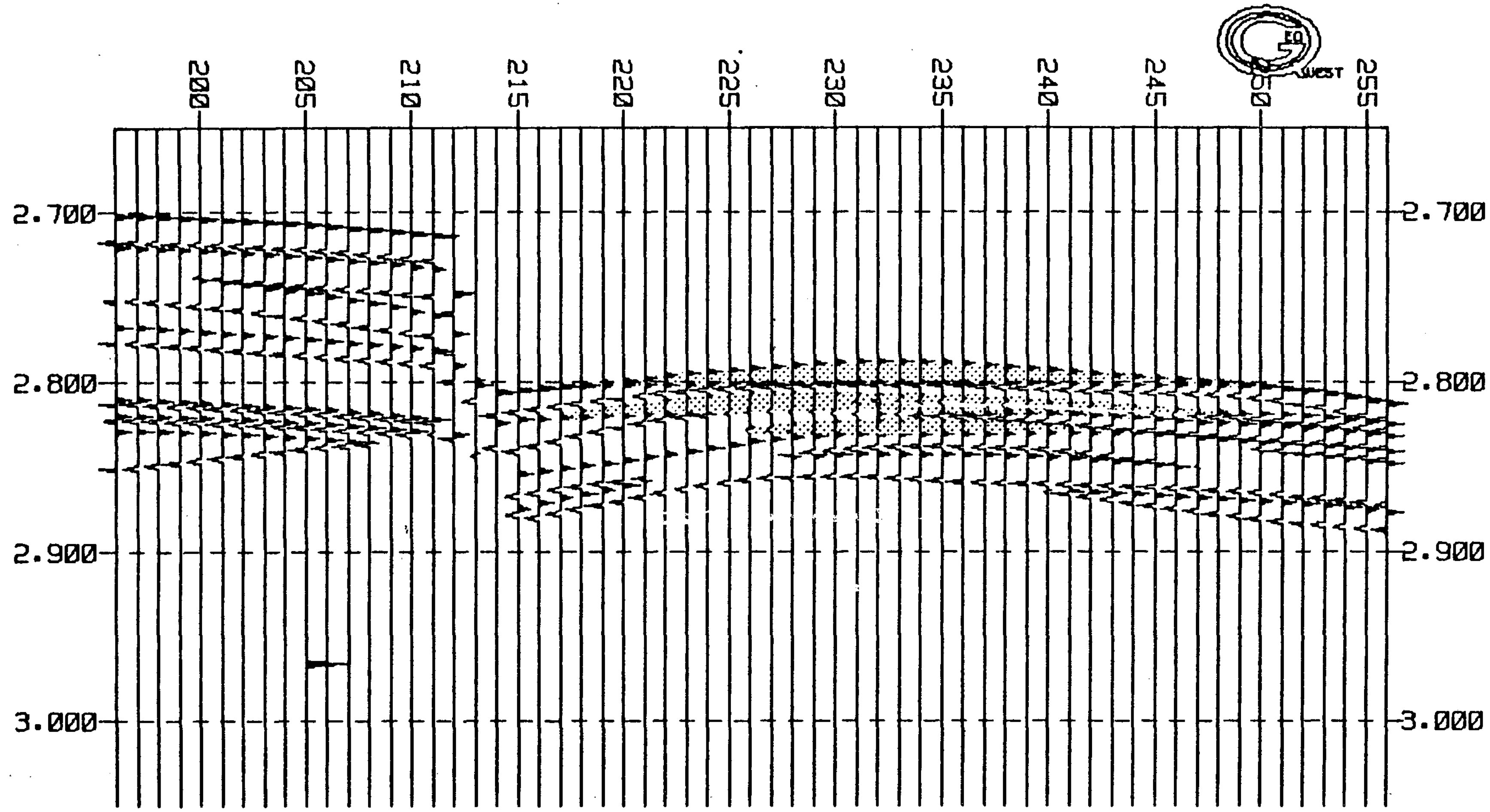

Figure 11B. Spike synthetic seismic section with gas sands shaded, (Model 1).

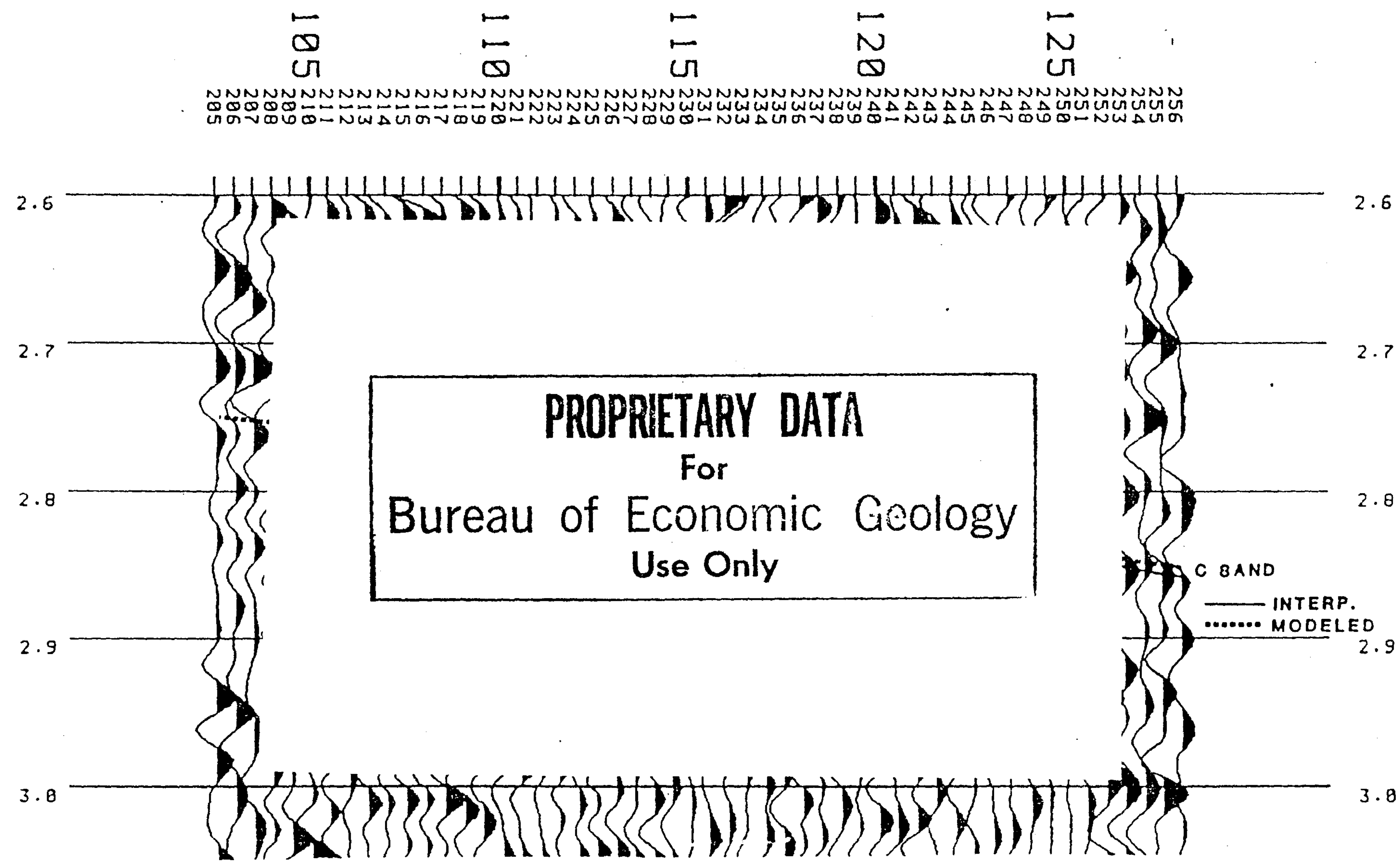

Figure 12. Line 3 showing interpreted and modeled C-Sand top.

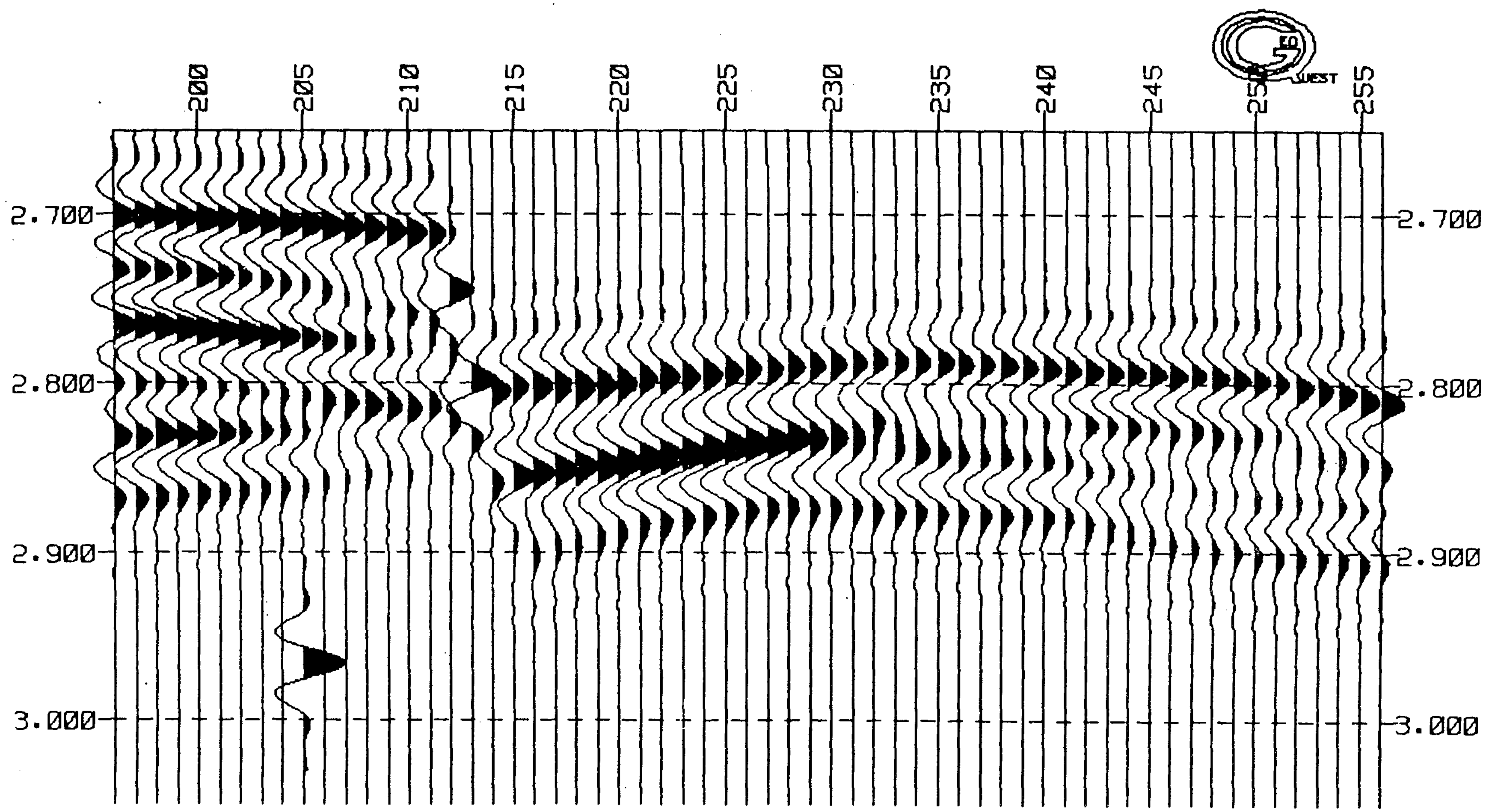

Figure 13. Synthetic seismic section with wavelet bandpass= 15-35 Hz.(Model 1)

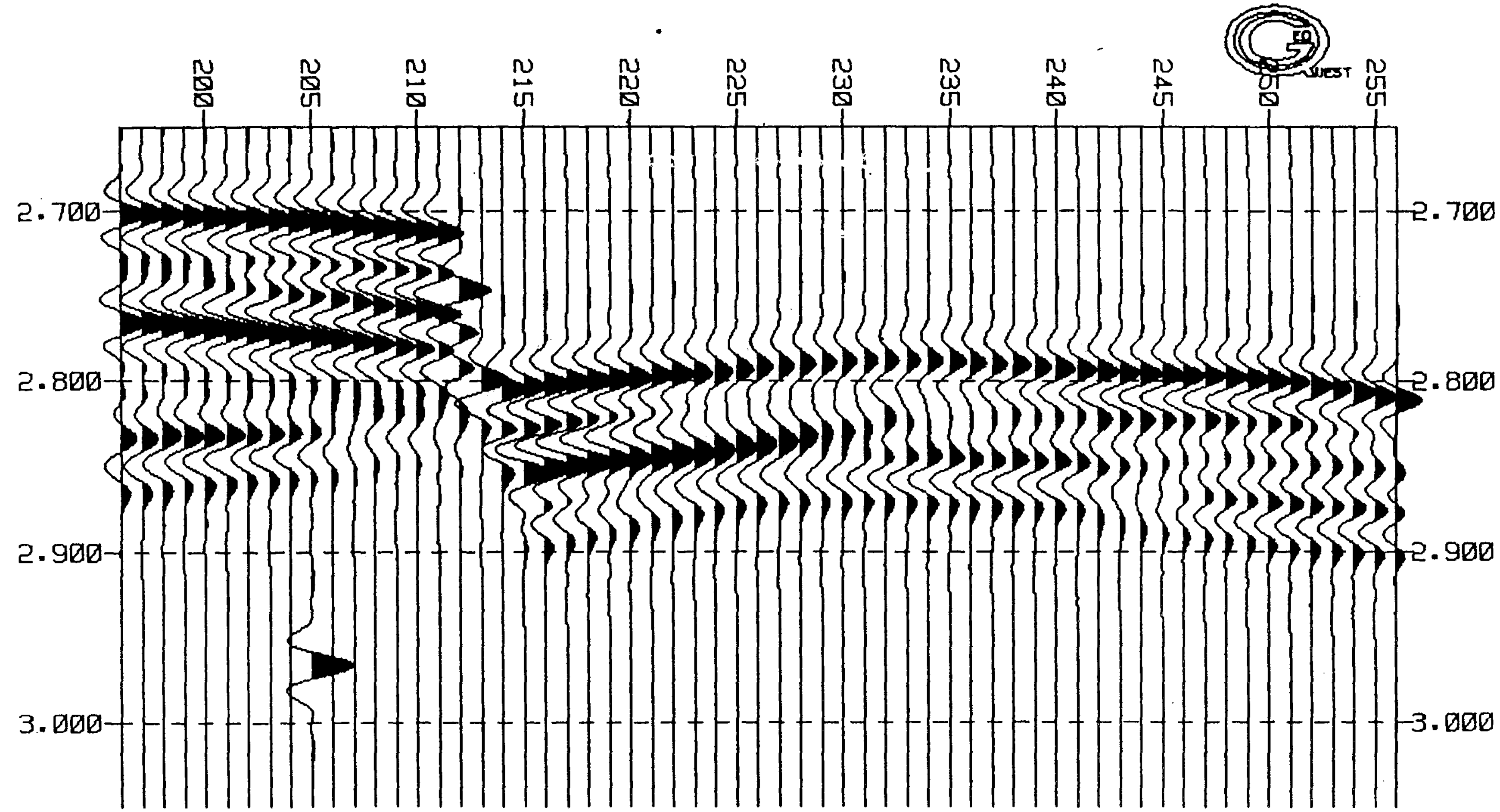

Figure 14. Synthetic seismic section with wavelet bandpass= 15-45 Hz.(Model 1)

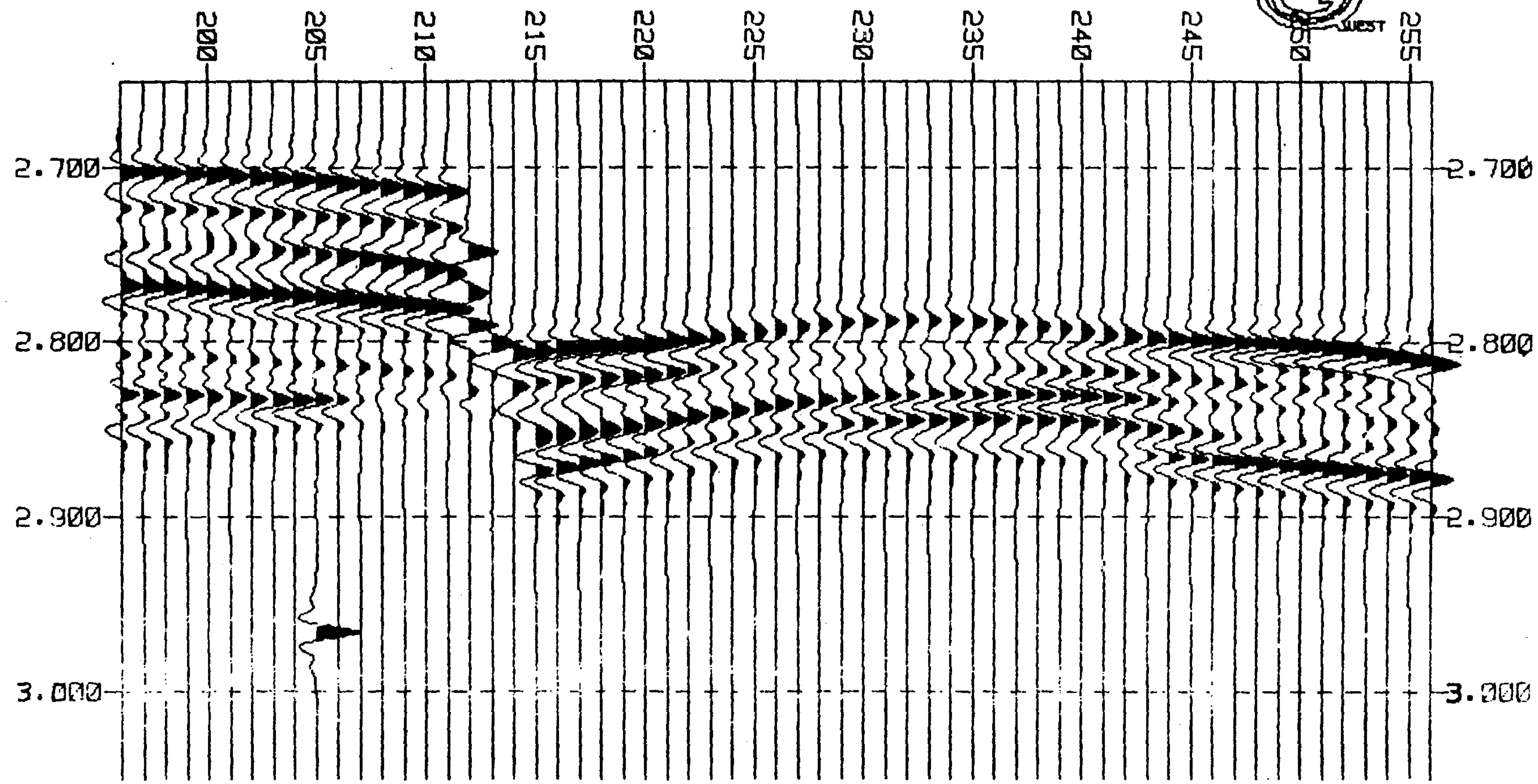

Figure 16. Synthetic seismic section with wavelet bandpass= 15-85 Hz.(Model 1)

GEOQUEST INTERNATIONAL, INC.

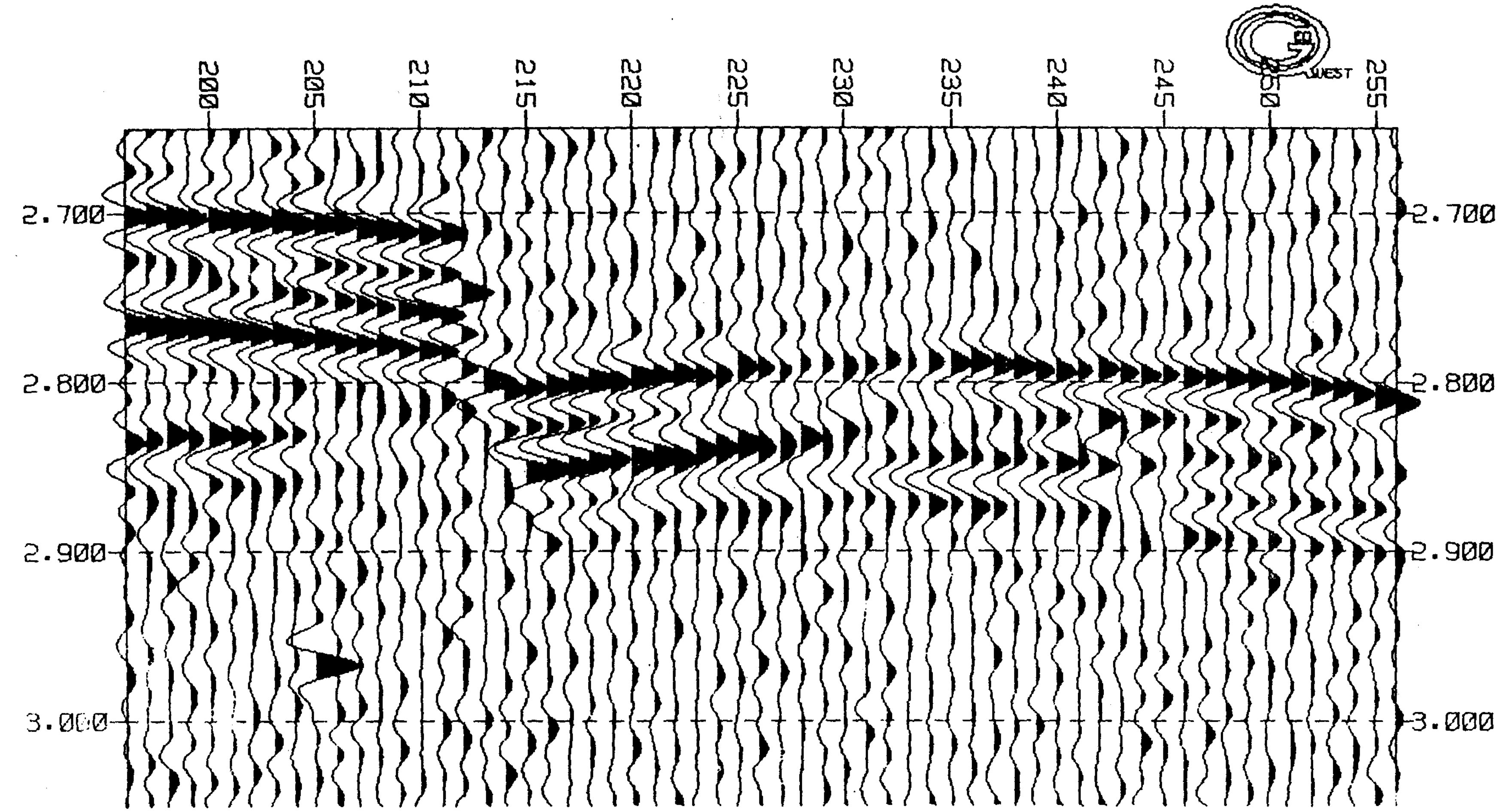

Figure 17. Synthetic seismic section with signal-to-noise= 25.1 (Bandpass= 15-45 Hz,Model 1).

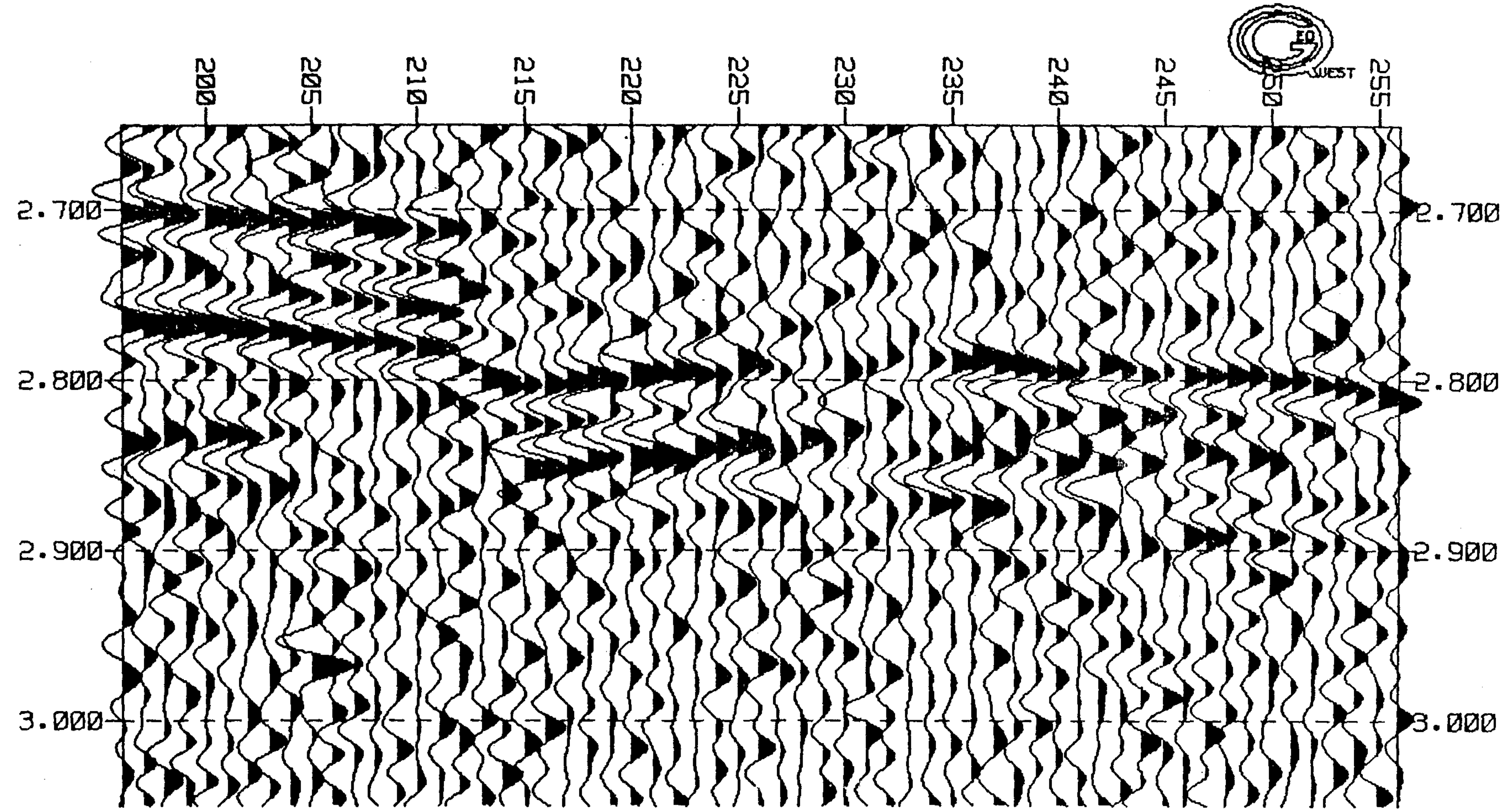

Figure 18. Synthetic seismic section with signal-to-noise= 12.6 (Bandpass= 15-45 Hz. Model 1)

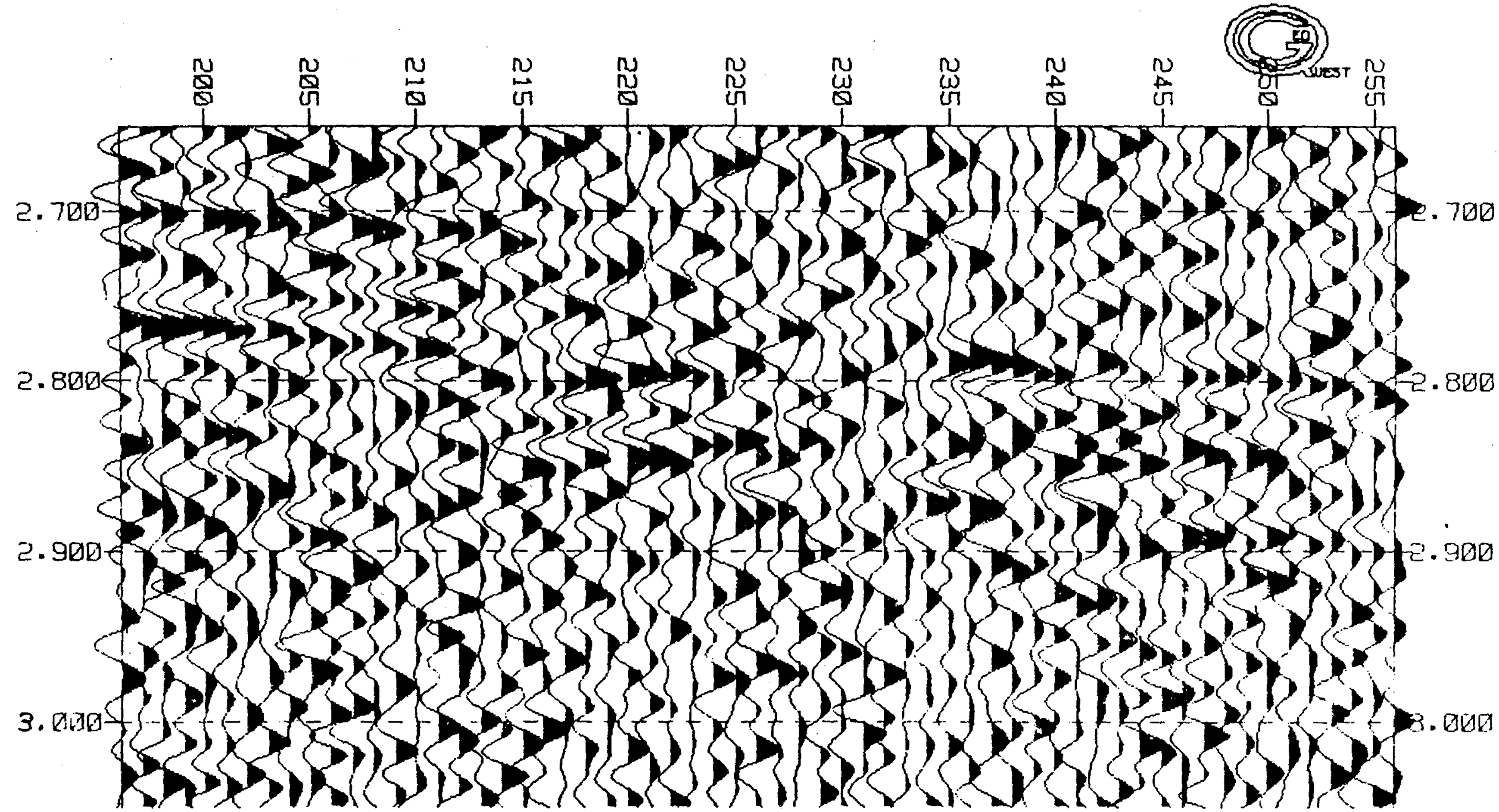

Figure 19. Synthetic seismic section with signal-to-noise= 6.3 (Bandpass= 15-45 Hz, Model 1).

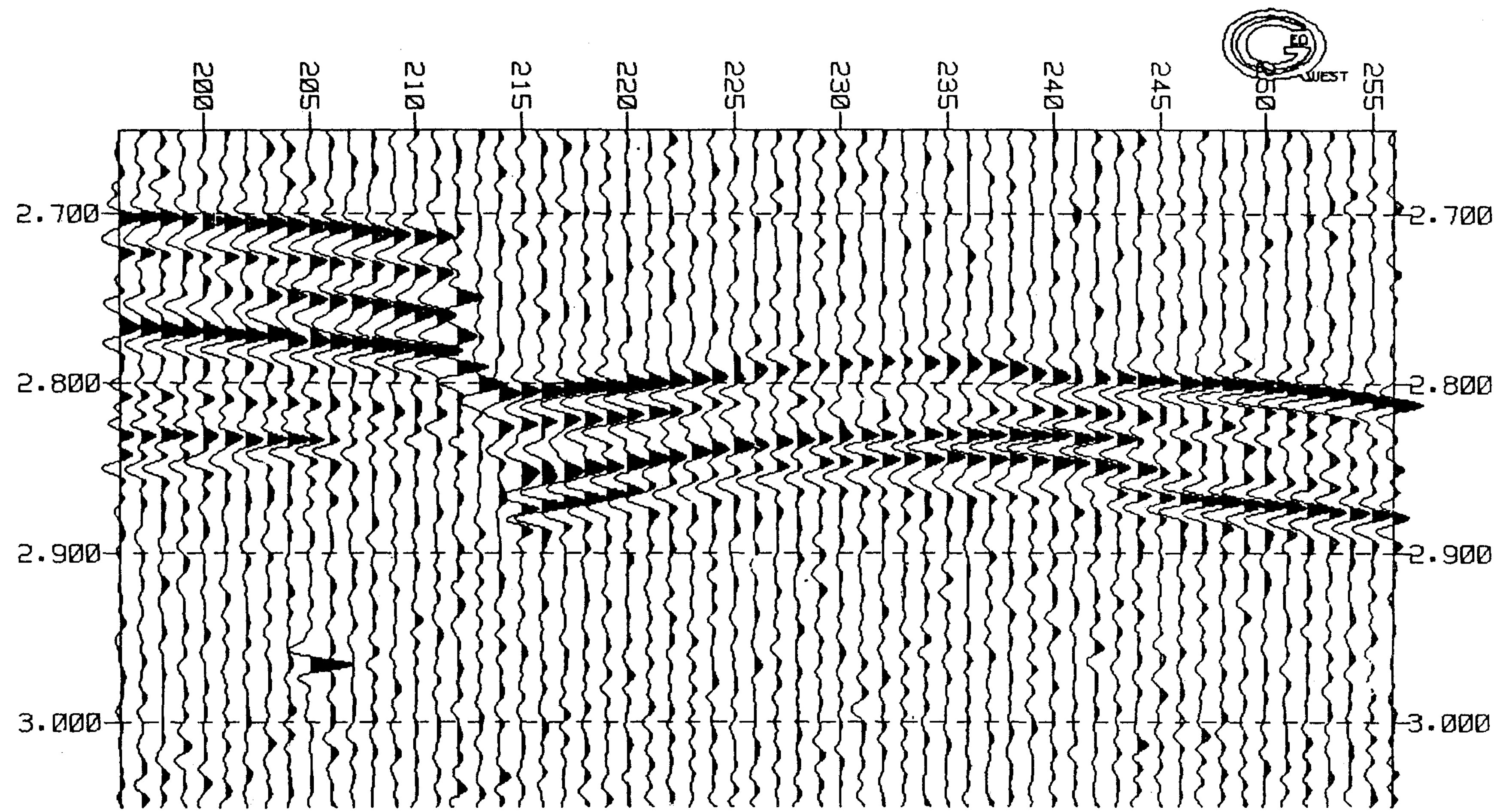

Figure 20. Synthetic seismic section with signal-to-noise= 25.1 (Bandpass= 15-85 Hz, Model 1)

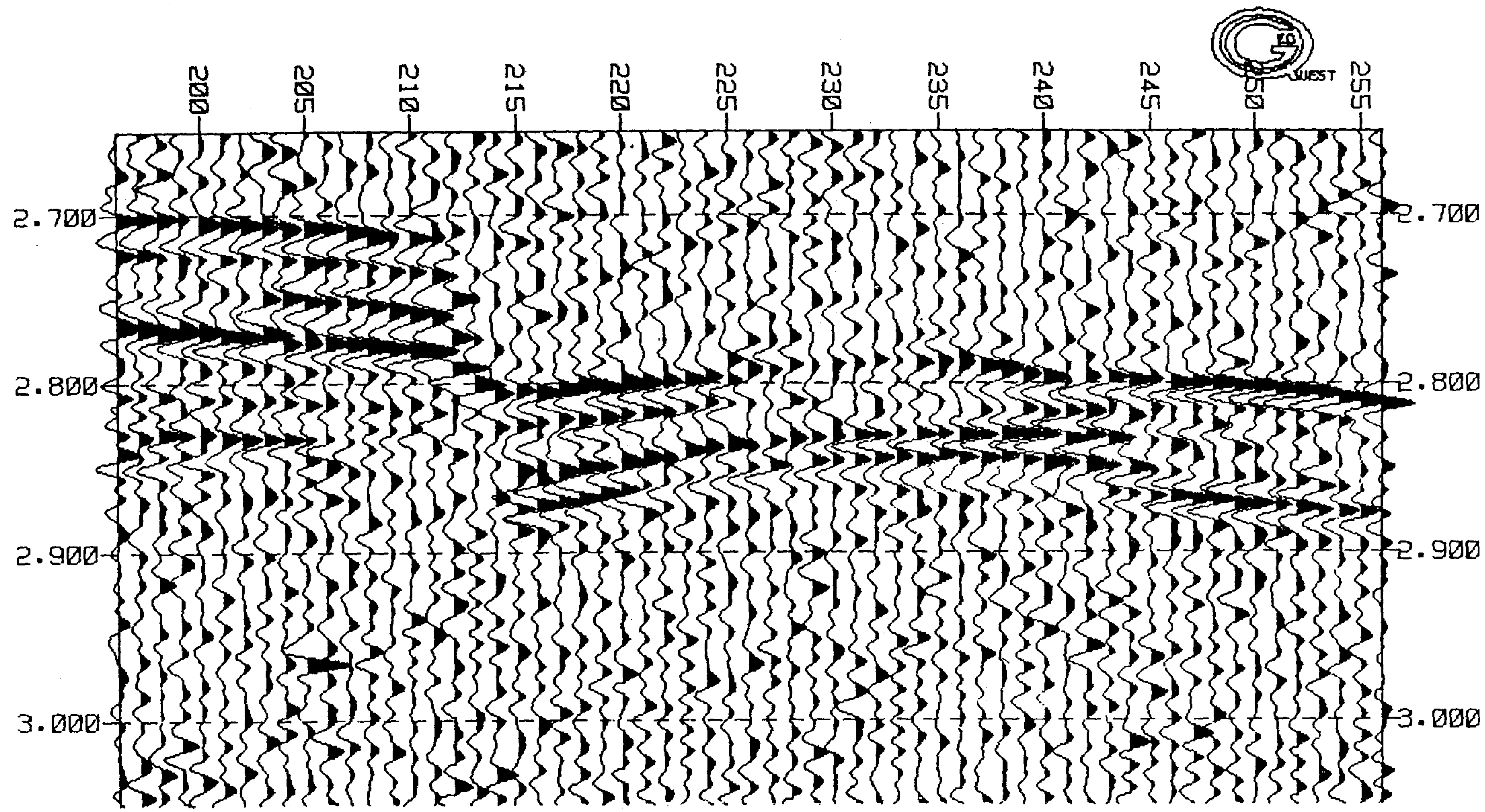

Figure 21. Synthetic seismic section with signal-to-noise= 12.6 (Bandpass= 15-85 Hz,Model 1).

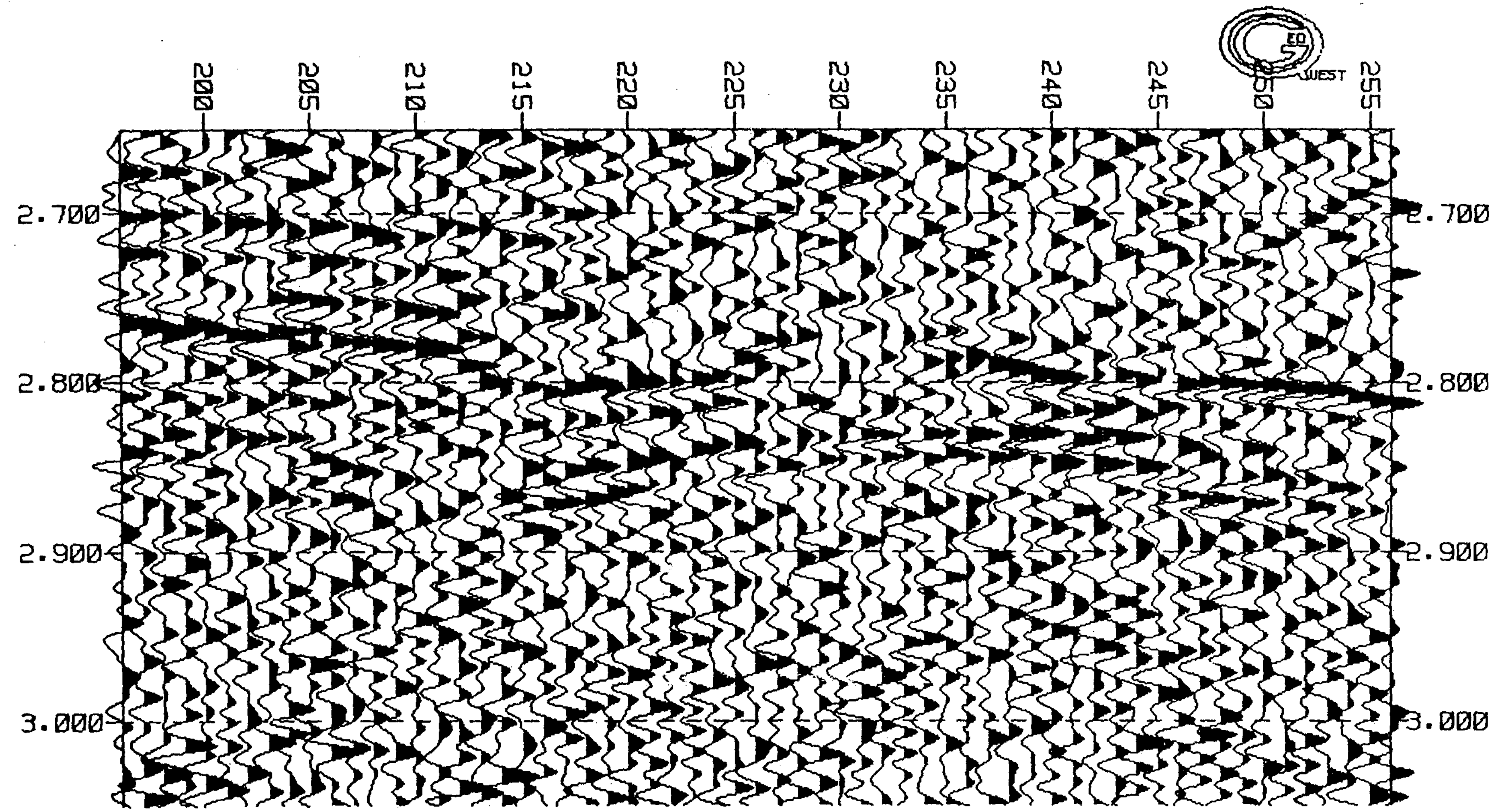

Figure 22. Synthetic seismic section with signal-to-noise= 6.3 (Bandpass= 15-85 Hz, Model 1)

GeoQuest International, Inc.

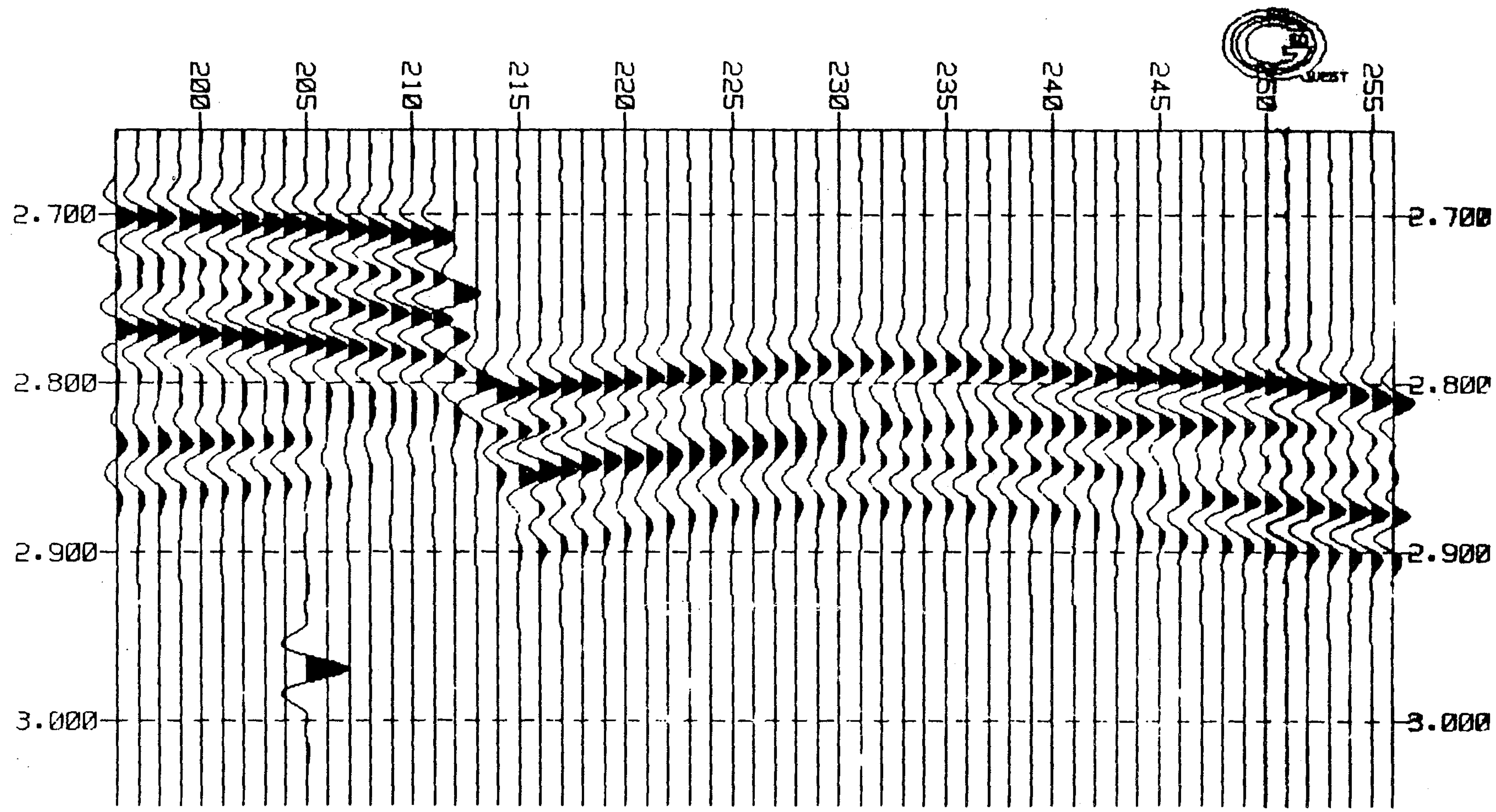

Figure 23. Synthetic seismic section with modified sand velocities. This is model 2 where channel sands have velocities 1000 f/s faster than the other sands. Wavelet bandpass= 15-45. Compare to figure 14.

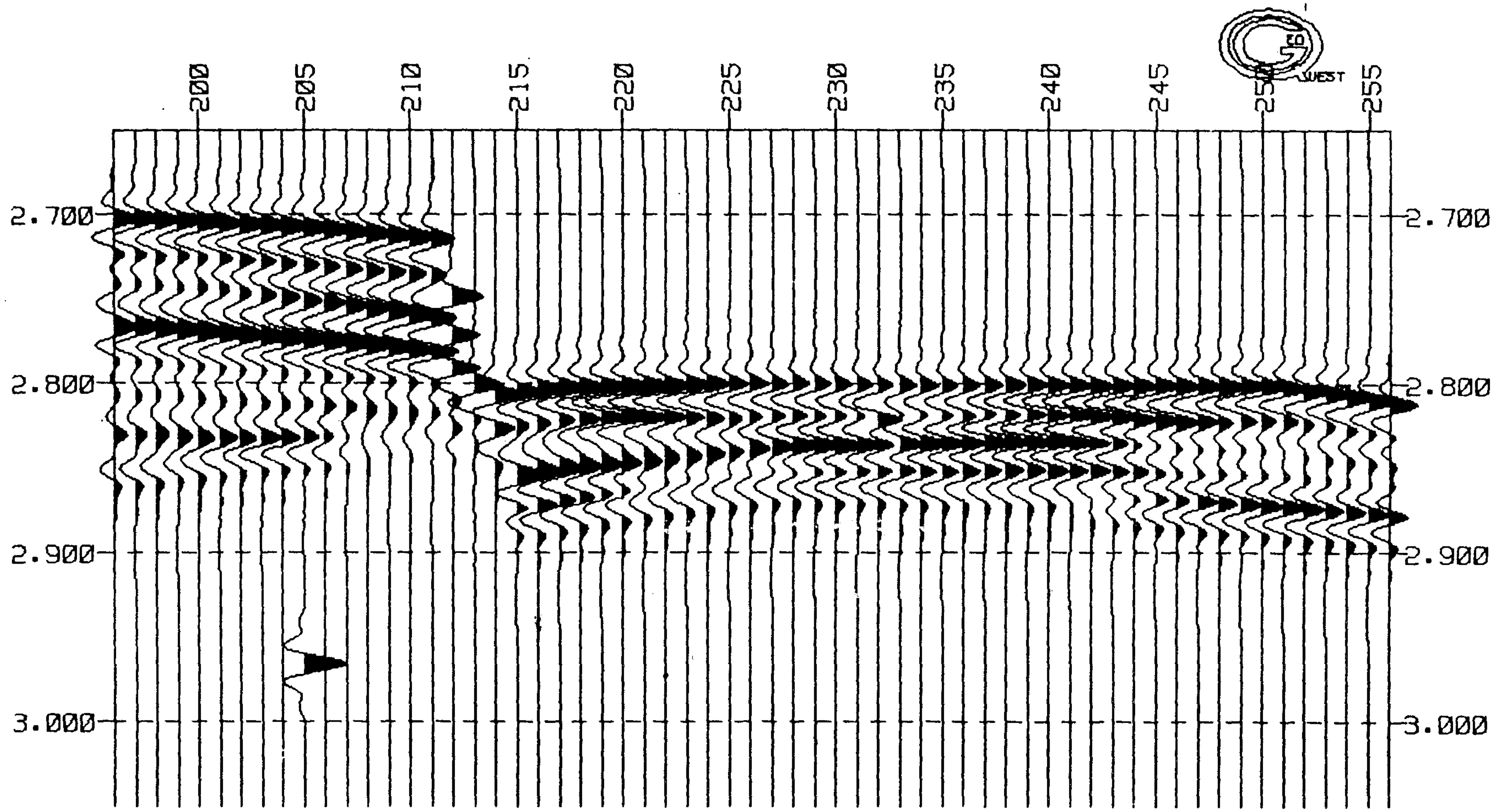

Figure 24. Synthetic seismic section with Low velocity gas (8000 f/s)-- Model 3. (bandpass= 15-65 Hz). Compare to figure 15.

GEOQUEST INTERNATIONAL, INC.

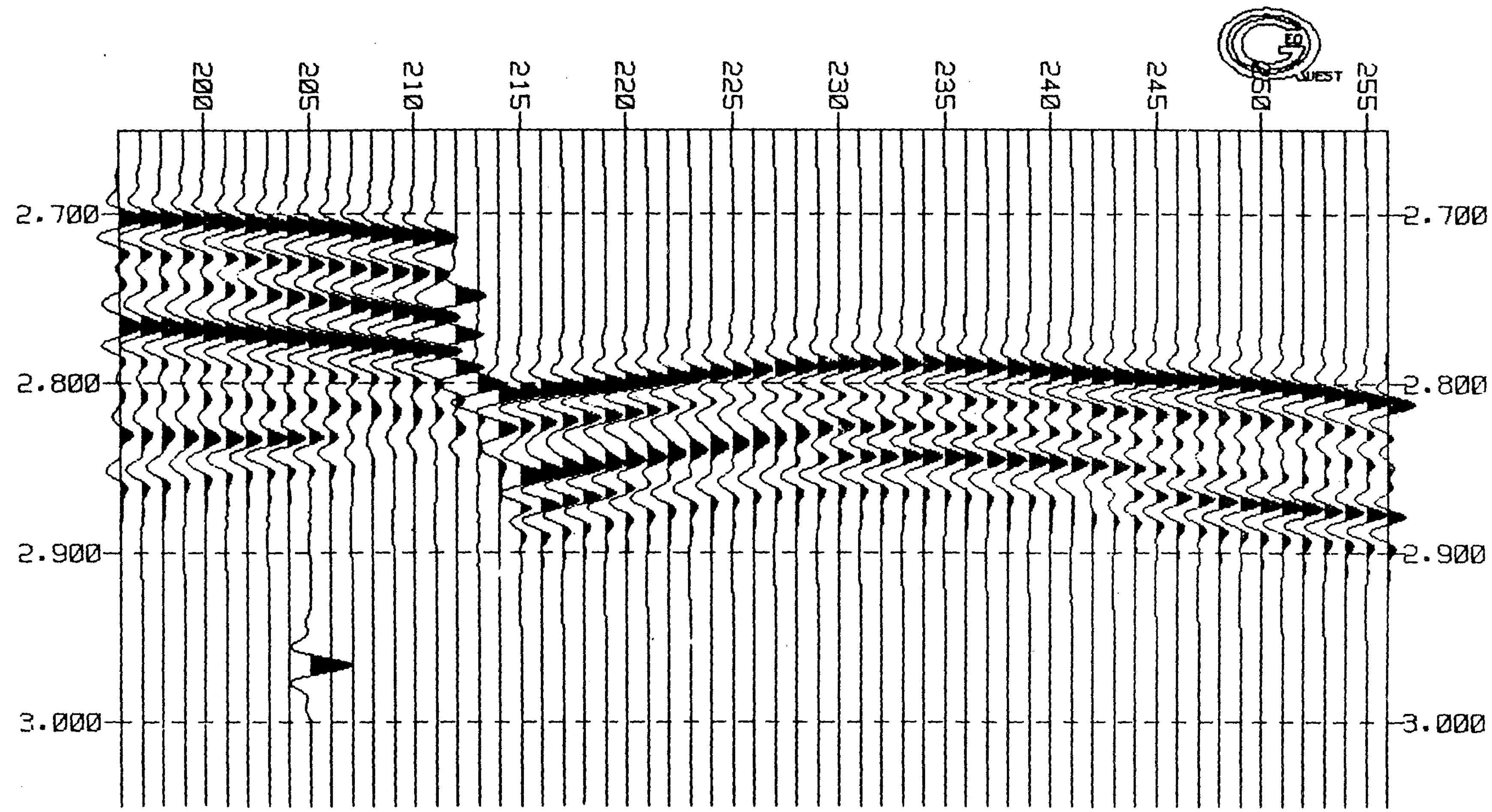

Figure 25. Synthetic seismic section with gas sand velocity= 10250 feet/second--Model 4. (bandpass= 15-65 Hz).

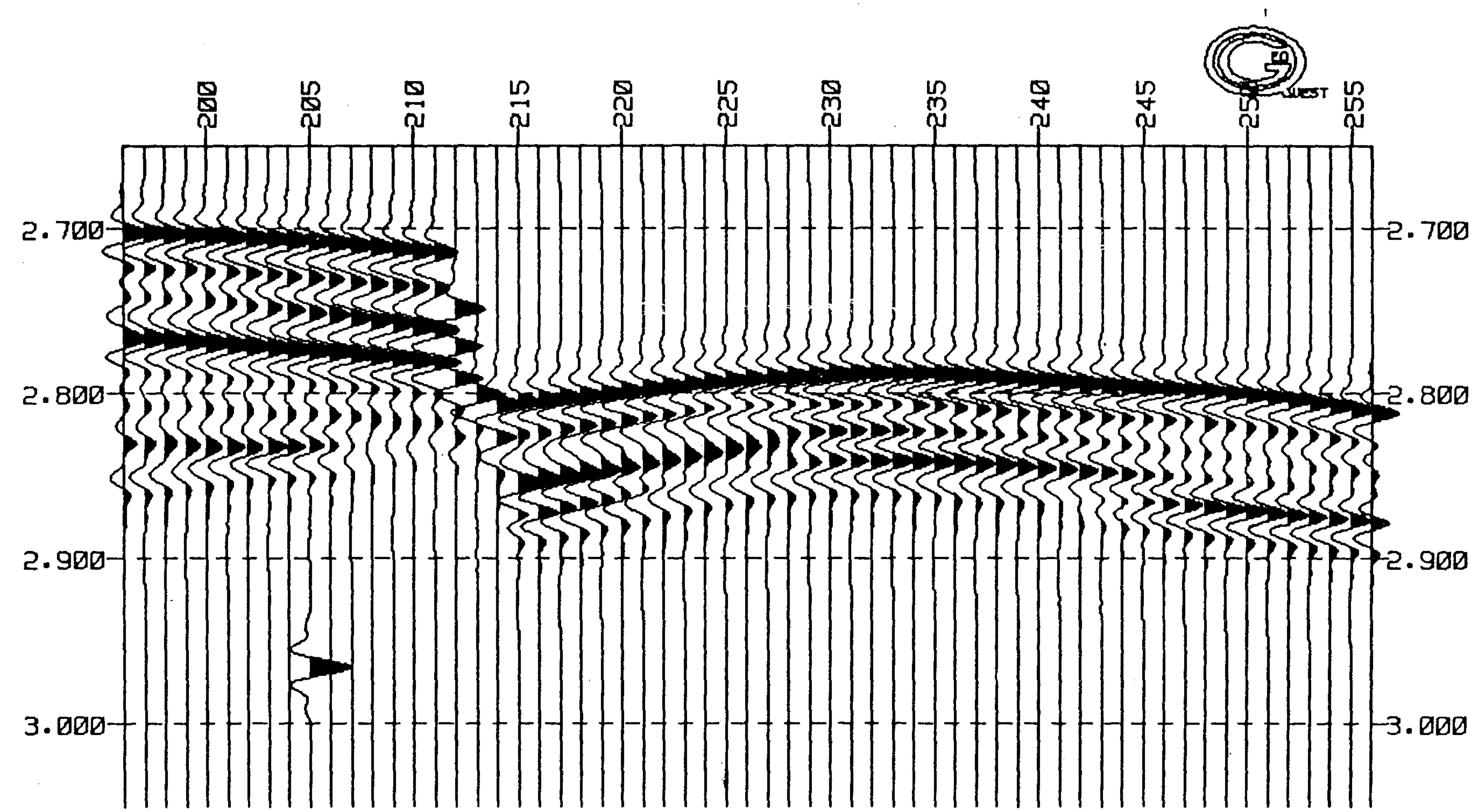

Figure 26. Synthetic seismic section with no gas--Model 5.(bandpass= 15-65 Hz).

APPENDIX A

WAVELET PROCESSING

The primary objective for processing applied to a recorded seismic signal is to more nearly approach the reflectivity series of the earth. The complex time series as recorded contains the following elements:

1. The basic seismic wavelet convolved with the reflectivity series of the earth.

2. Coherent noise which includes multiple events, diffractions, wave spreading, etc.

3. Random noise from instruments and earth filtering.

Careful field gathering combined with common-depth-point stacking procedures can appreciably decrease the contribution by the noise components. Frequency filtering and predictive deconvolution further attenuate these effects. However, traditional processing techniques have had limitations in resolution due to the constructive and destructive interference which results from the complex components and appreciable time length of the "basic wavelet". The complex shape of the basic wavelet is derived from:

1. Source signature.
2. Source ghost.
3. Receiver ghost.
4. Instrument phase distortion.
5. Cable and geophone phase distortion.

Traditionally, deconvolution has been used as the processing procedure to shorten the wavelet and thus decrease the complexity of the seismic trace. However, the results of deconvolution are unpredictable and variable. Some of the factors which affect the effectiveness of deconvolution are:

1. Spiking deconvolution uses the minimum-phase assumption in its operator derivations. Thus, mixed-phase or zero-phase data does not respond well.

2. Deconvolution designs its operator from the autocorrelation of a data window in each trace. Variable noise content from trace-to-trace dictates that the effectiveness of deconvolution varies as does the noise content.

3. Deconvolution does not remove the ambiguity associated with polarity. In fact, predictive deconvolution can produce an apparent polarity reversal if the prediction distance is changed.

Wavelet processing is a technique whereby the complex basic wavelet is converted to a simple, zero-phase wavelet of short time-domain length, whose amplitude spectrum can be optimized. Conversion to the zero-phase wavelet may be accomplished through a) wavelet extraction and Wiener filtering, and b) Statistical Wavelet Enhancement (SWE) filtering. The following results are achieved by the wavelet conversion:

1. The shortened wavelet reduces the destructive and constructive interference effects in the data. Resolution is increased and lateral character stability is greatly improved.

2. Bandwidth can be broadened without the decrease in signal-to-noise ratio, which often results when only deconvolution is used. This is possible since the spectral shape of the resulting data can be controlled in the operator design.

3. All polarity ambiguity is removed. The zero-phase wavelet in the processed data directly indicates the polarity of the reflecting boundary spike in the earth.

4. Correlation of seismic data to the stratigraphy can be accomplished with a degree of confidence not normally presented on conventionally processed data.

<u>Wiener Filtering</u>

Wiener filtering is an established wavelet shaping technique wherein the complex phase and amplitude spectrum of the basic seismic wavelet are converted to a zero-phase wavelet with a well shaped amplitude spectrum. The filter is designed by the well known Wiener-Levinson algorithm:

(Basic Wavelet)(Operator) = (Desired Wavelet)

Application of this operator to the pre-stack data converts the basic wavelet to the desired, and simplifies and shortens the response of each reflectivity spike. This simplification of the data results in more definitive velocity determination using standard algorithms which results in an improved bandwidth in the final data. Predictive deconvolution is commonly used after stack to reduce short-period multiples and further simplify the data.

SWE™ Filtering (Statistical Wavelet Enhancement)

The Wiener filter approach to wavelet shaping generates an inverting filter, within the band limitation of the spectral shape of the desired wavelet. Notches in the spectrum of the basic wavelet produce operators which are high in power at the notch frequency. Should the notch frequency vary slightly in the data, it is possible to overamplify some frequencies and produce "ringing".

The SWE approach separates the phase and amplitude correction steps. The complex phase spectrum of the basic seismic wavelet is removed before stacking by use of a phase correcting operator. This phase correction involves the generation of an operator which has a flat amplitude spectra over the bandwidth of the signal and a phase function which is the negative of that of the basic wavelet. Convolution with this operator removes the phase lag introduced by the seismic wavelet but leaves the amplitude spectrum unchanged.

The dephased data are then processed through stack using conventional methods. After stack, SWE is used to enhance the signal spectra. The term "Statistical Wavelet Enhancement" refers to a special application of an optimum coherency filtering technique to seismic data. As practiced, it is an after-stack process. The only special pre-stack process is phase correction of the total system phase distortion as determined from the basic seismic wavelet.

After correction for phase distortion and proper stacking of the seismic data, estimates of signal and noise properties are made using a data window and lateral distance selected on the basis of the lithologic section of interest and the data quality. Signal spectral properties are estimated by summing adjacent trace crosscorrelations with timing corrections, as needed. These crosscorrelations are defined to be estimates of the signal components only (the filtered reflectivity series) because they represent laterally correlatable data, and noise is assumed to be random over the same data domain. The resulting summation of the crosscorrelations usually is slightly skewed from perfect symmetry. The amount of skew may be taken as a measure of quality of the signal power spectrum estimated. The odd part, or skew portion, is removed, leaving a symmetrical function which represents the power spectral density of the seismic signal only.

The noise spectral properties are estimated from the sum of the autocorrelation functions measured over the same data domain. These

™GeoQuest International, Inc.

autocorrelations include signal as well as noise, since both are correlatable over a time window on a single data trace.

The optimum coherency filter according to Bendat[1] (1958) is defined as the operator:

$$H(\omega) = \frac{S_{*}(\omega)}{S^2(\omega) + N^2(\omega)}$$

The denominator is obtained directly from the autocorrelation sum. The numerator is obtained by factoring the crosscorrelation, after modification to symmetry, thus reducing from $S^2(\omega)$ to $S^*(\omega)$. The asterisk denotes the conjugate function (negative-phase or imaginary part). This conjugate function is meaningful only after a phase function has been assigned to the factored crosscorrelation sum. Since the data are made zero-phase before stacking, a zero-phase assumption is used.

Figure 1 demonstrates the generation of a Wiener filter. Figures 2 and 3 demonstrate the generation of a phase correcting and SWE filter.

[1]Bendat, Julius S. and Piersol, Allan G., Measurements and analysis of random data: John Wily and Sons, Inc., New York, N.Y.

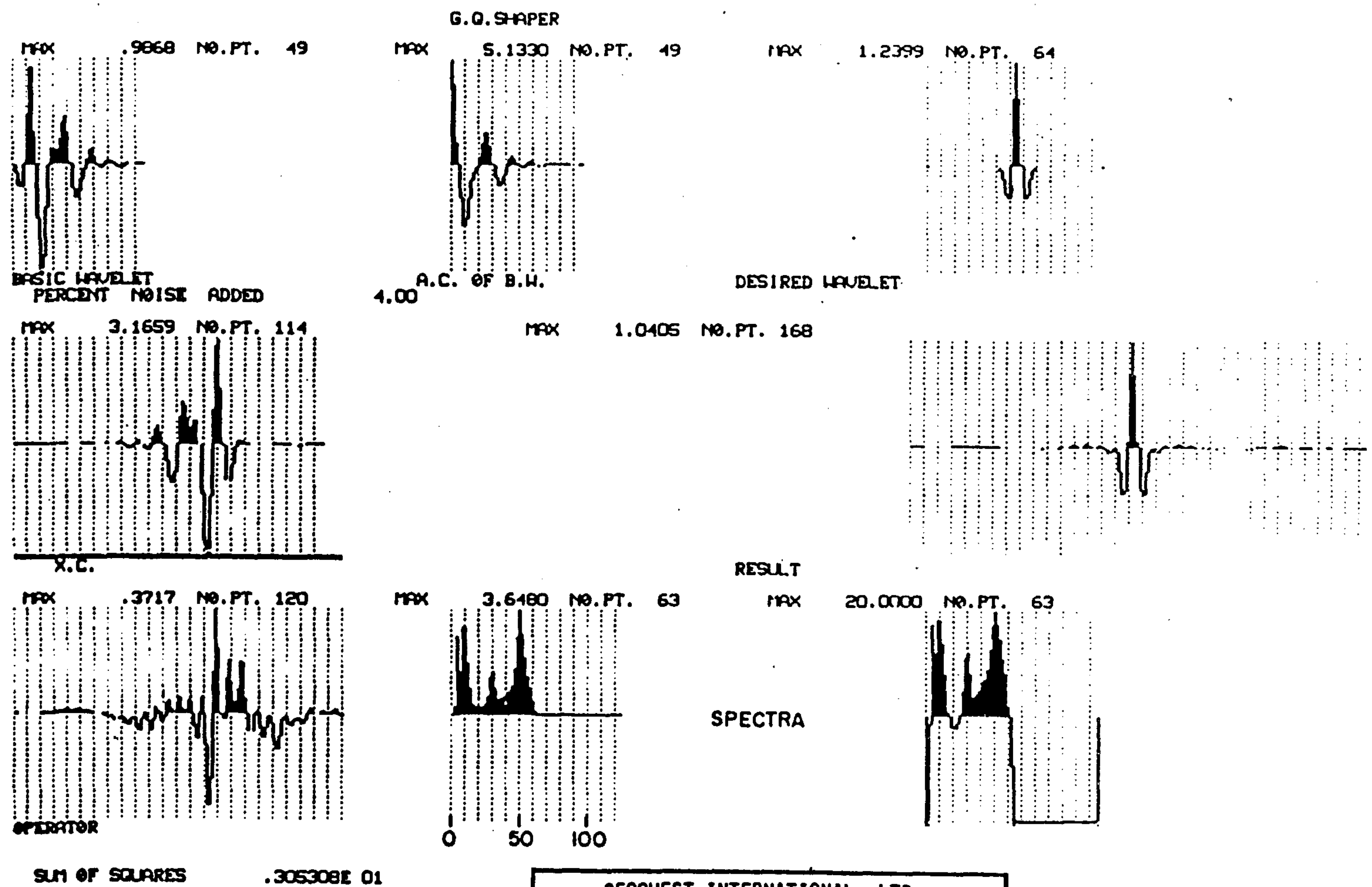

GEOQUEST INTERNATIONAL, LTD.

FIG. 1-A

COMPUTATION OF A WIENER FILTER OPERATOR

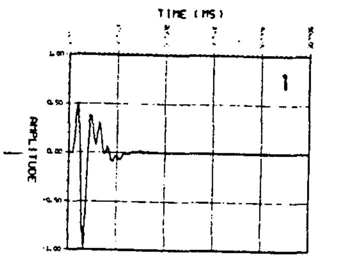

INSTRUMENT IMPULSE RESPONSE

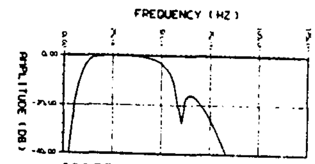

SPECTRUM OF 1

PHASE OF 1 IS NEGATED AND SPECTUM IS MODIFIED

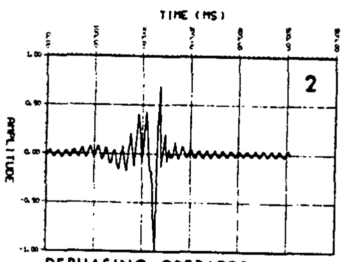

DEPHASING OPERATOR

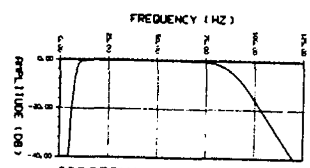

SPECTRUM OF 2

RESULT OF IMPULSE RESPONSE CONVOLVED WITH DEPHASING OPERATOR

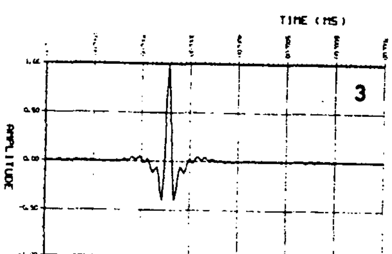

RESULT OF 1 CONVOLVED WITH 3

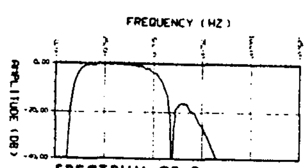

SPECTRUM OF 3

FIG.2-A GENERATION OF A DEPHASING OPERATOR

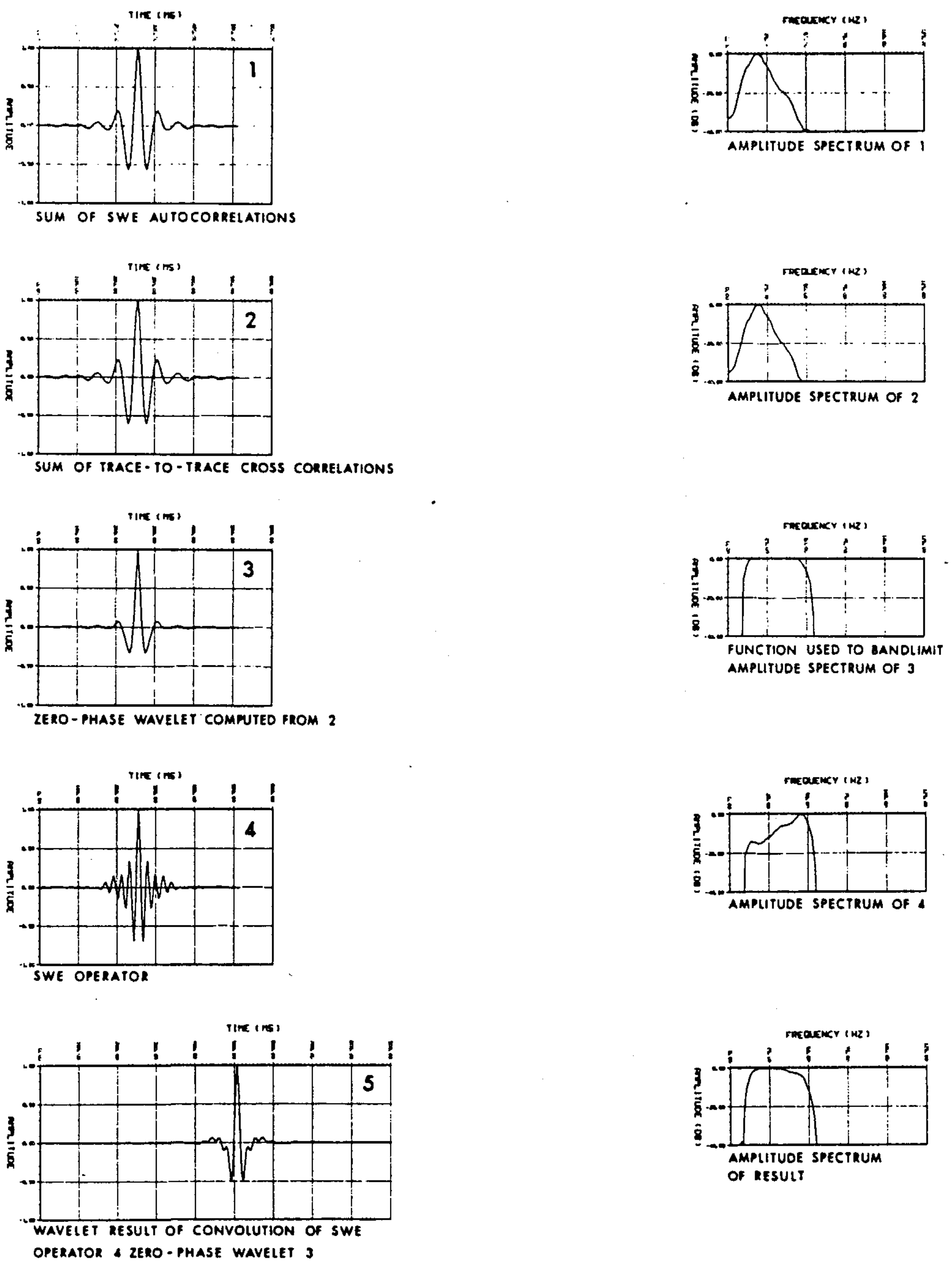

FIG. 3-A GENERATION OF A SWE OPERATOR

APPENDIX B

SWE

STATISTICAL WAVELET ENHANCEMENT

A method of processing seismic data which acknowledges properties of signal (the basic wavelet) and noise, and attempts to optimize the design of special filters (e.g. wavelet processing) has been developed by GeoQuest. This method is called SWE (Statistical Wavelet Enhancement) and involves special filtering both before and after stacking. The after stack filter operator design follows the coherency concepts set out in Bendat[1] as adapted to the seismic filtering and deconvolution problem. Two key measurements are made for this part of the SWE procedures: 1) the stack of autocorrelation functions, and 2) the stack of crosscorrelation functions. These are first discussed mathematically for establishing a background to describe the SWE method.

1. Averaging of Autocorrelation Functions

This mathematical model of a seismic trace $x_i(t)$ is usually expressed as:

$$x_i(t) = w(t) \star e_i\ (t) + n_i\ (t)$$

with

$$E\ \{e_i(t)e_i(t+\tau)\} = \delta(\tau)$$

$$E\ \{e_i(t)n_i(t+\tau)\} = 0$$

The autocorrelation function of $x_i(t)$ can be written as:

$$R_{x_i,\ x_i}(t) = \int x_i(\tau)x_i(\tau+t)d\tau$$

$$= \quad R_{w,w}(t) \star R_{e_i,e_i}\ (t) + R_{n_i,n_i}(t) + \varepsilon_i(t)$$

[1]Bendat, Julius S. and Piersol, Allan G., Measurements and Analysis of Random Data, John Wiley and Sons, Inc., New York, New York, 1958.

Averaging yields:

$$R_i(t) = \frac{1}{2N+1} \sum_{k=i-N}^{i+N} R_{x_k,x_k}(t)$$

$$= \quad R_{w,w}(t) * \left[\frac{1}{2N+1} \sum_{k=i-N}^{i+N} R_{e_k,e_k}(t) \right] +$$

$$\frac{1}{2N+1} \sum_{k=i-N}^{i+N} R_{n_k,n_k}(t) + \frac{1}{2N+1} \sum_{k=i-N}^{i+N} \varepsilon_i(t)$$

$$\approx R_{w,w}(t) + R_{n,n}(t)$$

Or, in terms of the Fourier spectrum,

$$R_i(f) \approx |W(f)|^2 + |N(f)|^2.$$

This expression says that an estimate of the "signal + noise" spectrum can be obtained by averaging autocorrelation functions. The weakest assumption inherent in deriving the expression is:

$$R_{e,e}(t) = \frac{1}{2N+1} \sum_{k=i-N}^{i+N} R_{e_k,e_k}(t) = \delta(t)$$

This is the equivalent to assuming an uncorrelated reflectivity plus noise spike series.

2. Averaging of Crosscorrelation Functions

The mathematical model of two neighboring seismic traces may be expressed as:

$$x_i(t) = w(t) * e_i(t) + n_i(t)$$

$$x_{i+1}(t) = w(t) * e_i(t+\Delta t_i) + n_{i+1}(t)$$

with

$$E\,\{e_i(t)e_i(t+\tau)\} = \delta(\tau)$$

$$E\,\{e_i(t)n_j(t+\tau)\} = 0$$

$$E\,\{n_i(t)n_j(t+\tau)\} = 0$$

The crosscorrelation function of $x_i(t)$ and $x_{i+1}(t)$ can be written as:

$$R_{x_i,x_i+1}(t) = \int x_i(\tau)x_{i+1}(\tau+t)d\tau$$

$$= \quad R_{w,w}(t) * R_{e_i,e_i}(t+\Delta t_i) + \varepsilon_i(t)$$

Averaging yields:

$$C_i(t) = \frac{1}{2N+1} \sum_{k=i-N}^{i+N} R_{x_k,x_{k+1}} \;(t-\Delta t_k)$$

$$= \quad R_{w,w}(t) * \left[\frac{1}{2N+1} \sum_{k=i-N}^{i+N} R_{e_k,e_k}(t) \right]$$

$$+ \frac{1}{2N+1} \sum_{k=i-N}^{i+N} \varepsilon_k(t-\Delta t_k)$$

$$\approx R_{w,w}(t)$$

or, in terms of the Fourier spectrum,

$$C_i(f) \approx |W(f)|^2$$

This expression says that an estimate of the "signal" spectrum can be obtained by averaging crosscorrelation functions. This weakest assumption inherent in deriving this expression is:

$$R_{e,e}(t) = \frac{1}{2N+1} \sum_{k=i-N}^{i+N} R_{e_k,e_k}(t) = \delta(t)$$

Note that if well data is available, then $R_{e,e}(t)$ can be estimated and used for a better signal spectrum estimate:

$$|W(f)|^2 \approx C_i(f)/R_{e,e}(f)$$

The functions $|W(f)|^2$ and $|W(f)|^2 + |N(f)|^2$ are used in establishing special deconvolution operators during the processing of seismic data. The processing procedure makes use of the seismic basic wavelet if it is known, and deduces it under one or more phase assumptions if it is not specifically known. The entire procedure called SWE is outlined as follows:

1. Basic Seismic Wavelet is Known, $w_0(t)$:

a) Pre-Stack Deconvolution

Apply phase-spectrum deconvolution for the outgoing wavelet:

$$F_1(f) = e^{-j\phi_0(f)}$$

$\phi_0(f)$ being the phase spectrum of wavelet $w_0(t)$.

In some instances, only the recording system phase spectrum is accounted for since this can always be documented. Phase spectrum deconvolution decreases the length of the seismic wavelet and improves the peak signal-to-noise ratio. The phase-spectrum deconvolution filter should be derived via the frequency domain, as stabilized least-squares inverse procedures will always give rise to phase distortions.

b) Post-Stack Deconvolution

i. Estimate total spectrum, $|W(f)|^2 + |N(f)|^2$ by averaging autocorrelation functions.

ii. Estimate wavelet amplitude spectrum, $|W(f)|$ by averaging crosscorrelation functions.

iiia. Compute absorption amplitude spectrum,

$$A\, e^{-\alpha f t_0} \leftrightarrow \frac{|W(f)|}{|W_0(f)|}$$

by a least-squares fit in the logarithmic domain.

iiib. If α has physical meaning, compute the minimum-phase spectrum, $\alpha(f)$, that is related to $e^{\alpha f t_0}$.

iv. Compute post-stack decon filter:

$$F_2(f) = \frac{|W(f)|e^{-j\alpha(f)}}{|W(f)|^2 + |N(f)|^2}$$

If the least-squares fit in, step iiia. is not satisfactory; $\alpha(f)$ should be taken as zero and $F_2(f)$ will represent a zero-phase deconvolution filter.

2. Basic Seismic Wavelet is Not Known:

a) Pre-Stack Deconvolution

ia. Estimate wavelet amplitude spectrum, $|W(f)|$ by averaging crosscorrelation functions in common offset domains.

ib. Compute minimum-phase spectrum, $\phi(f)$ that is related to $|W(f)|$.

ii. Apply phase-spectrum deconvolution for the estimated pre-stack minimum-phase seismic wavelet:

$$F_1(f) = e^{-j\phi(f)}$$

Note that this procedure could be done for each offset. A more practical procedure would be to combine a number of related offsets (e.g. divide total data set in 4 distance ranges).

b) Post-Stack Deconvolution

i. Estimate total spectrum, $|W(f)|^2 + |N(f)|^2$ by averaging autocorrelation functions.

ii. Estimate wavelet amplitude spectrum, $|W(f)|$ by averaging crosscorrelation functions.

iii. Compute zero-phase post-stack decon filter:

$$F_2(f) = \frac{|W(f)|}{|W(f)|^2 + |N(f)|^2} D(f)$$

D(f) represents a zero-phase band-pass filter with some desirable bandwidth. This extra bandlimitation might be necessary if the seismic wavelet is not "completely" minimum phase.

3. Outgoing Wavelet is Not Known (Post-Stack Decon Only):

Pre-stack deconvolution is expensive. Moreover, with noisy data, an accurate estimate of a pre-stack minimum-phase wavelet is difficult to obtain. Therefore, one may expect that in many practical situations (land data) "post-stack deconvolution only" is an attractive alternative:

ia. Estimate wavelet amplitude spectrum, $|W(f)|$ by averaging crosscorrelation functions.

ib. Compute minimum-phase spectrum, $\phi(f)$, that is related to $|W(f)|$.

ii. Estimate total spectrum, $|W(f)|^2 + |N(f)|^2$ by averaging autocorrelation functions.

iii. Compute post-stack decon filter:

$$F(f) = \frac{|W(f)|e^{-j\phi(f)}}{|W(f)|^2 + |N(f)|^2} D(f)$$

In the situation that the outgoing wavelet is far from minimum phase and is <u>not</u> known, it is important to have the option available of applying zero-phase deconvolution by:

$$F(f) = |W(f)| \,/\, \left[\, |W(f)|^2 + |N(f)|^2 \right]$$

If conventional predictive deconvolution has preceded the application of the SWE process, other phase assumptions are appropriate. Specifically, a second zero-crossing predictive deconvolution would suggest a $\pi/2$ constant phase assumption for the SWE process.

APPENDIX C

SYN-LOG

Conversion of Seismic Sections Into SYN-LOG Sections

Conversion to SYN-LOG involves converting reflectivity to relative acoustic impedance. After proper wavelet processing, the seismic trace represents a bandlimited reflectivity series and may be represented by

$$y(t) = w_0(t) * r(t) + n_0(t) \quad , \qquad \text{(III-1)}$$

$w_0(t)$ being a minimum-length zero phase wavelet and $n_0(t)$ having minimum power such that $y(t)$ represents an optimum least-squares estimate of reflectivity $r(t)$.

Since the seismic wavelet $w_0(t)$ is band limited we may replace in (III-1) reflectivity $r(t)$ by a discrete function:

$$r(t) = \Delta t \sum_n r(n\Delta t)\delta(t - n\ t)$$

$$= \sum_n r_n \delta(t - n\Delta t) \quad . \qquad \text{(III-2a)}$$

Equation (III-2a) describes a layered earth with acoustic discontinuities being defined by reflection coefficients r_n. Using some fundamental properties of acoustic wave theory, it can be easily shown that

$$r_n = \frac{a_{n+1} - a_n}{a_{n+1} + a_n} \quad , \qquad \text{(III-2b)}$$

a_n representing the acoustic impedance of the nth layer (Figure II-1).

It can be seen from Figure C-1 that a blocked impedance log is related to discrete reflectivity and vice versa. By making use of (III-2b), we will derive a relationship between reflectivity t(r) and acoustic impedance a(t).

Let us write (III-2b) somewhat differently (Figure C-2):

$$\Delta t\ r(n\Delta t) = \frac{a\ (n+\frac{1}{2})\Delta t - a\ (n-\frac{1}{2})\Delta t}{a\ (n+\frac{1}{2})\Delta t + a\ (n-\frac{1}{2})\Delta t}$$

or

$$\Delta t\ r(n\Delta t) = \frac{\Delta a(n\Delta t)}{2a(n\Delta t)} \qquad \text{for } \Delta t \text{ sufficiently small}$$

or

$$\Delta t\ r(n\Delta t) = \tfrac{1}{2}\Delta\{\ell n a(n\Delta t)\} \qquad \text{for } \Delta t \text{ sufficiently small} \quad \text{(III-3a)}$$

or

$$\boxed{r(t) = \tfrac{1}{2}\frac{d\ell n a(t)}{dt}} \qquad \text{(III-3b)}$$

Hence we have derived the interesting and important property that, apart from a constant,

"reflectivity equals the derivative of logarithmic acoustic impedance".

From (III-3a) it follows:

$$\sum_{k=n_o}^{n} \Delta\{\ell n a(k\Delta t)\} = 2\sum_{k=n_o}^{n} r(k\Delta t)\Delta t$$

or

$$\ell n a(n\Delta t) - \ell n a(n_o\Delta t) = 2\sum_{k=n_o}^{n} r(k\Delta t)\Delta t \qquad \text{(III-4a)}$$

or

$$\boxed{\tfrac{1}{2}\Delta\{na(t)\} = \int_{t_0}^{t} r(t)\ dt} \qquad \text{(III-4b)}$$

Hence, we have also shown that, apart from a constant, "change of logarithmic acoustic impedance equals <u>integrated</u> reflectivity".

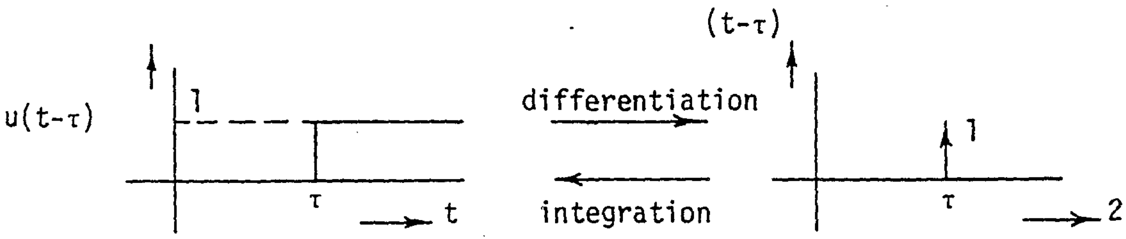

Bearing in mind that the unit step-function, U(t), is obtained from the unit impulse by integration and the unit impulse, δ(t), is obtained from the unit step function by differentiation, equations (III-3b) and (III-4b) fully explain the property that blocked acoustic impedance is related to discrete reflectivity and vice versa.

If, within the time gate (t_0, t), $\Delta a(t)$ is small then we can write

$$\ell n\ \frac{a(t)}{a(t_0)} = \ell n\ \frac{a(t_0) + \Delta a(t)}{a(t_0)}$$

$$= \ell n\ \left(1 + \frac{\Delta a(t)}{a(t_0)}\right)$$

$$\ell n\ \frac{a(t)}{a(t_0)} = \frac{\Delta a(t)}{a(t_0)}$$

and (III-4b) may be approximated by

$$\boxed{\frac{1}{2}\,\frac{\Delta a(t)}{a(t_0)} = \int_{t_0}^{t} r(t)dt \quad .} \qquad \text{(III-4c)}$$

from the foregoing it follows that for a given reflectivity, acoustic impedance can be computed apart from a constant $a(t_0)$. In other words, from integrated reflectivity data the d.c. component of the acoustic impedance is not recovered.

Now let us integrate seismic tract $y(t)$:

$$\int_{t_0}^{t} y(\tau)d\tau = \int_{t_0}^{t} \left[w_0(\tau) * r(\tau) \quad d\tau\right] + \int_{t_0}^{t} n_0(\tau)d\tau \; .$$

Since convolution and integration are linear processes we may interchange the order:

$$\int_{t_0}^{t} y(\tau)d\tau = w_0(t) * \int_{t_0}^{t} r(\tau)d\tau + \int_{t_0}^{t} n_0(\tau)d\tau$$

$$= w_0(t) * \Delta\{\ell n a(t)\} + n_0'(t)$$

$$= w_0(t) * \ell n a(t) + n_0'(t) \quad , \qquad \text{(III-5)}$$

as $w_0(t)$ has no d.c. component.

From (III-5) it follows that integrated seismic data will differ from acoustic impedance data by

1) d.c. component $a(t_0)$
2) integrated seismic noise $n_0'(t)$
3) amplitude characteristics of seismic wavelet $w_0(t)$.

In particular the band limited property of wavelet $w_0(t)$ causes two important deficiencies of seismic acoustic impedance data:

lack of high frequencies —— no detail

lack of low frequencies —— no trend.

In absence of high frequencies is a basic limitation of the seismic method.

In conclusion the following remarks can now be made:

1) Acoustic impedance logs can be synthesized from seismic data by integration.

2) Due to the lack of high frequency information in seismic data, synthetic logs have less detail than well logs.

3) Due to the lack of low frequency information in seismic data, synthetic logs do not contain any trend information.

Hence synthetic logs show relative acoustic impedance only.

Description of the SQUARE-PLOT Algorithm

Band-limited seismic data that has been integrated to produce an acoustic log display is smooth in transitioning from one polarity to another. Logs on the other hand are typically more abrupt in transition from one rock type to another. In order to restore the general appearance of log-type data, and also to reveal information usually hidden in inflection points on the acoustic seismic sections, GeoQuest has devised a SQUARE-PLOT algorithm. Unlike simple data clipping, SQUARE-PLOT retains amplitude information as it improves visual resolution.

The SQUARE-PLOT algorithm is explained with reference to the enclosed Figure C-3 Points of change in curvature are determined in the SYN-LOG data. Once sample transitions in the level are established at these points with the levels being equal to the maxima between such points. In the event of a local minimum not changing polarity, as at level "c" in the figure, the curvature changes and level sets are as shown. In an interior zone such as between "f" and "g" levels and "g" and "h" levels, the magnitude is computed as the average of the adjacent levels at the points of curvature change.

Application of SYN-LOG

The application of the SQUARE-PLOT algorithm to integrated seismic data is shown in Figure C-4.The wavelet processed seismic data is shown in the left panel of the figure and the integrated, SQUARE-PLOT display continues with the same data in the right panel. The juncture between the two display formats shows how intervals in the SQUARE-PLOT display correspond to a -1, + 0.4 relative reflection sequence in the seismic display. The zone being examined is a low acoustic impedance sand embedded in a higher acoustic impedance shale. This is noted usually as the correspondence of a seismic white trough with a transition from black to white (high to lower acoustic impedances) on the log data. Conversely a black peak on seismic corresponds to a transition from white to black (low to high acoustic impedance) on the log data.

The magnitude of change on the log display is indicative of acoustic contrast. The magnitude of relative acoustic impedance for a given indicated layer is also an indication of the absolute acoustic impedance deviation from the local trend or base value of acoustic impedance.

Figure C5 shows another example of wavelet processed seismic data with the log display having the SQUARE-PLOT format. This example is a response to locally soft or low velocity reservoir sands in a lenticular depositional environment. These sands are seen in the log display as correlatable white intervals. The correlatable black intervals are characterizing adjacent higher velocity shales with some amplitude boost from the overshoot which results from the lack of low frequencies in the seismic data.

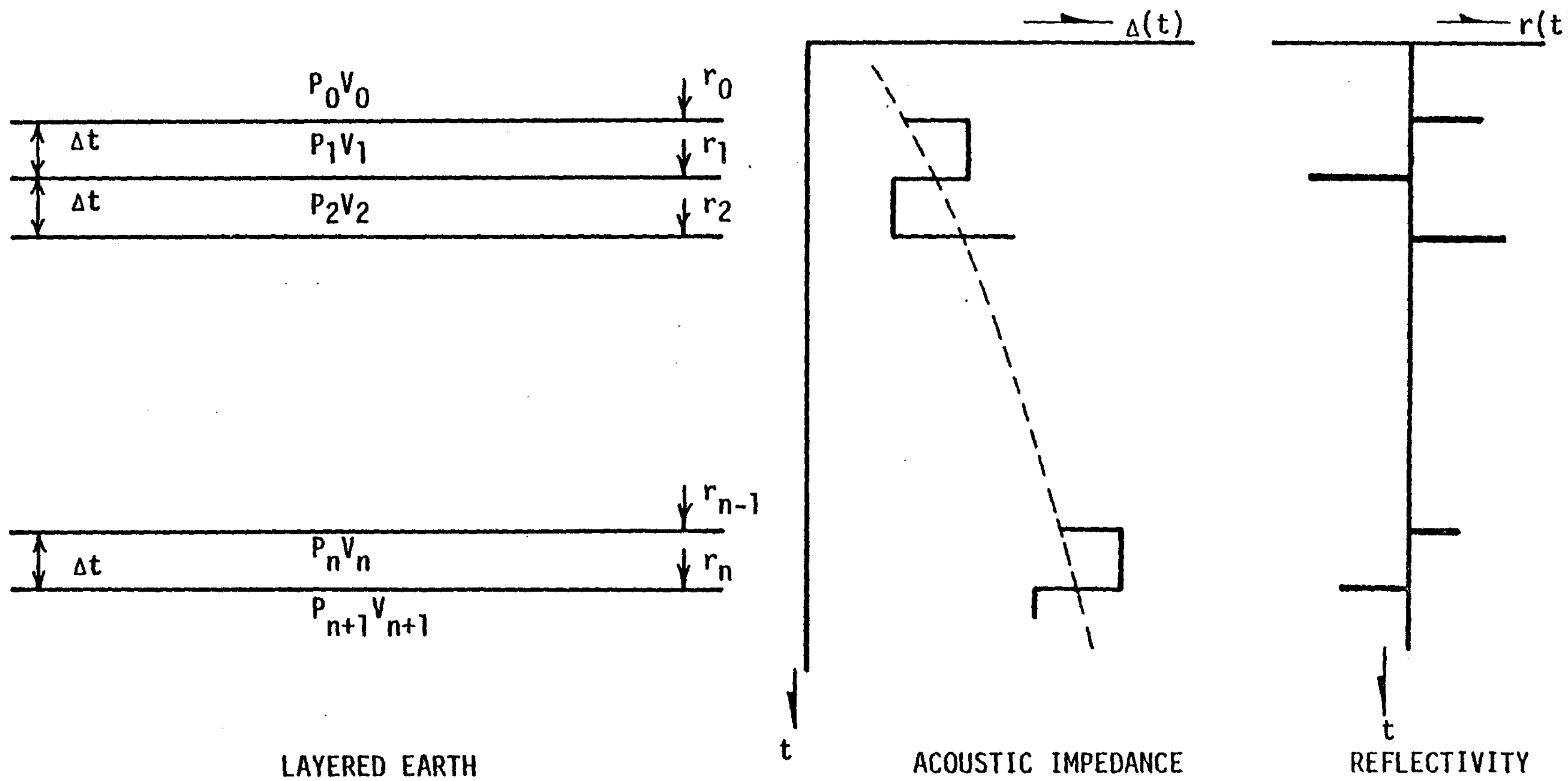

FIGURE C-1

BASIC RELATIONSHIP BETWEEN LITHOLOGY, ACOUSTIC IMPEDANCE AND REFLECTIVITY

FIGURE C-2

DERIVATION OF THE REFLECTIVITY - ACOUSTIC IMPEDANCE

FUNCTIONAL RELATIONSHIP

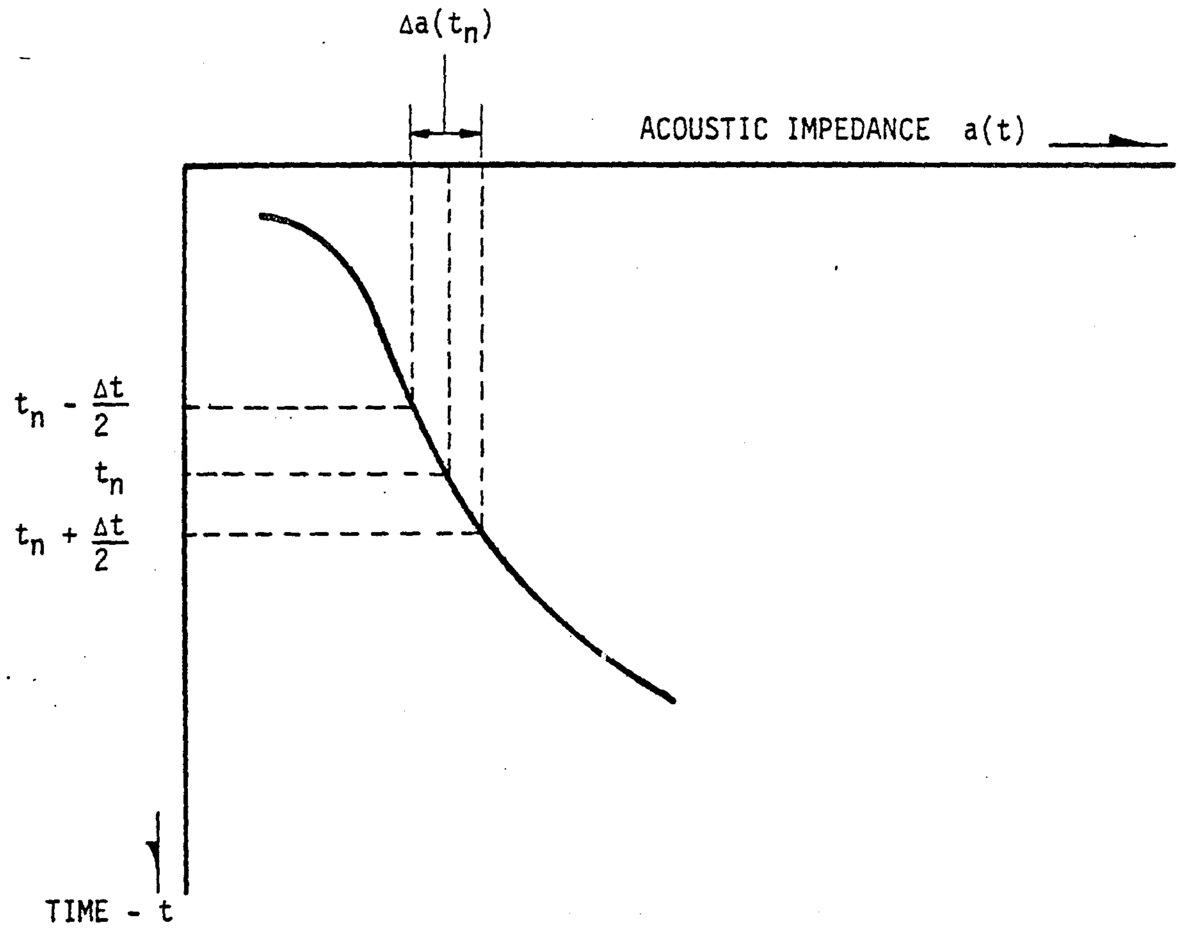

$$r_n = \frac{a(t_n + \frac{\Delta t}{2}) - a(t_n - \frac{\Delta t}{2})}{a(t_n + \frac{\Delta t}{2}) + a(t_n - \frac{\Delta t}{2})}$$

$$\approx \frac{\Delta a(t_n)}{2a(t_n)}$$

$$\lim_{\Delta t \to 0} r_n = \frac{1}{2} \frac{d}{dt} \ln a(t_n)$$

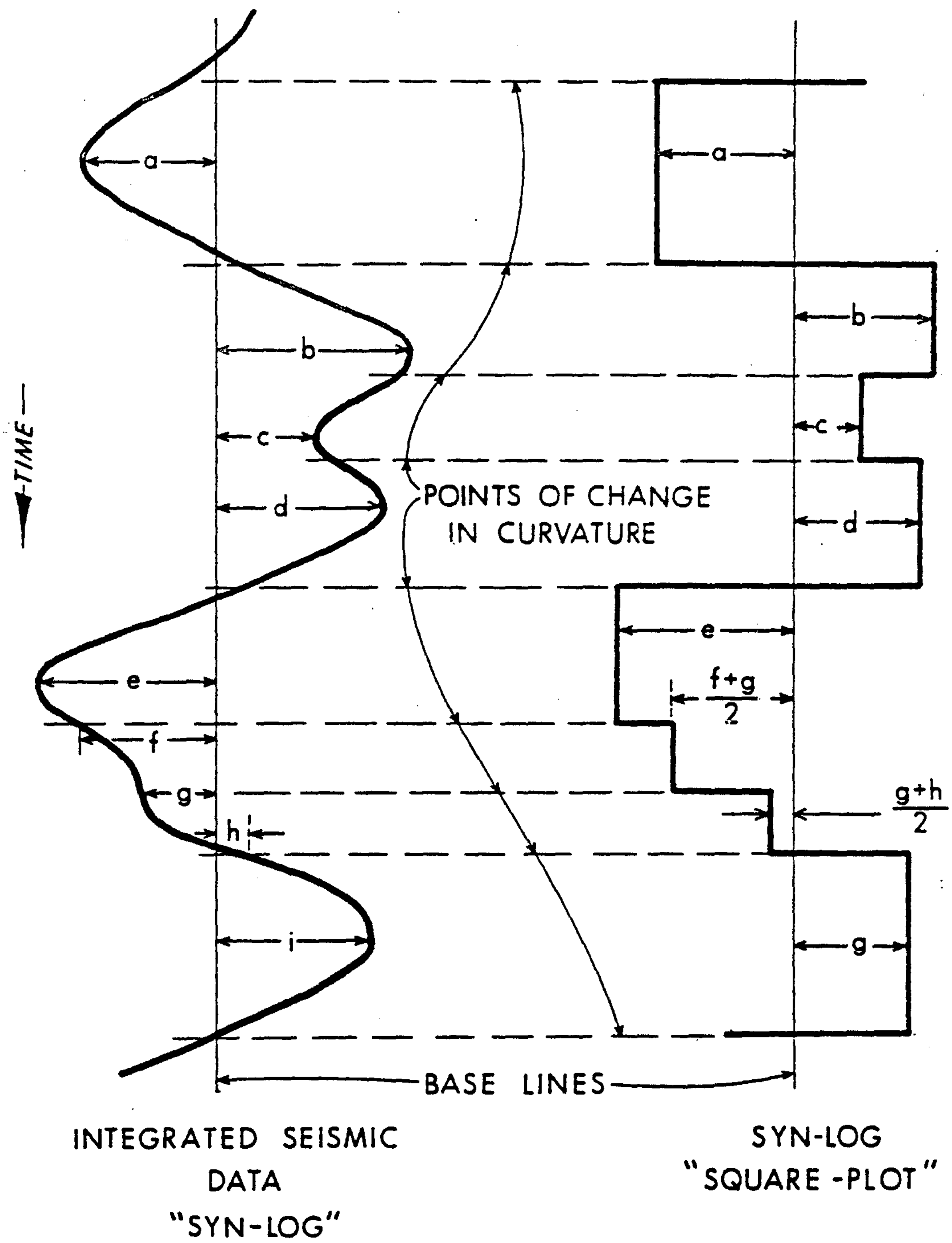

SYN-LOG SQUARE PLOT GENERATION

FIGURE C-3

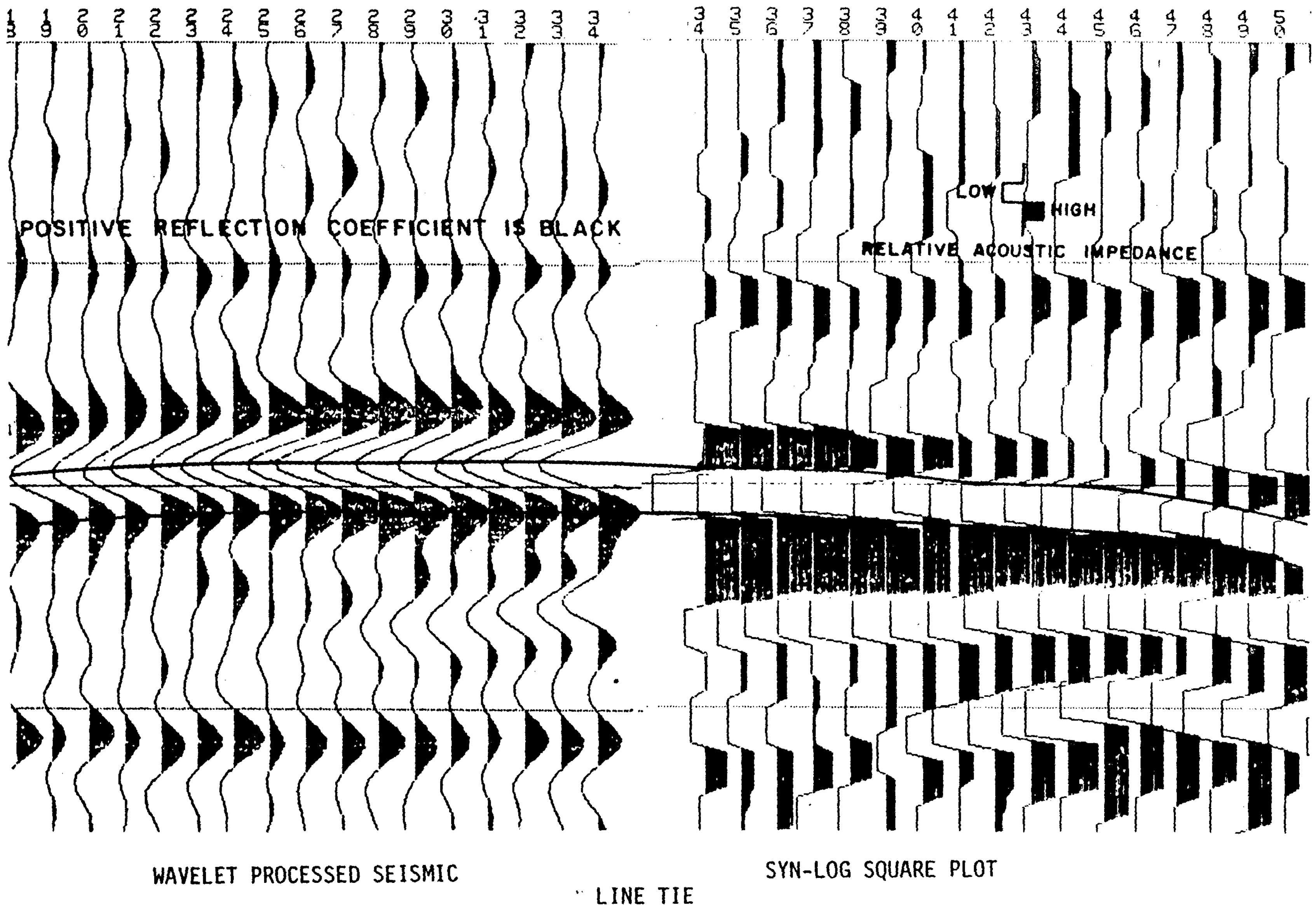

FIGURE C-4

LINE TIE COMPARISON FOR WAVELET PROCESSED AND SYNLOG VERSIONS OF THE SAME LINE

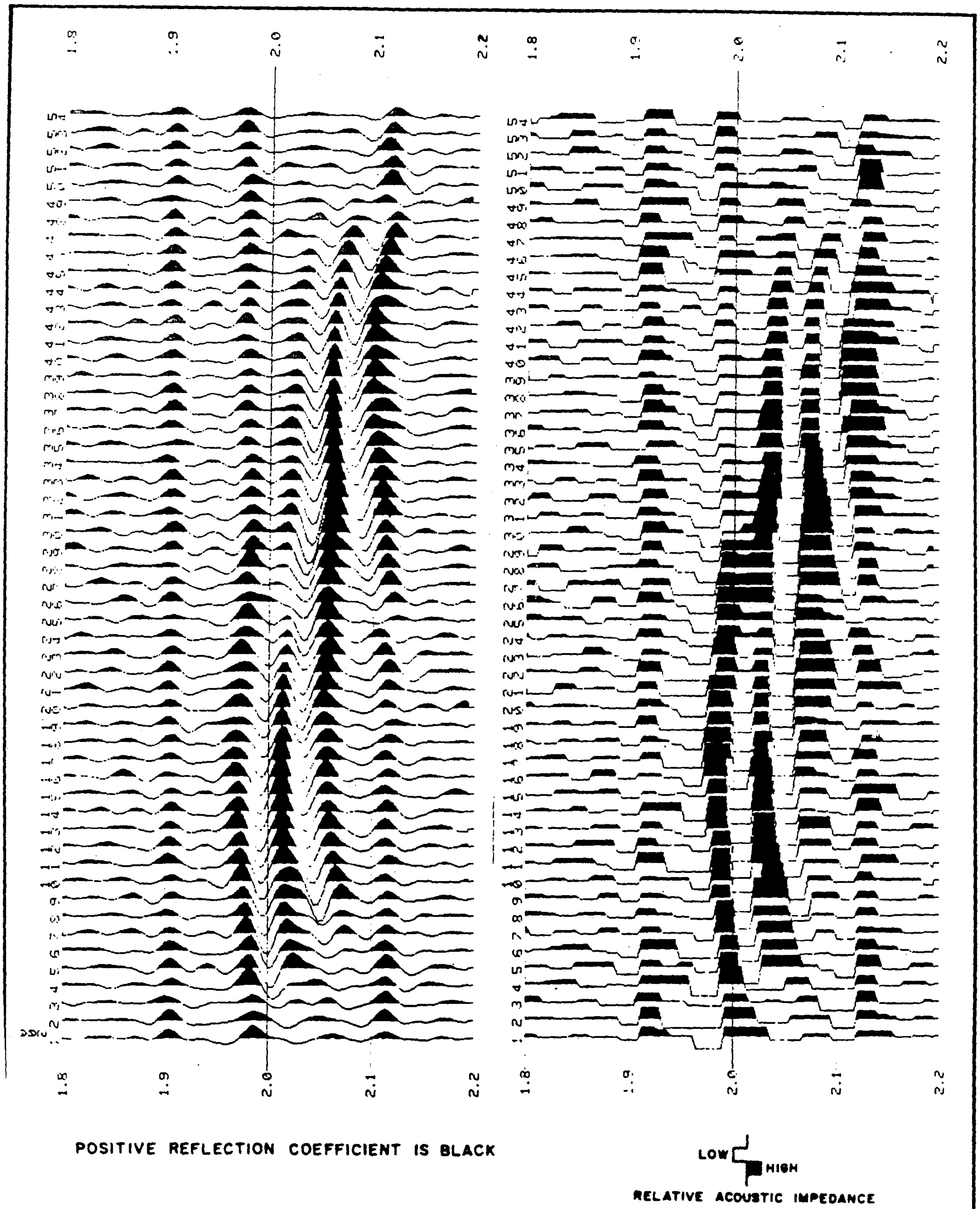

WAVELET PROCESSED SECTION

SYNLOG SQUARE PLOT SECTION

FIGURE C-5
COMPARISON OF WAVELET PROCESSED AND SYNLOG DATA

PART 3

EVALUATION OF THE LOWER HACKBERRY "C" SAND, PORT ARTHUR FIELD

Prepared by

Robert Lewis Ridings

Lewis Technical Services, Inc.
Spring, Texas 77373

For

Gas Research Institute

Contract No. 5080-321-0398

GRI Project Manager
Leo A. Rogers
Co-Production of Gas and Water

October 1982

CONTENTS

INTRODUCTION

This study was authorized by the Gas Research Institute as an independent evaluation of the lower Hackberry "C" Sand in the Port Arthur Field as a prospect for future production of gas.

During the period 1960 to 1971 gas was produced from four wells in the lower Hackberry "C" Sand. Production from the "C" Sand indicated a geopressured gas reservoir with substantial aquifer support. Gas production was accompanied by increasing amounts of water and, in 1971, the last well was abandoned as uneconomical under the conditions at the time.

The objective of this study was to estimate the quantities of gas which may be produced at this time by the drilling of a new well, installation of appropriate production facilities, and co-production of gas and gas-saturated reservoir brine.

The study approach consisted of the use of a numerical reservoir simulator model to approximate the physical system, a match of observed history to confirm certain physical parameters, and a prediction of future performance under assumed operating conditions.

The bulk of the data used was gathered by the Bureau of Economic Geology and the work done was carried out with their assistance and advice.

CONCLUSIONS

Based on the mathematical simulation of the lower Hackberry "C" Sand in the Port Arthur Field, the following conclusions are implied:

1. The original gas in place is estimated to have been about 50 Bcf.

2. The strength of the water drive and the observed pressure performance is consistent with a finite aquifer of about 850 million barrels.

3. Wells #14 and #23 indicate an inter-well communication of much less than the average sand permeability of 300 md.

4. A new well drilled as a twin to Well # 14 and equipped to handle high water production should have an initial capacity of some 5 MMcf/d declining to less than 1 MMcf/d over a ten-year period.

5. A well, as above, should produce between 4.5 and 5.0 Bcf over a ten-year period.

6. Economics of drilling and producing a new well will be enhanced by gas released from solution from the reservoir brine and a possible 50,000 STB of condensate over a ten-year period.

7. Production will be limited by pressure decline and aquifer depletion.

DESCRIPTION OF MODEL

The grid model used to represent the "C" Sand reservoir is shown in Figure 1. In the area of initial gas saturation, a block dimension of 500 ft by 500 ft was selected as being sufficient to represent the reservoir variations. A coarser grid was used to represent the water saturated areas away from the gas. This resulted in an overall grid dimension of 10 x 13 blocks with certain blocks deleted from the active system as they were deemed to represent areas not in communication with the area of interest.

Elevation and thickness values were assigned to each grid block by overlaying the grid on the "C" Sand structure and isopach maps (figs. 2 and 3).

Based on well tests, an average permeability of 300 md was assigned to the sand. An average porosity of 30% was estimated from available data. As is discussed in the following section, these data were modified during the history matching phase of the study as required to reflect observed performance.

Table I reflects the model data as determined by measurement and resulting from the match of history.

ANALYSIS OF HISTORY

The well test history of the wells completed in the "C" Sand is presented in Table II as reported by the operator.

From the producing characteristics of well # 11, it became apparent that this well was not in the same producing regime as wells #14 and #23. In 1962, Hurst estimated that well # 11 had a limited drainage area of just over 200 ft and the well was later depleted to hydrostatic pressure. As a result, the sand area containing that well was deemed to be outside of the area of current interest and was eliminated from the study area. Well #6 was not modeled because it produced a negligible amount of gas compared to the other wells in the "C" sand.

In establishing the reference base for the matching of calculated pressures, the formation pressures in the vicinity of the well were chosen over the instantaneous flowing pressures to eliminate the unknowns of well flowing characteristics. Table III lists the measured bottom-hole static pressures (formation pressures) which were measured for wells # 14 and #23.

Well # 14 was completed in the "C" Sand in July 1961 with an initial measured formation pressure of 9115 psi at 11,140 ft. Well # 23 was completed in the "C" Sand in July 1965 with an initial measured formation pressure of 8398 psi, or some 700 psi below original sand pressure. This indicates that the well was in communication with existing production at the time. However, it is estimated that the pressure around well # 14 in July 1965 was about 8100 psi, or some 300 psi less. This tends to indicate that the degree of communication between the wells is small although finite.

The small degree of communication between wells #14 and #23 is confirmed by the comparative rates of pressure decline during the time that well # 23 was producing. During the period mid-1965 to mid-1971, well # 23 experienced a pressure decline of 1200-1400 psi. Over the same period, well # 14 experienced a pressure decline of about half that amount. Adjustments to permeability in successive runs to match the observed performance resulted in a streak of reduced permeability (less than 0.5 md) between wells # 14 and #23. This, along with a restriction in aquifer support to well # 23 led to a reasonable match of pressure levels and rates of decline.

The history matching procedure led to an adjusted finite aquifer volume of about 850 million barrels. This aquifer volume was sufficient to agree with observed reservoir behavior.

The measured formation pressures at the wells were extrapolated based on analysis of shut-in tubing-head pressures from well tests. These extrapolations are shown on Figures 4 and 5 along with the calculated formation pressures. It must be emphasized that inferring static bottom-hole pressures from shut-in tubing-head pressures in these cases is less than precise due to inexact measurements of water production and assumptions on the static water column in a shut-in well. Therefore, these analyses were used only as a means of implying pressure trends. The methods of Orkiszewski (1967) and Beggs and Brill (1973) were used for this purpose with comparable results.

The gas production rates for wells # 14 and #23 are shown on Figures 6 and 7. During the producing life of the reservoir well # 14 produced a total of 10.5 Bcf and well # 23 produced a total of 1.3 Bcf for a reservoir total of 11.8 Bcf.

The calculated and observed water production rates for the wells are compared in Figures 8 and 9. Well #14 produced water-free gas from mid-1961 to mid-1963 with rapidly increasing water-gas ratio after breakthrough. Well #23 produced water from the point of initial production. The accuracy of the field water measurements are uncertain under the conditions of fluctuating rates and frequent down times. However, it is felt that the match of calculated and observed water productions are acceptable for the purposes of this study. The experience gained during the progress of the study indicated that further refinements of the parameters affecting water production made no significant differences in predicting performance once a reasonable match had been obtained.

Lacking special core analysis data, assumptions were necessary on gas and water relative permeabilities. Using the method of Corey (1954), a number of assumptions were made attempting to achieve a reasonable match of performance. The assumptions of connate water saturation of 35%,residual gas saturation of 25%, and Corey exponents of m=4 and n=2 appear to result in an acceptable match. The resulting relative permeability curves are shown in Figure 10.

As an aid in evaluating the simulation, water saturation maps were produced. Figure 11 shows the calculated water saturation map soon after the start of production on January 1, 1962. Figure 12 shows the calculated water saturation map just before the beginning of prediction at stable conditions on January, 1984. This indicates that a reasonable choice of location for a new well would be a twin of well #14 or possibly 500 ft to the west. Water saturation maps for January 1, 1989 and January 1, 1994 are shown in Figures 13 and 14 respectively.

PREDICTION OF PERFORMANCE

Prediction of performance was based on the assumption that well #14 would be twinned by a new well. Allowing time for committments, drilling, and installation of production facilities; it was assumed that production could begin around the first of 1984.

Model predictions were based on the calculated ability of such a well with 5-inch tubing to sustain high water production rates. A flowing bottom-hole pressure of 4,500 psi was calculated to enable production at a flowing well-head pressure of about 1,000 psi and the minimum flowing bottom-hole pressure of 4,500 psi was specified to the simulation model.

A target rate of 5 MMcf/d was specified to the model. From the initial rate of 5 MMcf/d the predicted rate declined to 0.8 MMcf/d over a period of ten years, producing some 4.8 Bcf over that period.

It should be noted that the above figures refer to free gas production only and not to gas released from solution from the reservoir brine nor the possible associated condensate production.

Based on correlations of gas-saturated brines, it is estimated that the produced water could yield some 20 scf of gas per bbl of brine. The predictions indicate that the 4.8 Bcf of free gas production would be associated with about 6 MMbbl of water production. Gas released from solution in the water could yield an additional 120 MMcf of gas.

Well tests on well #14 prior to abandonment indicated a condensate yield of about 15 STB/MMcf. On the assumption that over a ten-year period this could decline to an average value of 10 STB/MMcf, then approximately 50,000 STB of condensate could be expected over the same period.

For purposes of extrapolation beyond the ten-year model prediction, a decline rate of 8 percent per annum to the economic limit can be used.

REFERENCES

Beggs, H. D. and Brill, J. P., 1973, A study of two-phase flow in inclined pipes: Journal of Petroleum Technology, v. 25, p. 607-617.

Corey, A. T., 1954, The interrelation between gas and oil relative permeabilities: Producers Monthly, Nov. issue, p. 38-41.

Hurst, William, Gas reserves in place established by material balance studies with pressure build-up interpretation—Hackberry Unit, Port Arthur Field, Jefferson County, Texas: report prepared for Meridith and Company, Houston, Texas, Sep. 1962.

Orkiszewski, J, 1967, Predicting two-phase pressure drops in vertical pipe: Trans. AIME, v. 240, p. 829-838.

Table I

INITIAL CONDITIONS

LOWER HACKBERRY "C" SAND RESERVOIR

Initial Pressure	9115 psi @ -11,140 ft
Gas-Water Contact	-11,154 ft
Gas Gravity	0.7 (Air = 1.0)
Connate Water Saturation	35%
Residual Gas Saturation	25%
Reservoir Temperature	230°F
Water Compressibility	5×10^{-6} 1/psi
Water Viscosity	0.3 cp
Initial Gas Pore Volume	26.9 MM Res bbl
Initial Gas in Place	52.4 Bcf
Aquifer Volume	850 MM bbl

Table II B

PORT ARTHUR FIELD - "C" SAND, LOWER HACKBERRY—JEFFERSON COUNTY, TEXAS

Kilroy and MPS No. 1 Doornbos (BEG Well #23) Field Test Data

Date	Dry Gas Rate Mcf/d	Water/Gas Ratio bbl/MMcf	Cond./Gas Ratio bbl/MMcf	SIWHP psia
07-27-65	2413	--	68	--
08-02-65	2413	--	--	6751
01-12-66	1750	375	--	6215
06-29-66	1280	461	82	5515
01-12-67	688	--	--	--
03-13-67	1180	--	--	5115
09-11-67	1100	70	6	4515
02-05-68	600	830	--	4415
07-31-68	750	--	--	4215
04-30-69	431	934	--	4215
07-17-69	483	--	--	--
01-13-70	300	1533	--	4015
07-14-70	436	2294	38	--
01-26-71	373	1300	29	--
07-29-71	345	3246	29	--
08-01-71	abandoned	--	--	--

Table II A

PORT ARTHUR FIELD - "C" SAND, LOWER HACKBERRY—JEFFERSON COUNTY, TEXAS

Meredith No. 2 Doornbos (BEG Well #14) Field Test Data

Date	Dry Gas Rate Mcf/d	Water/Gas Ratio bbl/MMcf	Cond./Gas Ratio bbl/MMcf	SIWHP psia
07-28-61	6494	--	67	7454
12-06-61	8500	--	60	7015
06-06-62	8500	--	--	6915
12-13-62	9023	--	--	--
06-06-63	7000	24	52	6715
12-26-63	5500	45	52	6715
03-19-64	7000	77	47	6415
06-22-64	7000	91	47	6315
12-04-64	7200	106	39	6502
01-04-65	7300	--	--	6502
06-03-65	6400	353	39	6165
07-26-65	6400	353	--	6165
06-19-66	4500	--	--	5615
06-20-66	4500	332	59	5615
12-12-66	4400	274	--	5915
12-20-66	1240	1011	18	5515
01-12-67	1297	--	--	Shut In (Treatment)
03-13-67	3140	--	--	5415
03-19-67	3140	765	14	5415
09-11-67	1059	860	78	5415
02-05-68	600	819	--	5315
07-31-68	1000	--	--	4815
01-15-69	1000	1525	14	4815
04-30-69	826	828	--	4815
07-15-69	1800	1059	12	4815
07-17-69	749	--	--	4815
01-13-70	417	887	--	4815
01-15-70	900	2111	17	4215
07-14-70	568	1495	74	--
01-26-71	494	1061	7	4115
06-15-71	700	2214	7	4165
07-29-71	424	2616	19	--
12-07-71	400	5000	15	4015
06-02-72	128	3117	16	--

Table III

MEASURED BOTTOM-HOLE PRESSURES

LOWER HACKBERRY "C" SAND RESERVOIRS

Date	Formation Pressure, psi
Well #14, perfs 11,136 - 11,144 ft	
7-24-61	9115
3- 8-62	8705
7-20-62	8547
3-29-63	8470
12- 2-63	8275
10-26-64	8146
Well #23, perfs 11,128 - 11,131 ft	
7-27-65	8398

Table IV

PORT ARTHUR FIELD (LOWER HACKBERRY - C SAND)—WELL SUMMARY

Well No. 14

Date	Gas Rate (Mcf/d)	Water Rate (bbl/d)	Bottom-Hole Pressure (psi)	Avg. Block Pressure (psi)
1 Jan 1962	4994.	0.	8882.	8950.
1 Jul 1962	6205.	0.	8716.	8804.
1 Jan 1963	5874.	0.	8584.	8670.
1 Jul 1963	6545.	1.	8385.	8509.
1 Jan 1964	4957.	12.	8253.	8424.
1 Jul 1964	6001.	210.	7310.	8245.
1 Jan 1965	5692.	1219.	6236.	8036.
1 Jul 1965	3965.	1386.	6363.	7935.
1 Jan 1966	4118.	1658.	5822.	7763.
1 Jul 1966	2450.	1505.	6141.	7694.
1 Jan 1967	1691.	1348.	6302.	7632.
1 Jul 1967	1201.	1126.	6550.	7589.
1 Jan 1968	809.	822.	6822.	7563.
1 Jul 1968	681.	693.	6898.	7529.
1 Jan 1969	522.	565.	6977.	7499.
1 Jul 1969	597.	666.	6812.	7443.
1 Jan 1970	305.	465.	7009.	7425.
1 Jul 1970	329.	508.	6941.	7388.
1 Jan 1971	361.	564.	6832	7340.
1 Jul 1971	173.	367.	6989.	7323.
1 Jan 1972	220.	473.	6889.	7285.
1 Jul 1972	93.	232.	7063.	7279.
1 Jan 1973	74.	205.	7102.	7266.
1 Jan 1974	0.	0.	7270.	7270.
1 Jan 1975	0.	0.	7264.	7263.
1 Jan 1976	0.	0.	7259.	7259.
1 Jan 1977	0.	0.	7255.	7255.
1 Jan 1978	0.	0.	7252.	7252.
1 Jan 1979	0.	0.	7249.	7249.
1 Jan 1980	0.	0.	7248.	7248.
1 Jan 1981	0.	0.	7247.	7247.
1 Jan 1982	0.	0.	7246.	7246.
1 Jan 1983	0.	0.	7245.	7245.
1 Jan 1984	0.	0.	7245.	7245.
2 Jan 1984	5000.	1231.	5767.	7184.
1 Jan 1985	2983.	2422.	4500.	6757.
1 Jan 1986	1750.	2297.	4500.	6541.
1 Jan 1987	1483.	2059.	4500.	6354.
1 Jan 1988	1316.	1862.	4500.	6185.
1 Jan 1989	1168.	1696.	4500.	6035.
1 Jan 1990	1055.	1546.	4500.	5903.
1 Jan 1991	968.	1411.	4500.	5786.
1 Jan 1992	898.	1288.	4500.	5681.
1 Jan 1993	838.	1178.	4500.	5586.
1 Jan 1994	782.	1080.	4500.	5501.

Table V

PORT ARTHUR FIELD (LOWER HACKBERRY - C SAND)—WELL SUMMARY

Well No. 23

Date	Gas Rate (Mcf/d)	Water Rate (bbl/d)	Bottom-Hole Pressure (psi)	Avg. Block Pressure (psi)
1 Jan 1966	883.	30.	8274.	8518.
1 Jul 1966	1156.	72.	7649.	8314.
1 Jan 1967	1186.	331.	5719.	8042.
1 Jul 1967	638.	504.	5714.	7878.
1 Jan 1968	694.	900.	4130.	7575.
1 Jul 1968	397.	695.	5193.	7457.
1 Jan 1969	317.	572.	5597.	7360.
1 Jul 1969	442.	769.	4781.	7184.
1 Jan 1970	247.	377.	6071.	7185.
1 Jul 1970	237.	301.	6219.	7154.
1 Jan 1971	541.	698.	4609.	6966.
1 Jul 1971	242.	267.	6227.	7013.
1 Jan 1972	264.	227.	6245.	6996.
1 Jul 1972	0.	0.	7062.	7074.
1 Jan 1973	0.	0.	7098.	7101.
1 Jan 1974	0.	0.	7139.	7141.
1 Jan 1975	0.	0.	7161.	7162.
1 Jan 1976	0.	0.	7175.	7175.
1 Jan 1977	0.	0.	7186.	7186.
1 Jan 1978	0.	0.	7196.	7197.
1 Jan 1979	0.	0.	7207.	7208.
1 Jan 1980	0.	0.	7213.	7213.
1 Jan 1981	0.	0.	7217.	7217.
1 Jan 1982	0.	0.	7220.	7221.
1 Jan 1983	0.	0.	7224.	7224.
1 Jan 1984	0.	0.	7227.	7227.
2 Jan 1984	0.	0.	7227.	7227.
1 Jan 1985	0.	0.	7184.	7183.
1 Jan 1986	0.	0.	7118.	7116.
1 Jan 1987	0.	0.	7041.	7038.
1 Jan 1988	0.	0.	6957.	6954.
1 Jan 1989	0.	0.	6872.	6868.
1 Jan 1990	0.	0.	6783.	6781.
1 Jan 1991	0.	0.	6698.	6694.
1 Jan 1992	0.	0.	6611.	6608.
1 Jan 1993	0.	0.	6528.	6524.
1 Jan 1994	0.	0.	6444.	6442.

Table VI

PORT ARTHUR FIELD (LOWER HACKBERRY - C SAND)—RESERVOIR SUMMARY

Date	Gas Rate (Mcf/d)	Water Rate (bbl/d)	Datum Pressure (psi)
1 Jan 1962	4994.	0.	8985.
1 Jul 1962	6205.	0.	8859.
1 Jan 1963	5874.	0.	8741.
1 Jul 1963	6545.	1.	8604.
1 Jan 1964	4957.	12.	8522.
1 Jul 1964	6001.	210.	8377.
1 Jan 1965	5692.	1219.	8202.
1 Jul 1965	3965.	1386.	8098.
1 Jan 1966	5001.	1680.	7935.
1 Jul 1966	3606.	1577.	7840.
1 Jan 1967	2877.	1679.	7747.
1 Jul 1967	1839.	1629.	7676.
1 Jan 1968	1503.	1722.	7606.
1 Jul 1968	1078.	1388.	7553.
1 Jan 1969	839.	1137.	7508.
1 Jul 1969	1039.	1435.	7441.
1 Jan 1970	552.	842.	7414.
1 Jul 1970	566.	809.	7378.
1 Jan 1971	902.	1262.	7317.
1 Jul 1971	415.	634.	7297.
1 Jan 1972	484.	701.	7264.
1 Jul 1972	93.	232.	7260.
1 Jan 1973	74.	205.	7253.
1 Jan 1974	0.	0.	7256.
1 Jan 1975	0.	0.	7254.
1 Jan 1976	0.	0.	7252.
1 Jan 1977	0.	0.	7250.
1 Jan 1978	0.	0.	7249.
1 Jan 1979	0.	0.	7249.
1 Jan 1980	0.	0.	7248.
1 Jan 1981	0.	0.	7248.
1 Jan 1982	0.	0.	7248.
1 Jan 1983	0.	0.	7248.
1 Jan 1984	0.	0.	7248.
2 Jan 1984	5000.	1231.	7245.
1 Jan 1985	2988.	2422.	6908.
1 Jan 1986	1750.	2297.	6711.
1 Jan 1987	1483.	2059.	6538.
1 Jan 1988	1316.	1862	6377.
1 Jan 1989	1168.	1696.	6234.
1 Jan 1990	1055.	1546.	6105.
1 Jan 1991	968.	1411.	5989.
1 Jan 1992	898.	1288.	5883.
1 Jan 1993	838.	1178.	5786.
1 Jan 1994	782.	1080.	5699.

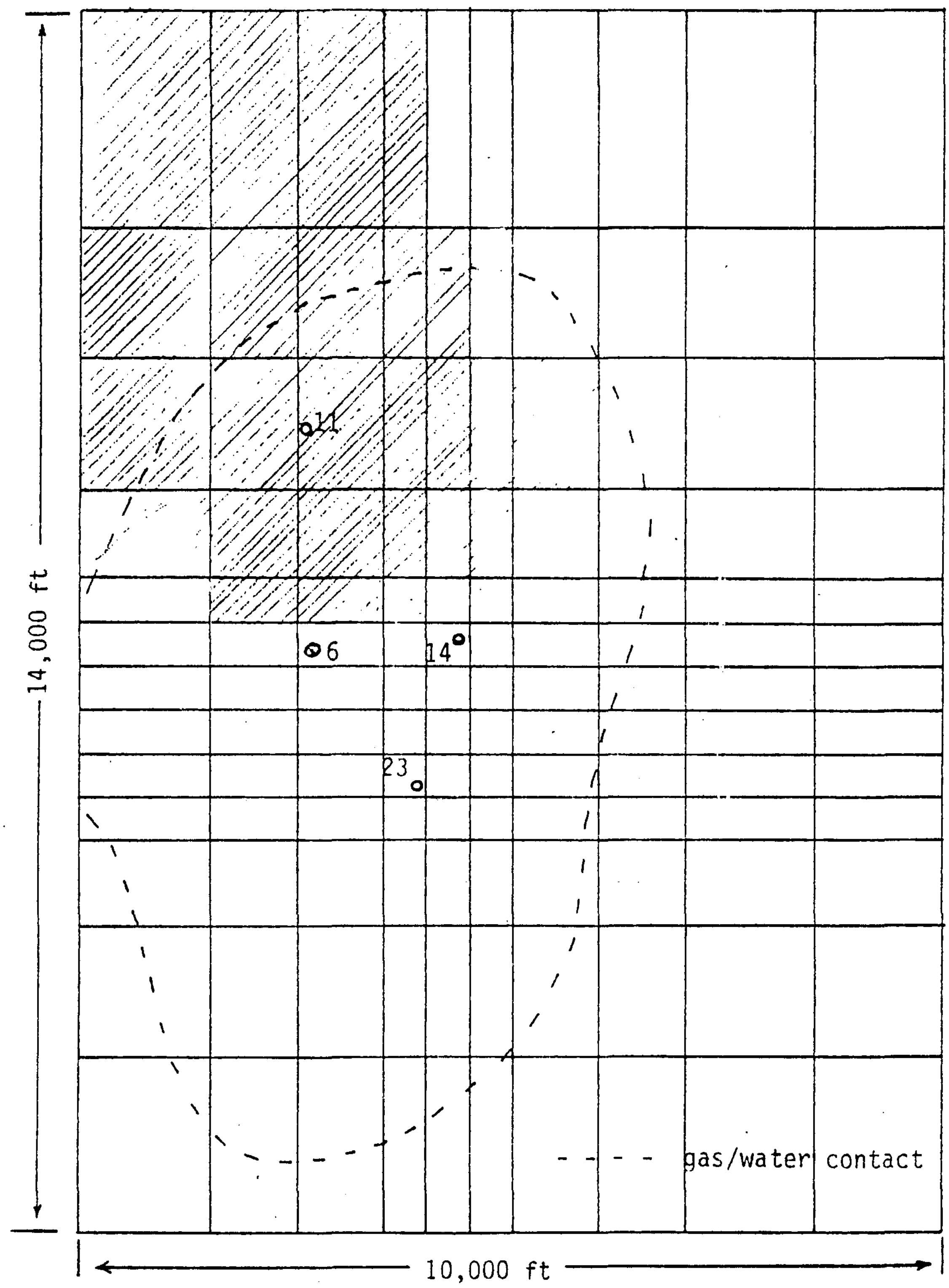

Figure 1. Simulator Grid

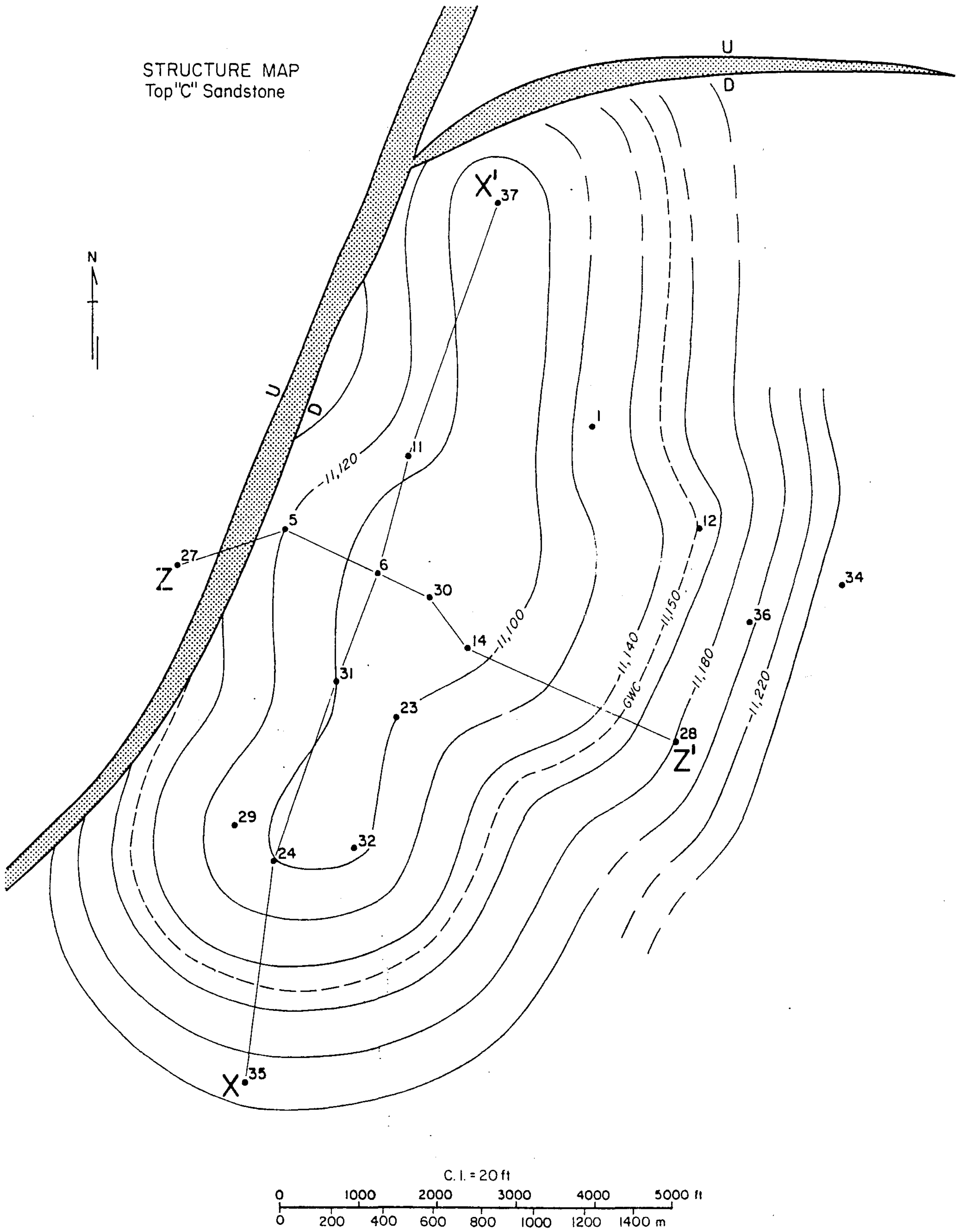

Figure 2. Structure map, "C" sandstone, Port Arthur field.

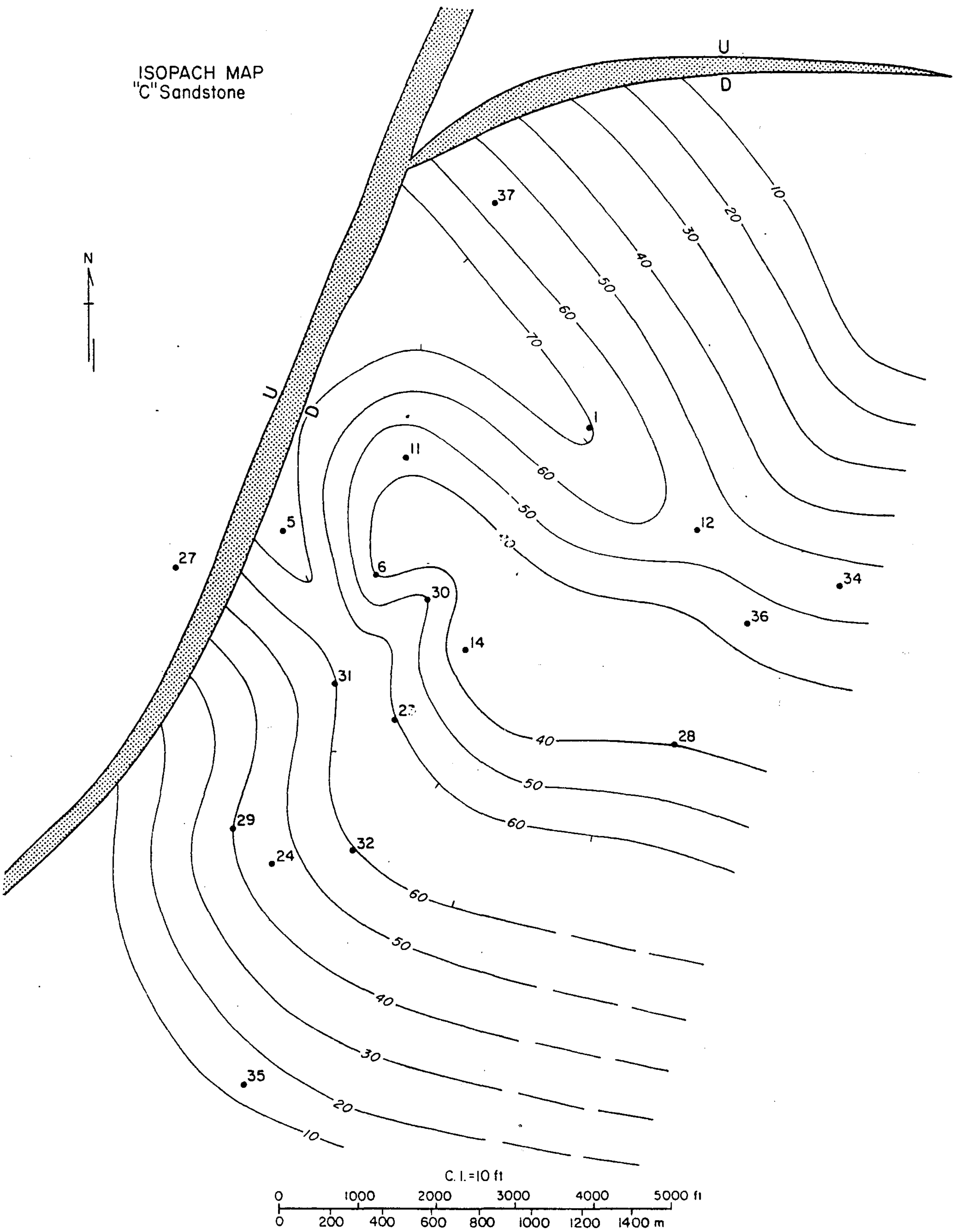

Figure 3. Isopach map, "C" sandstone, Port Arthur field.

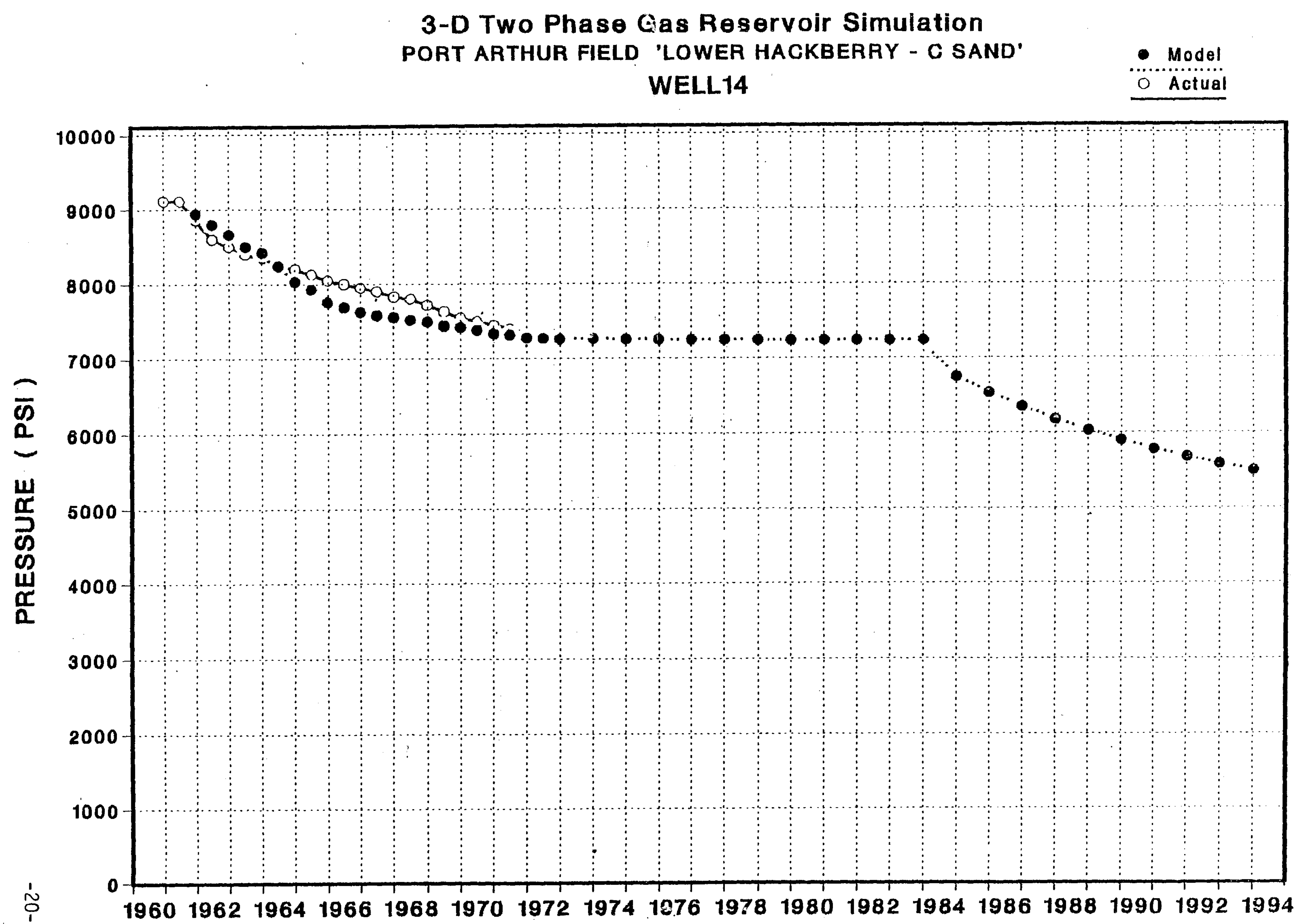

Figure 4. Formation Pressures - Well No. 14

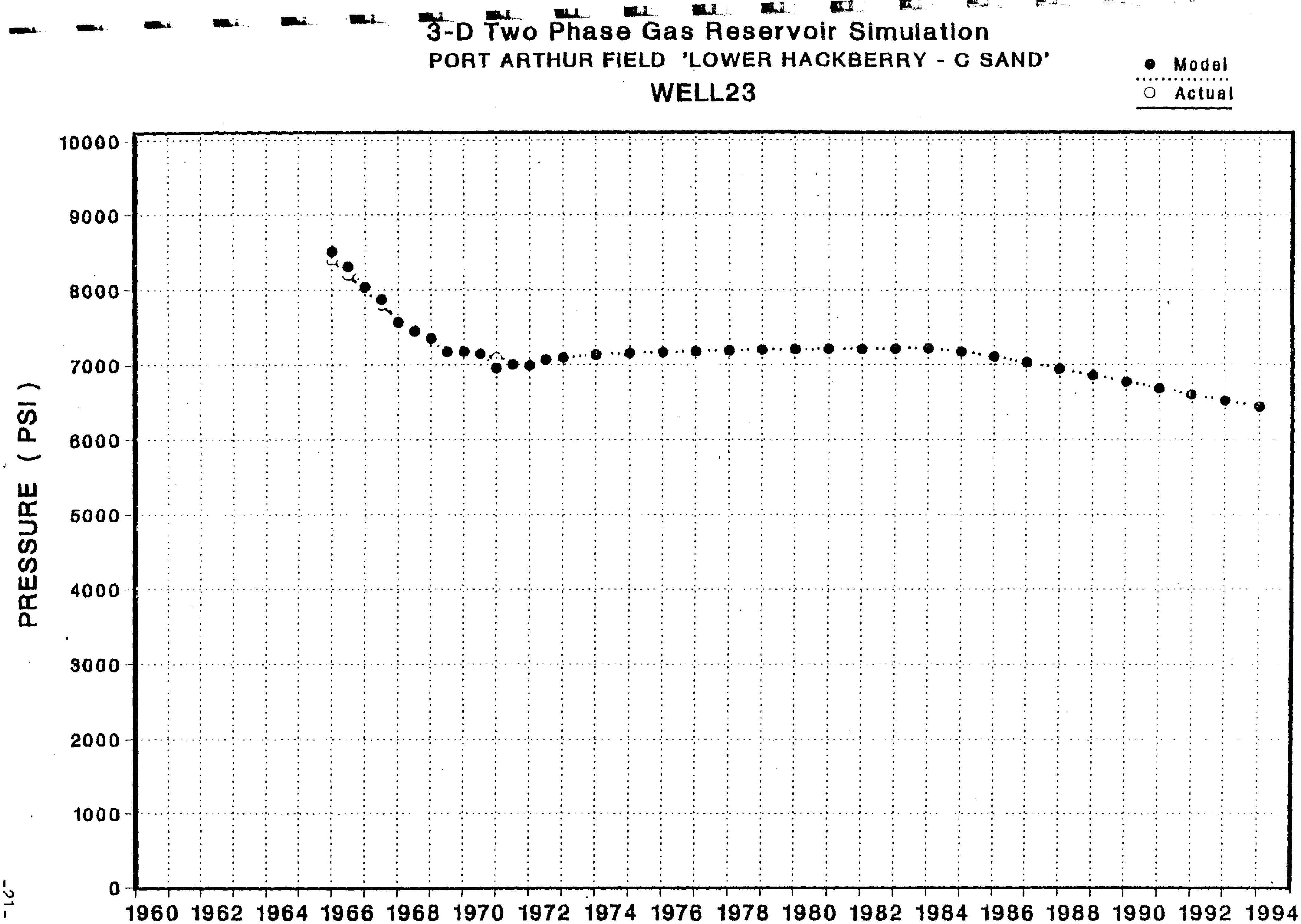

Figure 5. Formation Pressures - Well No. 23

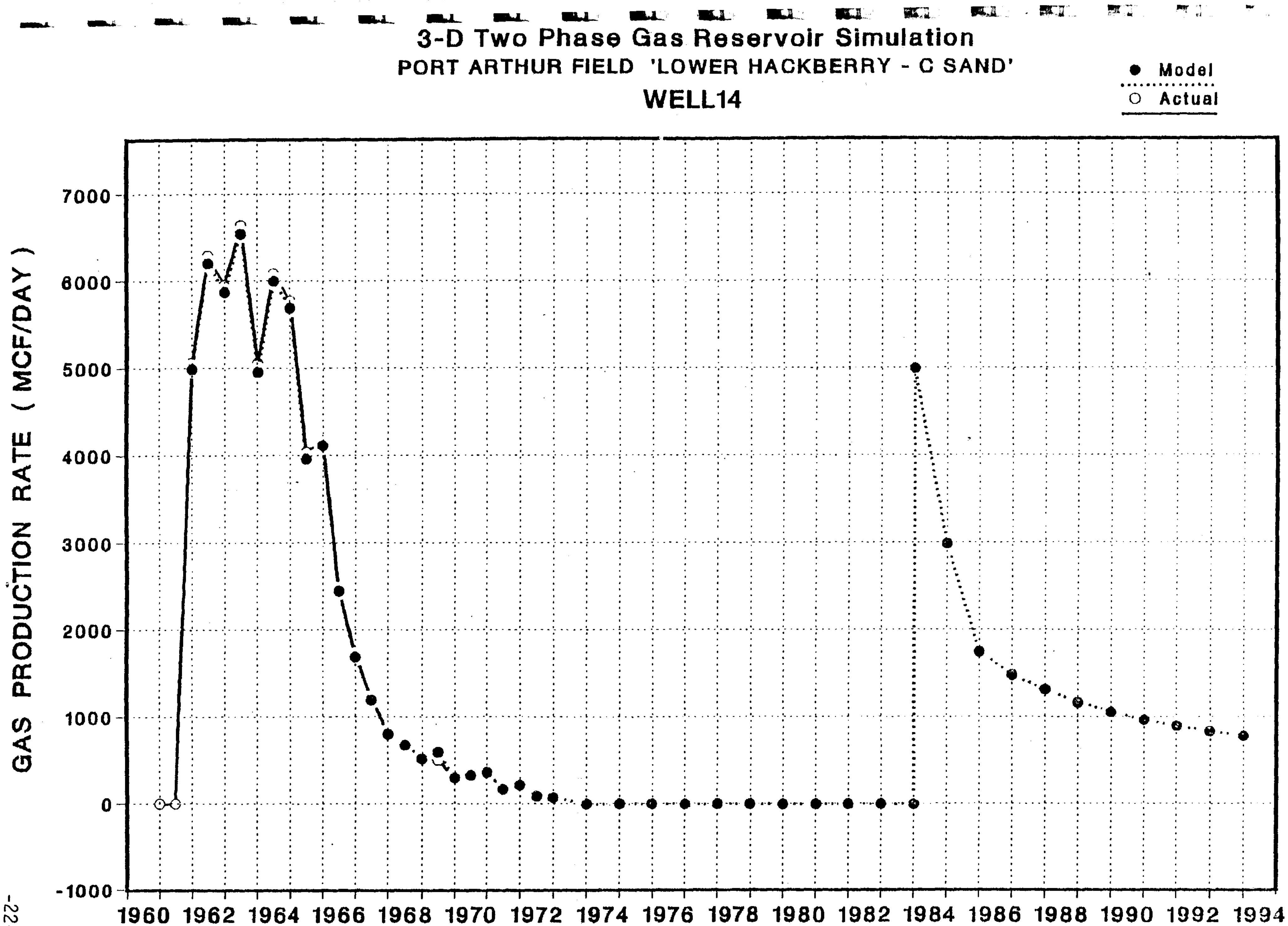

Figure 6. Gas Production Rate - Well No. 14.

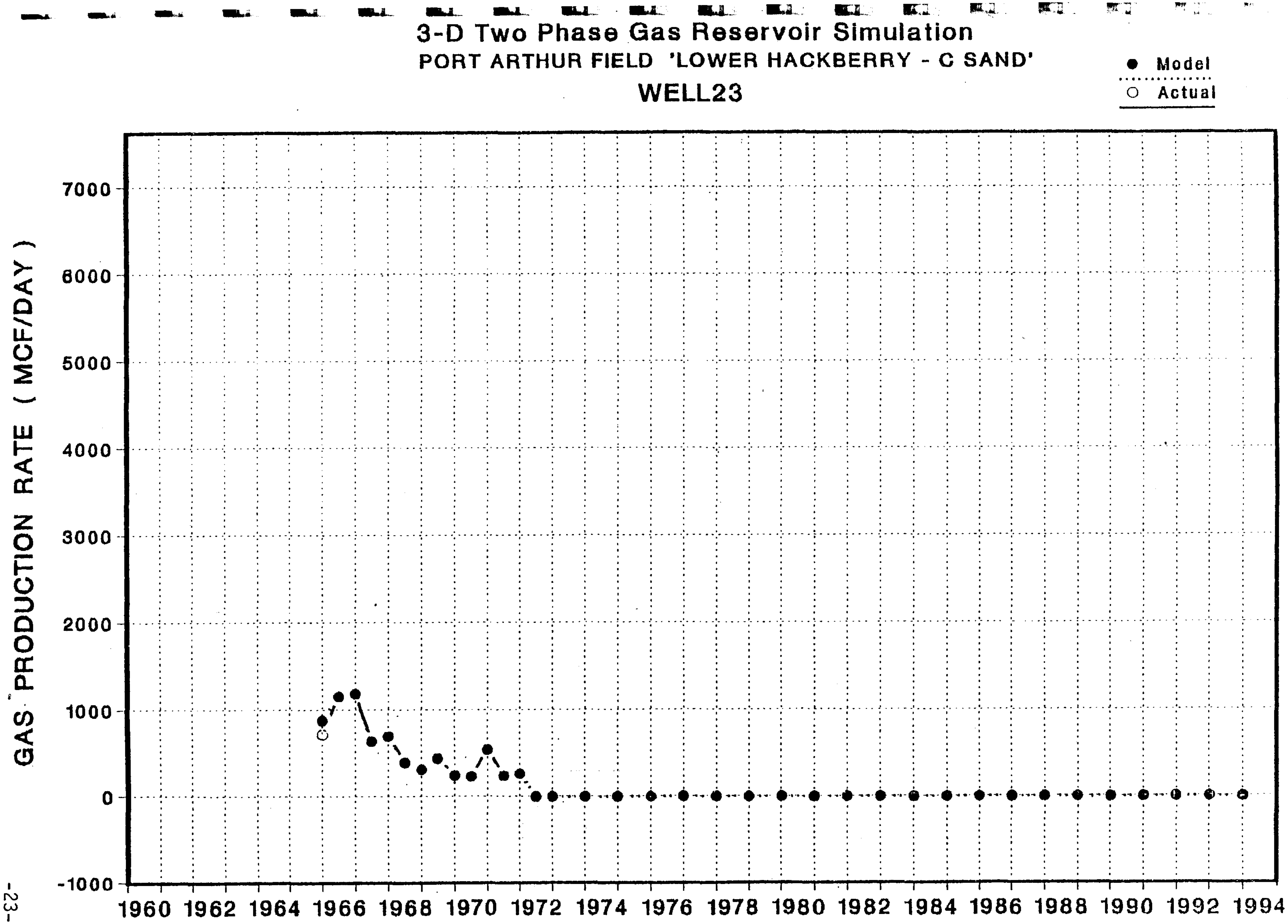

Figure 7. Gas Production Rate - Well No. 23.

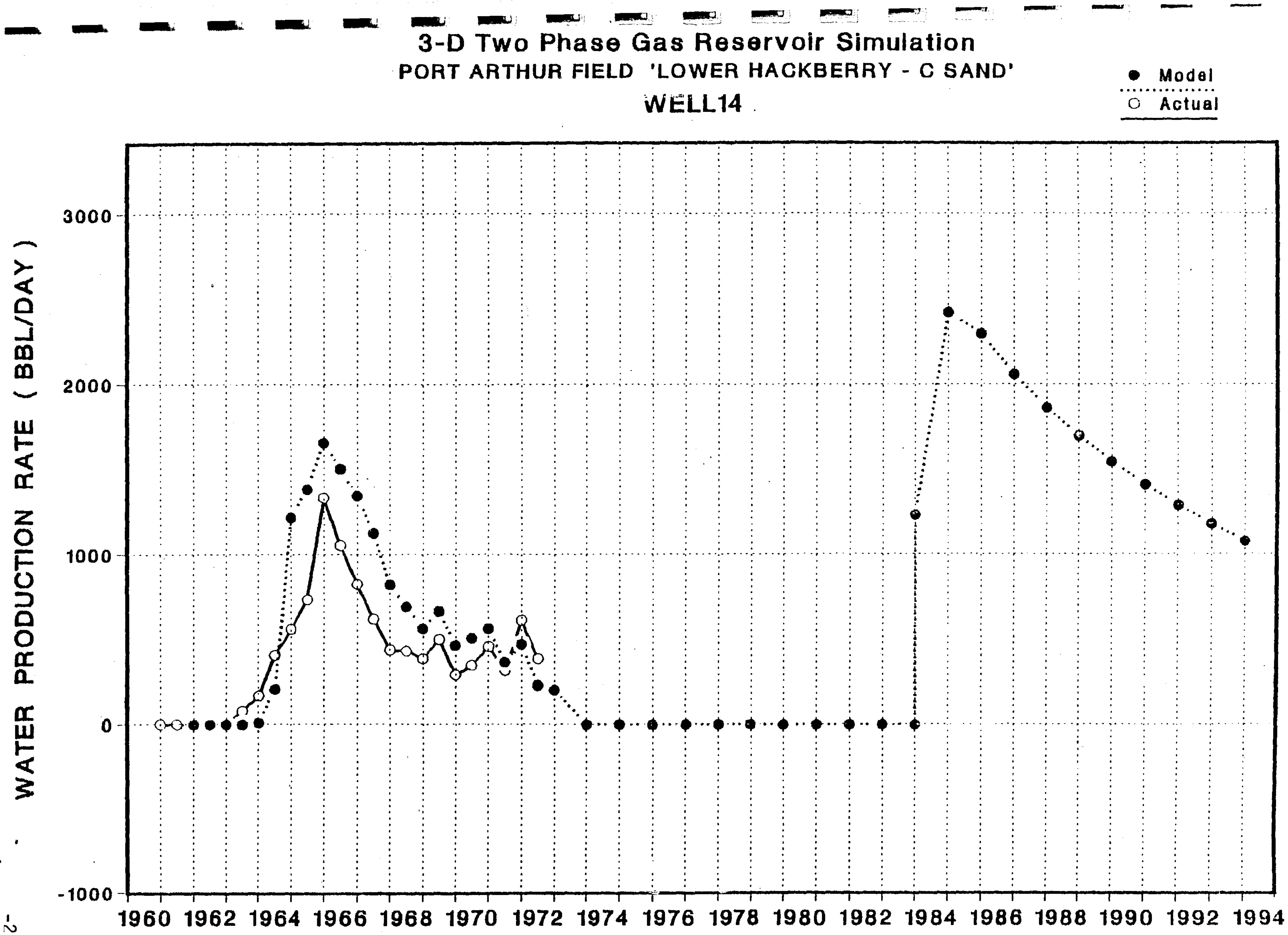

Figure 8. Water Production Rate - Well No. 14.

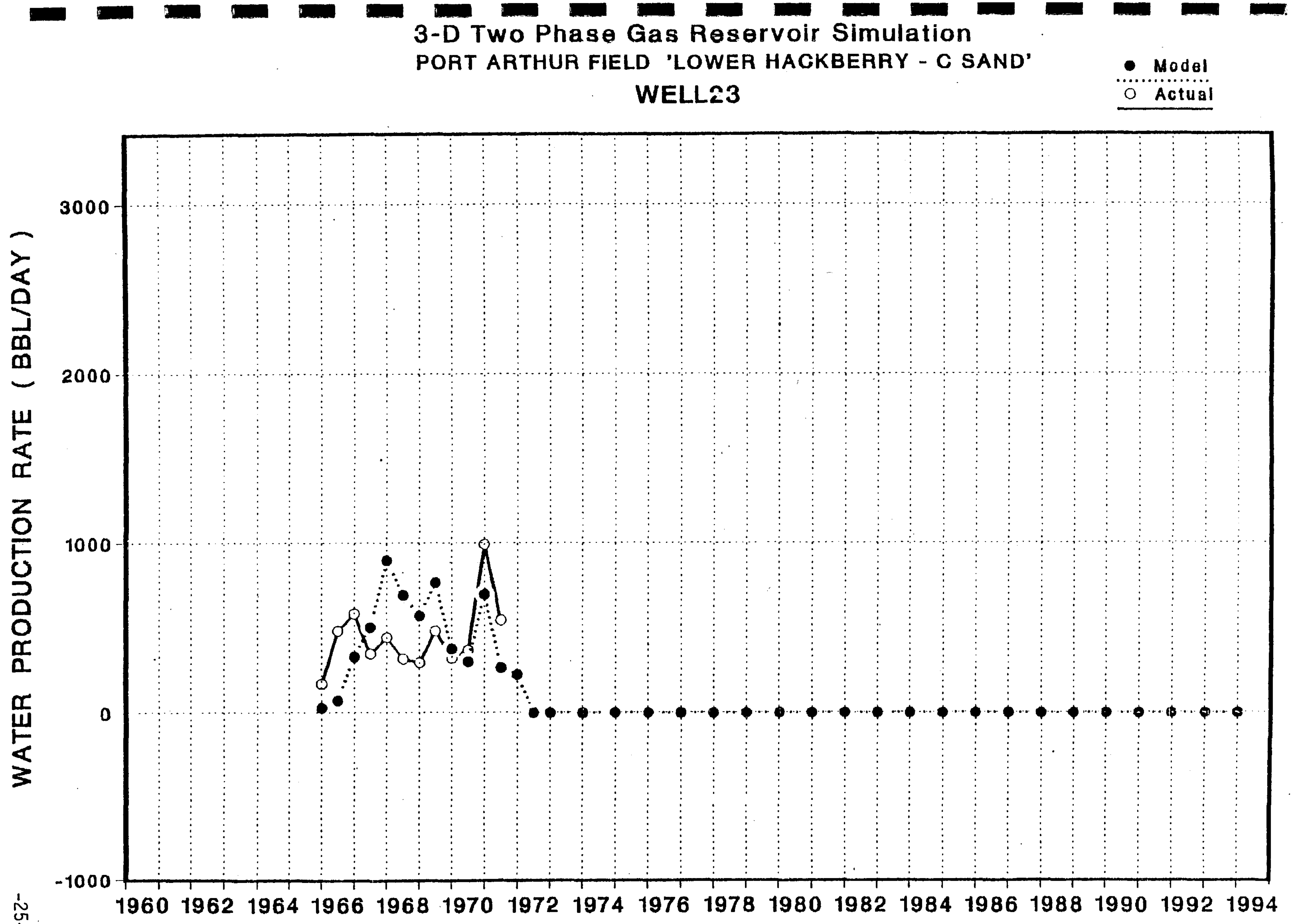

Figure 9. Water Production Rate - Well No. 23.

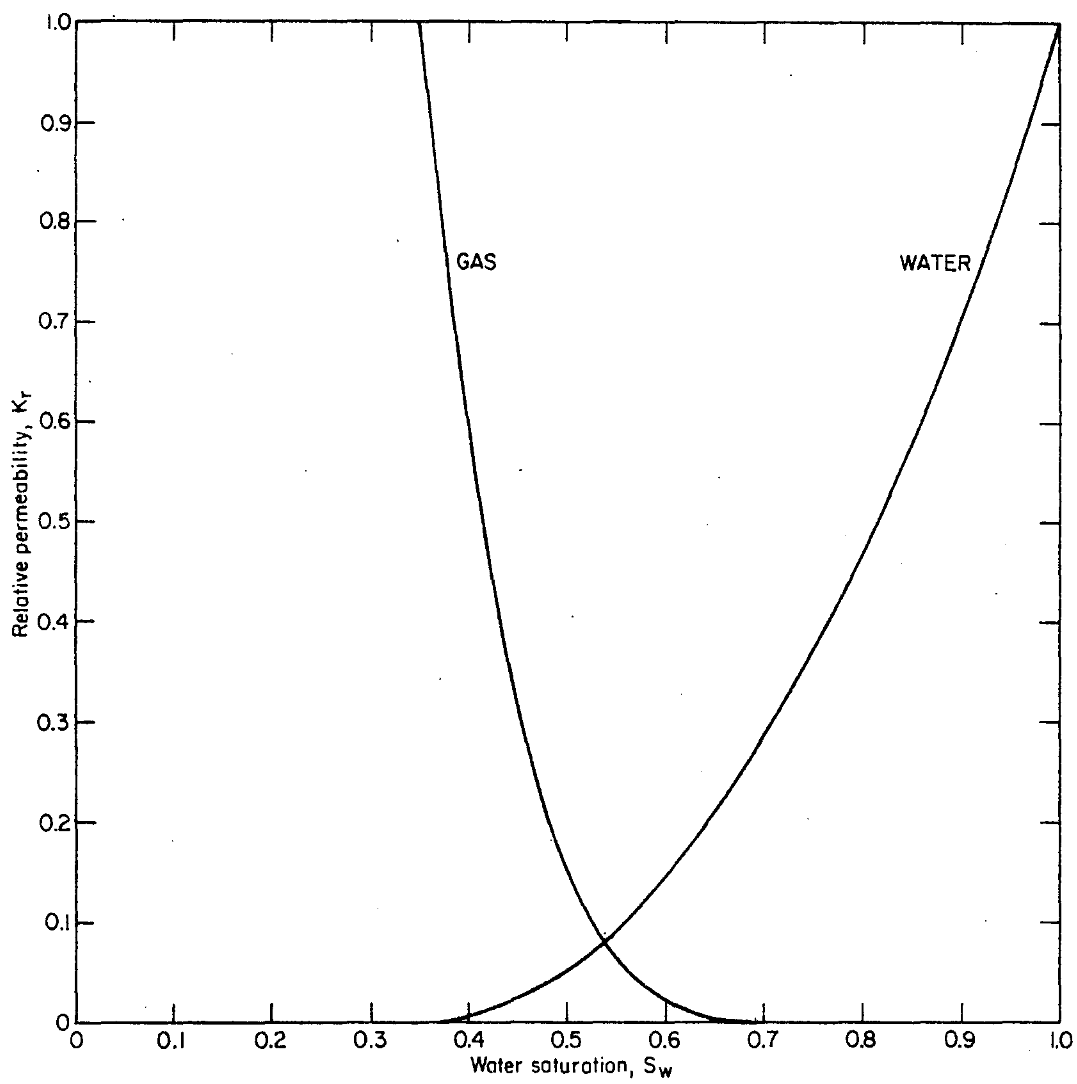

Figure 10. Gas-Water Relative Permeability Curves.

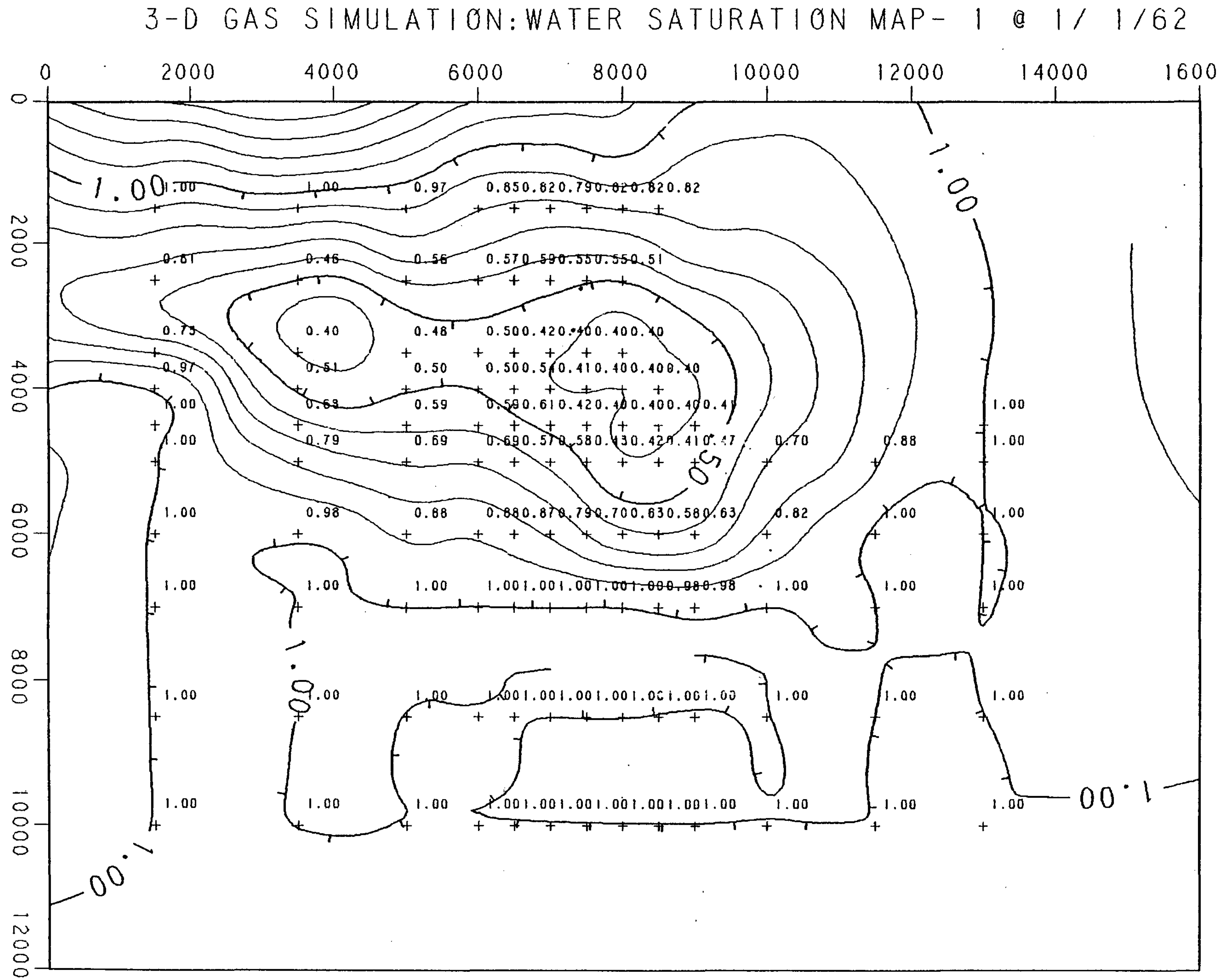

Figure 11. Water Saturation Map @ 1/1/62.

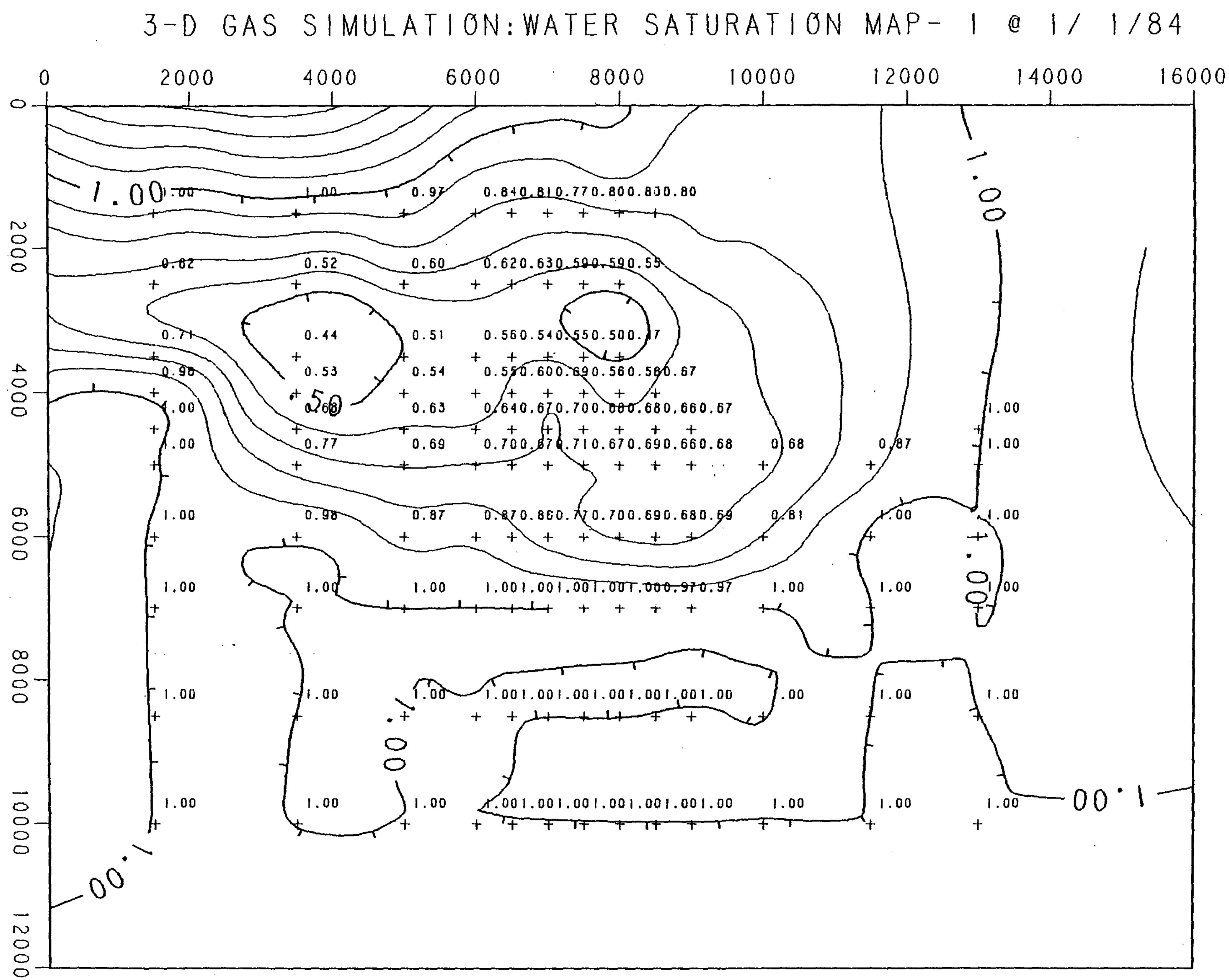

Figure 12. Water Saturation Map @ 1/1/84.

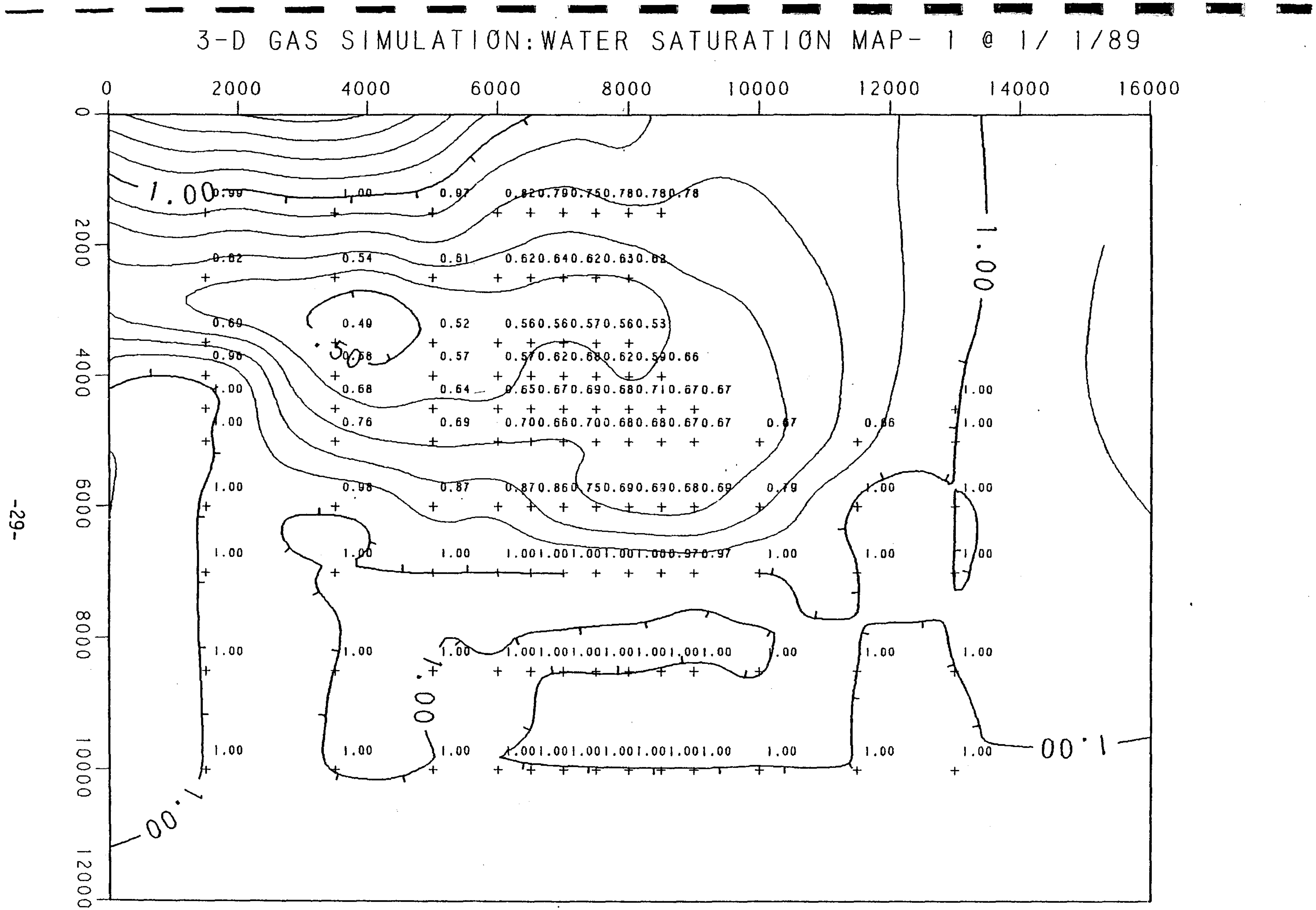

Figure 13. Water Saturation Map @ 1/1/89.

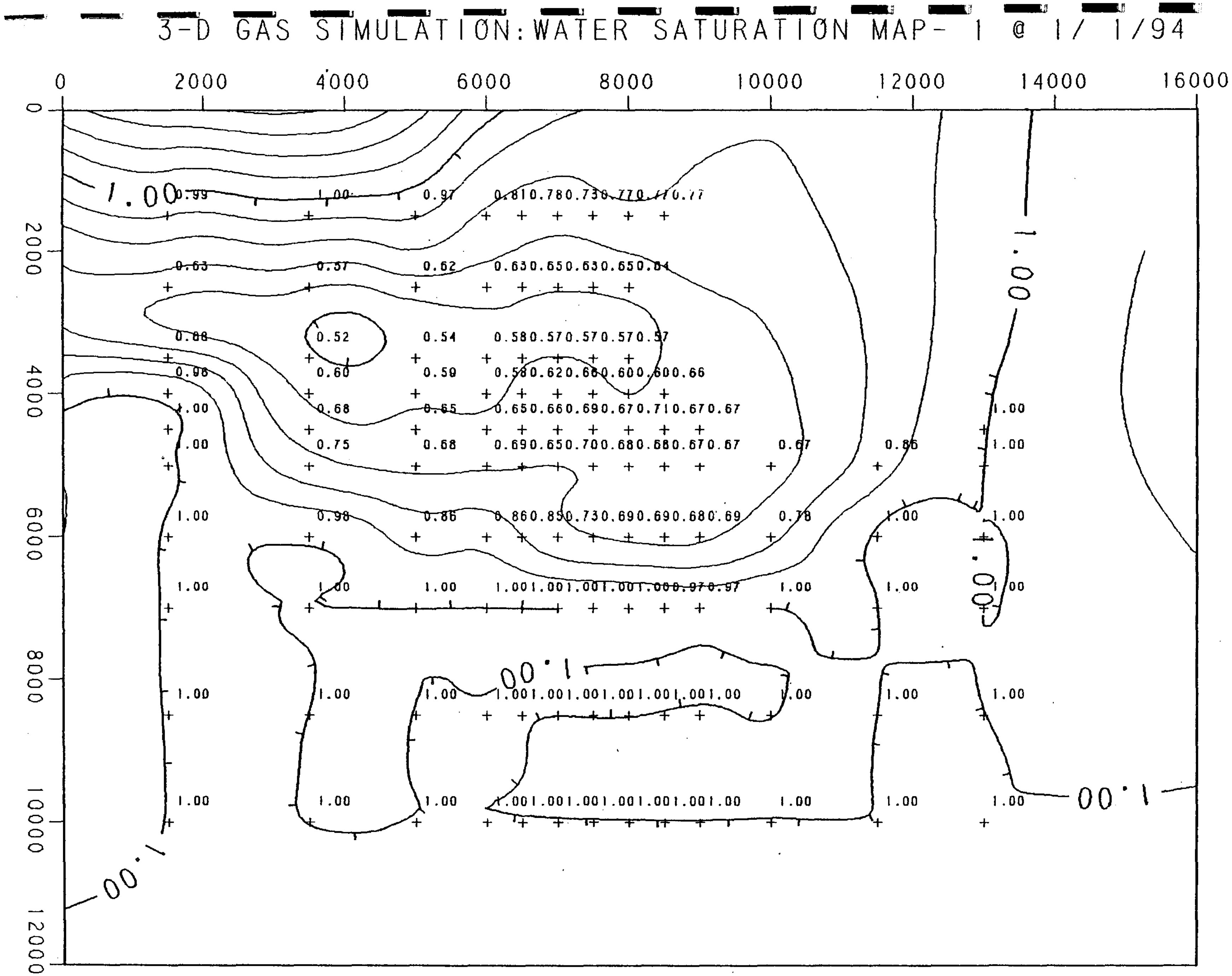

Figure 14. Water Saturation Map @ 1/1/94.

PART 4

ECONOMIC ANALYSIS

CONTENTS

SUMMARY OF ECONOMIC ANALYSIS

Predicted gas production (total)	4.837 Bcf
Predicted condensate production (total)	48 Mbbl
Initial production	January 1984
Production life	10 years
Prices in 1984	
Gas	$ 3.53/Mcf
Condensate	$38.49/bbl
Production and disposal well costs	(1984)
Tangible	$1,886,000
Intangible	$1,547,000
Other capital costs	$ 403,000
Operating costs	$ 33,000/month

Economic Indicators

	Case 1 (non-escalated)	Case 2 (escalated)
Net present worth at 15%		
BFIT	$2,000,000	$2,089,000
AFIT	$ 700,000	$1,079,000
Payout (BFIT)		
Undiscounted, years	2.1	2.48
Discounted, years	2.6	3.33
Break even gas price at 15%		
BFIT, $/Mcf	2.5	—
AFIT, $/Mcf	3.0	—

ECONOMIC ANALYSIS—DISCUSSION

This economic analysis is for the "C" sandstone, Port Arthur field, and is based on the reservoir simulation results (Table 1) of R. L. Ridings (Part 3, this report). Two cases, based on different assumptions, are reported here. In case 1, the prices of gas, condensate, and investment and expense costs are not escalated, whereas, in case 2 they are escalated as discussed below. In both bases it is assumed that production begins in January 1984. Basic cost information for 1984 is based on 1983 dollars which escalate at 12 percent per year (Table 2).

Case 1 (non-escalated)

Cost data are listed under 1984 in Table 2. The current gas price of \$3.27/Mcf is estimated to be \$3.53/Mcf in 1984. The analysis was carried out while varying the price of gas from \$3.00/Mcf to \$6.00/Mcf. At a 15 percent rate of return, the breakeven gas price is \$3.00/Mcf (A.F.I.T.) and \$2.50/Mcf (B.F.I.T.) as shown in Figure 1. The net present worth profiles are shown for different gas prices before and after federal income taxes in figures 2 and 3, respectively. For a gas price of \$3.53/Mcf and a 15 percent rate of return, the net present worth is 2 million dollars (B.F.I.T.) and \$700,000 (A.F.I.T.). The project payout (Figure 4) will be 2 years (B.F.I.T) and 2.5 years (A.F.I.T.) after initial production.

Case 2 (escalated)

A gas price of \$3.53/Mcf and a condensate price of \$38.49/bbl were used with production starting in 1984. Prices were escalated at 8 percent per year and operating costs were escalated at 10 percent per year. Basic cost data in 1984 are given in Table 2. Results of the economic analysis are shown in Table 3. The net present worth at a 15 percent rate of return is 2.09 million dollars (B.F.I.T.) and 1.08 million dollars (A.F.I.T.). Project payout will be 2-3 years after initial production.

TABLE 1. PREDICTED GAS, CONDENSATE, AND WATER PRODUCTION

Year	Gas Production		Condensate Production		Water Production	
	Annual (MMcf/year)	Daily (MMcf/d)	Annual (Mbbl/year)	Daily (Mbbl/D)	Annual (Mbbl/year)	Daily (Mbbl/D)
1984	1,096	3.002	10.96	0.03002	885	2.42
1985	639	1.750	6.39	0.01750	838	2.30
1986	541	1.482	5.41	0.01482	752	2.06
1987	480	1.315	4.80	0.01315	680	1.86
1988	427	1.169	4.27	0.01169	621	1.70
1989	385	1.054	3.85	0.01054	546	1.48
1990	353	0.967	3.53	0.00967	515	1.41
1991	328	0.898	3.28	0.00898	470	1.29
1992	307	0.841	3.07	0.00841	431	1.18
1993	286	0.783	2.86	0.00783	394	1.08

TABLE 2. COST INFORMATION

Items	1983 (M$)	1984 (M$)
Production and disposal well		
Tangible		
Production well	1,592	1,783
Disposal well	92	103
	1,684	1,886
Intangible		
Production well	1,181	1,323
Disposal well	200	224
	1,381	1,547
Other capital costs		
Intangible	360	403
Total (above items)	3,425	3,836
Operating cost	30/month	33/month

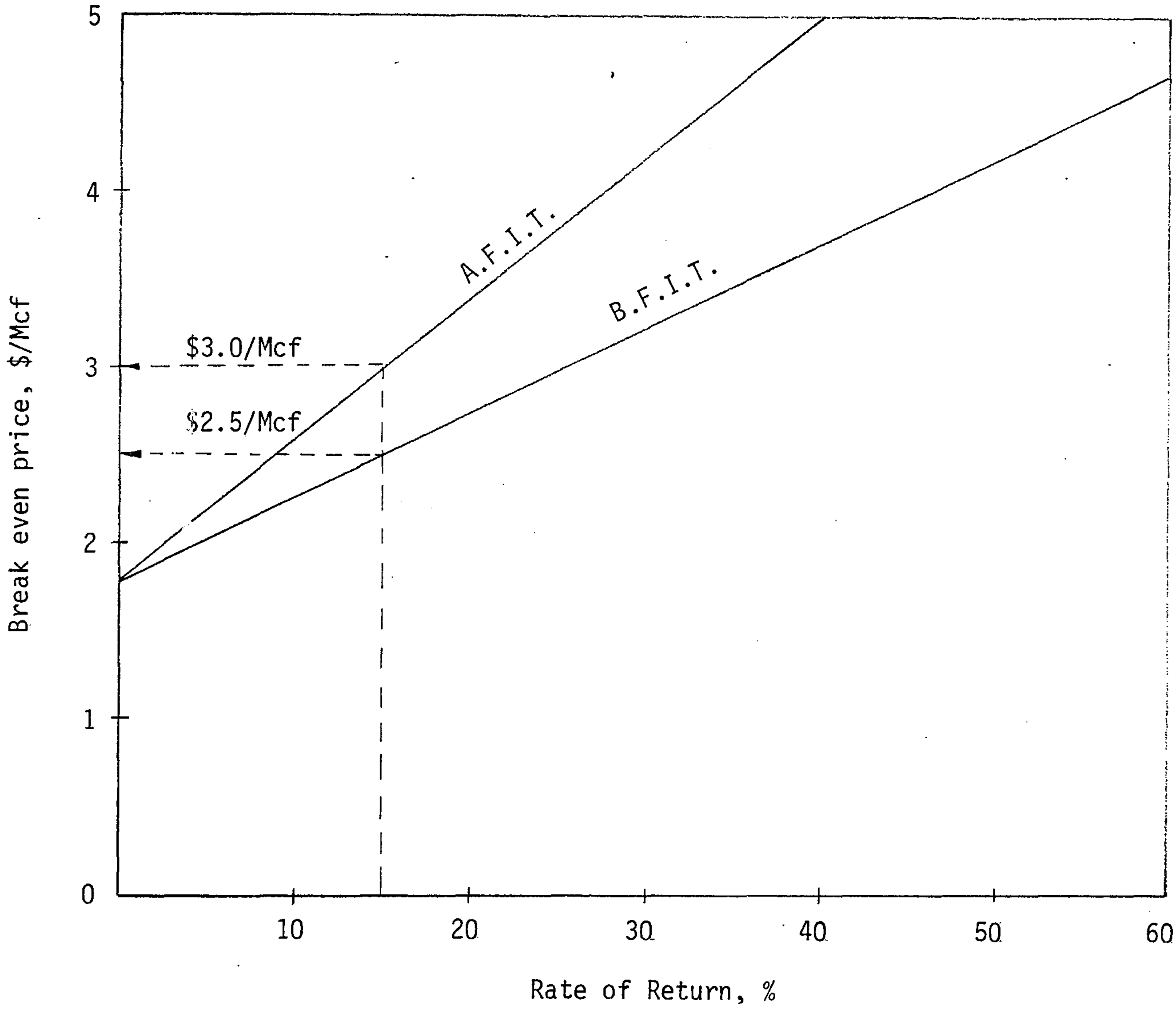

Figure 1. Breakeven gas price versus rate of return (before and after federal income tax).

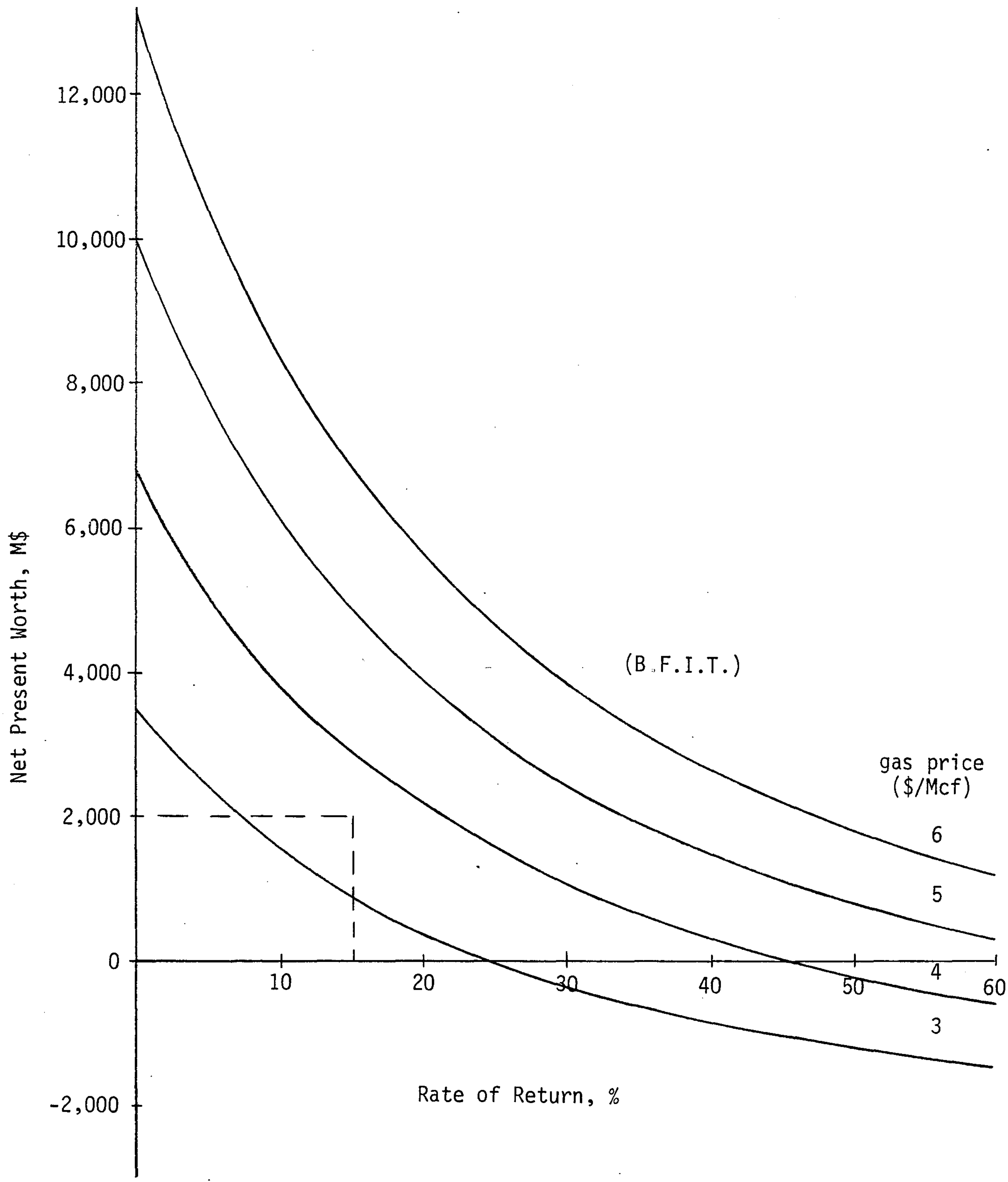

Figure 2. Net present worth versus rate of return (B.F.I.T.) for different gas prices.

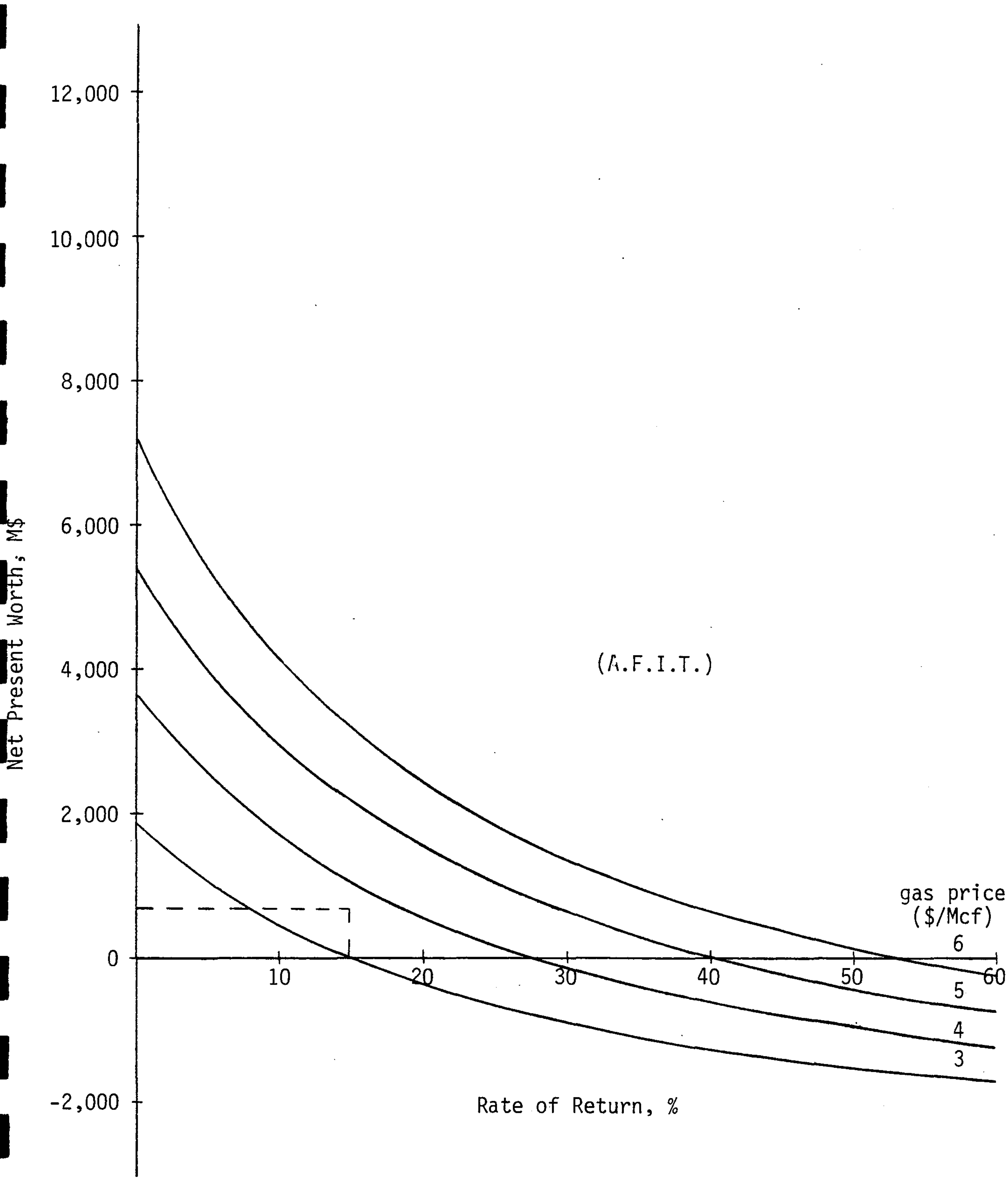

Figure 3. Net present worth versus rate of return (A.F.I.T.) for different gas prices.

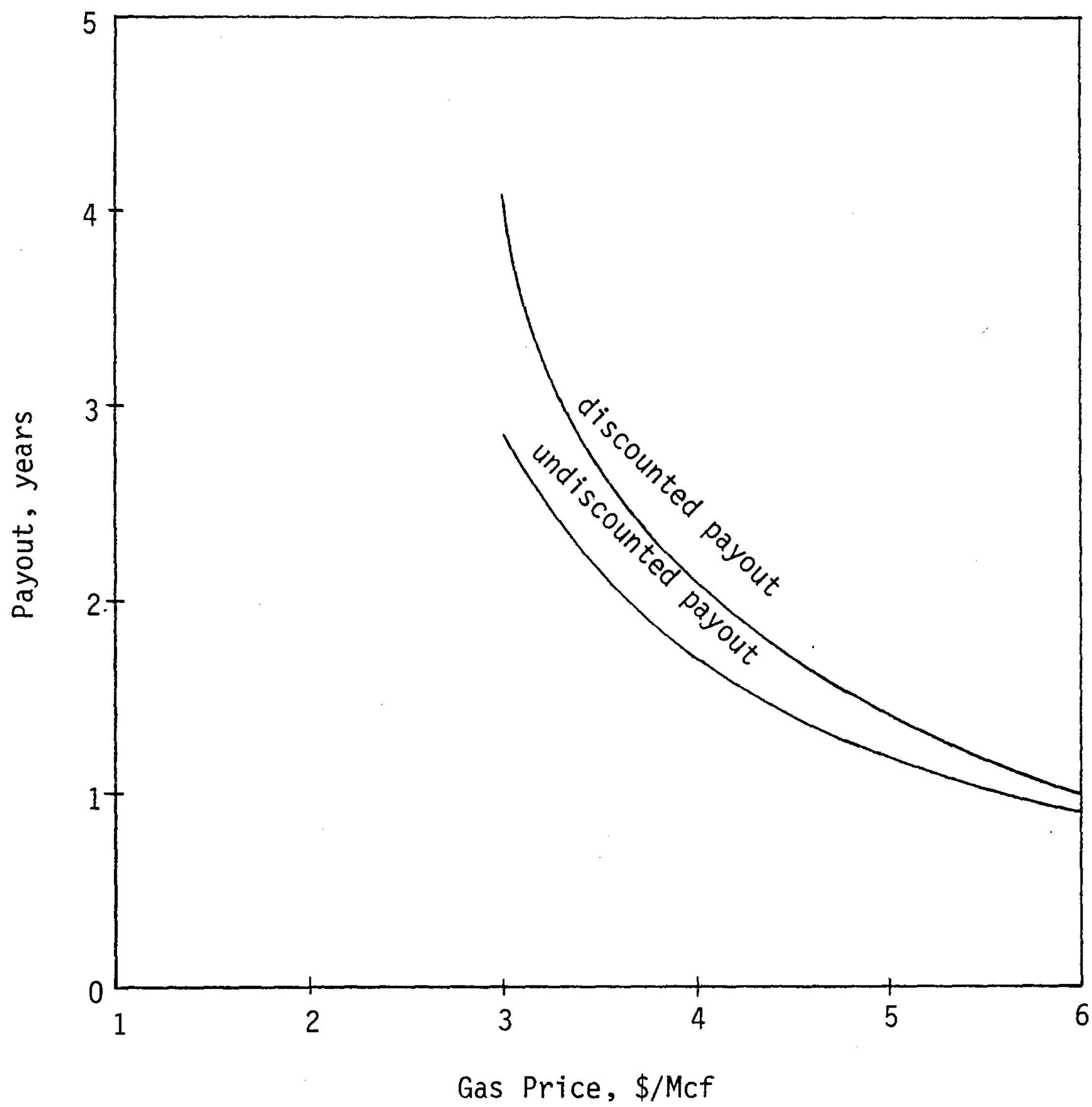

Figure 4. Payout versus gas price for discounted and non-discounted cases

TABLE 3 - 1

R E S E R V E S   A N D   E C O N O M I C S

AS OF DATE: 10/ 1/1983

PERIOD ENDING	12-83	12-84	12-85	12-86	12-87	12-88	12-89	12-90	12-91	12-92	12-93	10.2 YR TOTAL
OWNERSHIP												
1) WORKING INTEREST PCT	100.000	100.000	100.000	100.000	100.000	100.000	100.000	100.000	100.000	100.000	100.000	100.000
2) REVENUE PERCENT	75.000	75.000	75.000	75.000	75.000	75.000	75.000	75.000	75.000	75.000	75.000	75.000
INVESTMENTS, M$												
3) BORROWED CAPITAL	0.	0.	0.	0.	0.	0.	0.	0.	0.	0.	0.	0.
4) EQUITY INVESTMENTS	3570.6	0.	0.	0.	0.	0.	0.	0.	0.	0.	1120.1	4690.7
5) TOTAL	3570.6	0.	0.	0.	0.	0.	0.	0.	0.	0.	1120.1	4690.7
OIL PHASE												
6) GROSS OIL, MB	0.	11.0	6.4	5.4	4.8	4.3	3.8	3.5	3.3	3.1	2.9	48.4
7) NET OIL, MB	0.	8.2	4.8	4.1	3.6	3.2	2.9	2.6	2.5	2.3	2.1	36.3
8) OIL REVENUE, M$	0.	316.3	199.2	182.1	174.6	167.6	163.2	161.7	162.1	164.1	164.9	1855.7
9) OIL PRICE, $/B	0.	38.491	41.570	44.896	48.488	52.367	56.556	61.081	65.967	71.245	76.944	76.944
GAS PHASE												
10) GROSS GAS, MMF	0.	1095.7	638.8	540.9	480.0	426.7	384.7	353.0	327.8	307.0	285.8	4840.3
11) NET GAS, MMF	0.	821.8	479.1	405.7	360.0	320.0	288.5	264.7	245.8	230.2	214.3	3630.2
12) GAS REVENUE, M$	0.	2904.4	1828.5	1672.4	1602.7	1538.7	1498.3	1484.6	1489.0	1506.0	1514.3	17039.0
13) GAS PRICE, $/MCF	0.	3.5342	3.8169	4.1223	4.4521	4.8082	5.1929	5.6083	6.0570	6.5416	7.0649	7.0649
ECONOMICS, M$												
18) GROSS REV. TO INTR.	0.	3220.7	2027.7	1854.5	1777.2	1706.3	1661.5	1646.3	1651.2	1670.1	1679.3	18894.7
19) - SEV. TAX	0.	232.4	146.3	133.8	128.2	123.1	119.9	118.8	119.1	120.5	121.2	1363.3
20) - WINDFALL TAX PAID	0.	0.	0.	0.	0.	0.	0.	0.	0.	0.	0.	0.
21) + WINDFALL REFUND	0.	0.	0.	0.	0.	0.	0.	0.	0.	0.	0.	0.
22) - AD VALOREM TAX	0	119.5	75.3	68.8	66.0	63.3	61.7	61.1	61.3	62.0	62.3	701.3
23) - OPERATING COSTS	171.2	684.9	499.0	548.9	603.7	664.1	730.5	643.1	589.5	518.7	442.2	6095.8
24) - CAPITAL REPAYMENT	0.	0.	0.	0.	0.	0.	0.	0.	0.	0.	0.	0.
25) - INTEREST PAID	0.	0.	0.	0.	0.	0.	0.	0.	0.	0.	0.	0.
26) = NET INCOME	-171.2	2183.9	1307.2	1103.0	979.3	855.7	749.4	823.3	881.3	968.8	1053.5	10734.4
27) - EQUITY INVESTMENTS	3570.6	0.	0.	0.	0.	0.	0.	0.	0.	0.	1120.1	4690.7
28) = BFIT NET	-3741.8	2183.9	1307.2	1103.0	979.3	855.7	749.4	823.3	881.3	968.8	-66.6	6043.7
PRESENT WORTH AT 15.000 PERCENT												
29) NET INCOME	-168.0	1953.6	1006.5	731.1	558.7	420.3	316.8	299.6	276.1	261.3	244.6	5900.5
30) EQUITY INVESTMENTS	3570.0	0.	0.	0.	0.	0.	0.	0.	0.	0.	241.0	3811.0
31) BFIT NET	-3738.1	1953.6	1006.5	731.1	558.7	420.3	316.8	299.6	276.1	261.3	3.5	2089.5
32) CUM BFIT NET	-3738.1	-1784.5	-778.0	-46.9	511.9	932.2	1249.0	1548.6	1824.7	2086.0	2089.5	2089.5

TABLE 3 - 2

A F T E R   T A X   E C O N O M I C S

AS OF DATE: 10/ 1/1983

PERIOD ENDING	12-83	12-84	12-85	12-86	12-87	12-88	12-89	12-90	12-91	12-92	12-93	10.2 YR TOTAL
INVESTMENTS, M$												
1) EXPENSED	1547.3	0.	0.	0.	0.	0.	0.	0.	0.	0.	1120.1	2667.4
2) DEPLETABLE	137.2	0.	0.	0.	0.	0.	0.	0.	0.	0.	0.	137.2
3) DEPRECIABLE	1886.1	0.	0.	0.	0.	0.	0.	0.	0.	0.	0.	1886.1
4) TOTAL	3570.6	0.	0.	0.	0.	0.	0.	0.	0.	0.	1120.1	4690.7
TAX CALCULATIONS, M$												
5) GROSS REV. TO INTR.	0.	3220.7	2027.7	1854.5	1777.2	1706.3	1661.5	1646.3	1651.2	1670.1	1679.3	18894.7
6) - SEVERANCE TAX	0.	232.4	146.3	133.8	128.2	123.1	119.9	118.8	119.1	120.5	121.2	1363.3
7) - WINDFALL TAX	0.	0.	0.	0.	0.	0.	0.	0.	0.	0.	0.	0.
8) - OPR. COSTS	171.2	804.4	574.2	617.7	669.7	727.4	792.2	704.2	650.8	580.7	504.6	6797.1
9) - OVERHEAD	0.	0.	0.	0.	0.	0.	0.	0.	0.	0.	0.	0.
10) - INTANG. EXPENSED	1547.3	0.	0.	0.	0.	0.	0.	0.	0.	0.	1120.1	2667.4
11) - DEPRECIATION	282.9	414.9	396.1	396.1	396.1	0.0	0.	0.	0.	0.	0.	1996.1
12) = NET	-2001.4	1769.0	911.1	707.0	583.2	855.7	749.4	823.3	881.3	968.8	-66.6	6180.9
13) NET	-2001.4	1769.0	911.1	707.0	583.2	855.7	749.4	823.3	881.3	968.8	-66.6	6180.9
14) - DEPLETION	0.	31.1	18.1	15.3	13.6	12.1	10.9	10.0	9.3	8.7	8.1	137.2
15) - INTEREST	0.	0.	0.	0.	0.	0.	0.	0.	0.	0.	0.	0.
16) = TAXABLE	-2001.4	1737.9	893.0	691.6	569.6	843.6	738.5	813.3	872.0	960.1	-74.7	6043.7
17) TAXABLE	-2001.4	1737.9	893.0	691.6	569.6	843.6	738.5	813.3	872.0	960.1	-74.7	6043.7
18) * TAX RATE	0.4600	0.4600	0.4600	0.4600	0.4600	0.4600	0.4600	0.4600	0.4600	0.4600	0.4600	0.4600
19) - INV. CREDIT	188.6	0.	0.	0.	0.	0.	0.	0.	0.	0.	0.	188.6
20) + PREF. TAX	0.	0.	0.	0.	0.	0.	0.	0.	0.	0.	0.	0.
21) = F.I.T.	-1109.3	799.5	410.8	318.2	262.0	388.1	339.7	374.1	401.1	441.7	-34.3	2591.5
22) REVENUE - SEV. TAXES	0.	2988.3	1881.4	1720.7	1649.0	1583.2	1541.6	1527.5	1532.0	1549.6	1558.1	17531.4
23) - OPR. COSTS	171.2	804.4	574.2	617.7	669.7	727.4	792.2	704.2	650.8	580.7	504.6	6797.1
24) - F.I.T.	-1109.3	799.5	410.8	318.2	262.0	388.1	339.7	374.1	401.1	441.7	-34.3	2591.5
25) - LOAN REPAYMENT	0.	0.	0.	0.	0.	0.	0.	0.	0.	0.	0.	0.
26) - INTEREST	0.	0.	0.	0.	0.	0.	0.	0.	0.	0.	0.	0.
27) = NET INCOME	938.0	1384.5	896.4	784.9	717.3	467.7	409.7	449.2	480.2	527.2	1087.9	8142.9
28) - EQUITY INVESTMENTS	3570.6	0.	0.	0.	0.	0.	0.	0.	0.	0.	1120.1	4690.7
29) = AFIT NET	-2632.5	1384.5	896.4	784.9	717.3	467.7	409.7	449.2	480.2	527.2	-32.2	3452.2
PRESENT WORTH AT 15.000 PERCENT												
30) NET INCOME	920.7	1238.4	690.2	520.2	409.2	229.7	173.2	163.5	150.4	142.2	252.5	4890.3
31) EQUITY INVESTMENTS	3570.0	0.	0.	0.	0.	0.	0.	0.	0.	0.	241.0	3811.0
32) AFIT NET	-2649.3	1238.4	690.2	520.2	409.2	229.7	173.2	163.5	150.4	142.2	11.5	1079.3
33) CUM AFIT NET	-2649.3	-1410.9	-720.7	-200.4	208.8	438.5	611.7	775.2	925.6	1067.8	1079.3	1079.3

TABLE 3 - 3

E C O N O M I C   I N D I C A T O R S

AS OF DATE: 10/ 1/1983

	B.F.I.T. WORTH M$------	A.F.I.T. WORTH M$------
PRESENT WORTH PROFILE AND RATE-OF-RETURN VS. BONUS TABLE		
0.	6043.699	3452.206
5.	4359.468	2456.309
10.	3077.662	1684.479
15.	2089.508	1079.283
20.	1317.210	598.635
25.	704.841	211.661
30.	212.170	-104.228
35.	-190.002	-365.672
40.	-522.922	-584.936
50.	-1039.501	-931.187
60.	-1420.446	-1192.108
70.	-1712.881	-1396.231
80.	-1944.763	-1560.836
90.	-2133.443	-1696.853
100.	-2290.151	-1811.485
RATE OF RETURN, PCT.	32.6	28.4
UNDISCOUNTED PAYOUT, YRS.	2.48	2.70
DISCOUNTED PAYOUT, YRS.	3.33	3.74
UNDISCOUNTED NET/INVEST.	2.29	1.74
DISCOUNTED NET/INVEST.	1.55	1.28